Supercooled sulphuric acid solutions: Desorption of water, mass accommodation and residence time of HCl at 213, 218 and 228 K

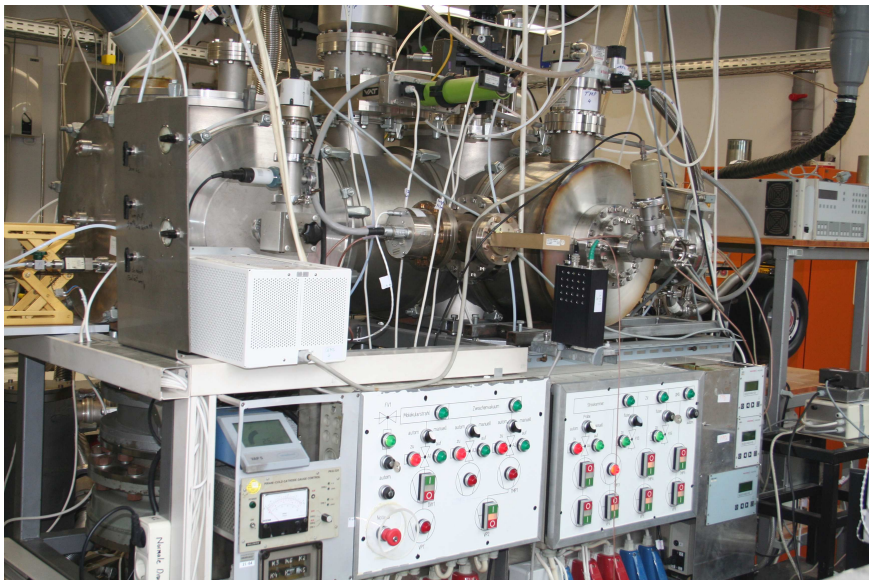

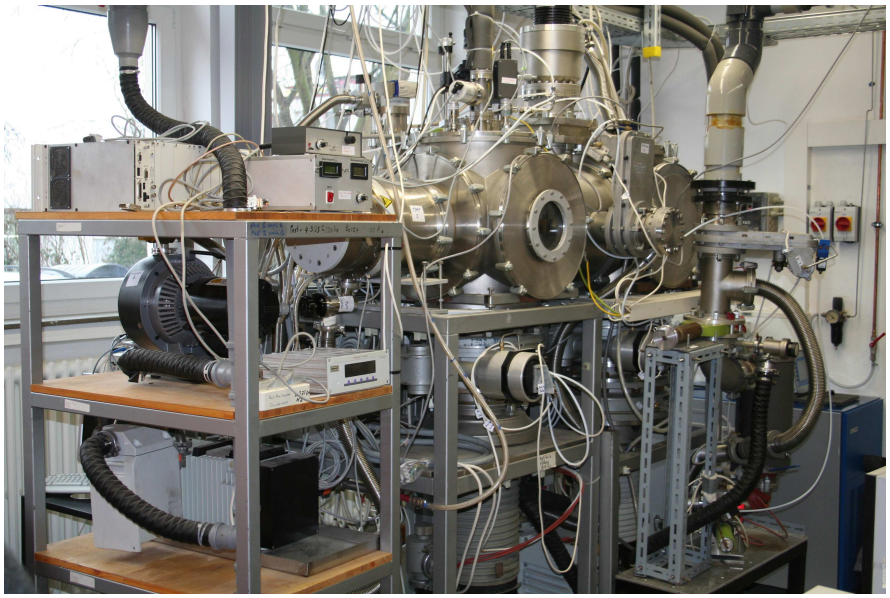

Dissertation
Faculty of chemistry
University of Duisburg- Essen
21.12.2012

Khaled Ataya

Supercooled sulphuric acid solutions: Desorption of water, mass accommodation and residence time of HCl at 213, 218 and 228 K

Dissertation

Submitted to

Faculty of chemistry
University of Duisburg- Essen

In partial fulfilment of the
requirements for a

Doctor of Natural Sciences
(Dr. rer. nat.)

Khaled Ataya
from
Damascus/ Syria

Tag der Disputation: 29.01.2013

Vorsitzender: Prof. Dr. O. Schmitz

1. Gutachter: Prof. Dr. Dr. h. c. R. Zellner
2. Gutachter: Prof. Dr. C. Mayer

Acknowledgements

Here is the place where I would like to thank Prof. Dr. Dr. h. c. R. Zellner, who allowed me to join his group and gave me a chance to write my PhD thesis at the University of Duisburg-Essen.

My very sincere thanks also to Dr. Peter Behr. He is an inspiration and wonderful human being. He is not only my supervisor but also my best brother in Germany. Thank you for making me the scientist.

I also give thanks to all of the Zellner group and LUAT group members who helped me in the lab and made me laugh.

I would like to thank specially Mr. Schnichels and Mr. Türksch.

Finally, I would like to thank Prof. Dr. –Ing. habil. K. Görner, who supported this work.

Erklärung

Hiermit versichere ich, dass ich die vorlegende Arbeit mit dem Titel

„Supercooled sulphuric acid solutions:
Desorption of water, mass accommodation
and residence time of HCl at 213, 218 and 228 K“

selbst verfasst und keine außer den angegebenen Hilfsmitteln und Quellen benutzt habe, und dass die arbeit in dieser oder ähnlicher Form noch bei keiner anderen Universität eingerichtet wurde.

Essen, im Oktober 2012

Khaled Ataya

Khaled Ataya
Oberdorf Str. 29
45143 Essen

atayakhaled@yahoo.com
Tel: 0201/4338447

Curriculum Vitae

Personal Data

Name	Ataya Khaled
Birth date	13.11.1979
Birth place	Damascus (Syria)
Nationality	Syrian

Educations

2008 – 2013	Ph.D. student at the faculty of chemistry, university of Duisburg- Essen
2007 – 2008	Advanced project in the physical chemistry, department of physical chemistry, university of Duisburg- Essen
2003 – 2004	Diploma of higher studies in general chemistry, department of chemistry, university of Damascus
1998 – 2003	Bachelor of chemical sciences (applied chemistry), faculty of science, university of Damascus
1998	Secondary education certificate (scientific section) in Damascus

Work experience

2009 – 2012	Scientist at the University of Duisburg- Essen, LUAT (Chair of Environmental Process Engineering and Plant Design), in the teamwork of Prof. Dr. Ing. habil. K. Görner
10.2009	Scientific visitor, one week, BER II, Neutron Scattering Centre, Helmholtz- Zentrum Berlin für Materialien und Energie GmbH in der Helmholtz Gemeinschaft, Dr. Hoser, (Flat- Cone Signal Crystal Diffractometer “thermal neutrons“), Focal point: thermal evolution of the powder diffraction pattern of D_2O crystal
2008 – 2009	Scientist at the University of Duisburg- Essen, Institute of theoretical and physical Chemistry, in the teamwork of Prof. Dr. Dr. h. c. R. Zellner

2004 – 2007	Chemist at the Italian detergent industry, department of sodium silicate production, in Damascus

Related experiences

Environmental chemistry, Analysis chemistry

Heterogeneous reactions

Atomic and molecular beam scattering technique, vacuum evaporation experiments

Mass, IR, NIR, VIS spectrometer

Skills and Qualifications

Language	English (very good) German (DSH- 2) Arabic (very good)
EDV/Graphic/Internet	Microsoft Office (Word, Excel, Power Point) Internet (Outlook, Internet Explorer), Origin, Spectroscopy software, data analysis applications, Visual Basic, FORTRAN 77, SAP Program

Khaled Ataya

List of publications

Paper

Behr P., U. Scharfenort, K. Ataya, R. Zellner, *Dynamic and mass accommodation of HCl molecules on surface acid- water surfaces*, Phys. Chem. Chem. Phys., 11, 1- 8, **2009**.

Oral presentation

P. Behr, U. Scharfenort, K. Ataya, R. Zellner, *Dynamics and mass accommodation of HCl molecules on sulphuric acid/ water surfaces*, 109. Hauptversammlung der Deutschen Bunsen- Gesellschaft für Physikalische Chemie e.V., Universität Bielefeld, **2010**.

Poster presentation

Peter Behr, Khaled Ataya, *Thermal and non- thermal translational energy distributions of D_2O molecules desorbing from liquid and solid D_2O/ D_2SO_4 surfaces*, P. 367, III. Hauptversammlung der Deutschen Bunsen- Gesellschaft für Physikalische Chemie e.V., Tagungshandbuch, Universität Leipzig, **2012**.

Contents

Introduction

Interactions between gas and liquid molecules are of importance for understanding atmospheric and industrial processes. For example, heterogeneous reactions of hydrogen chloride gas with the solution of sulphuric acid aerosols play an important role in stratospheric ozone depletion [e.g. Anderson et al., 2000]. This hydrogen chloride reacts with dissolved molecules such as $ClONO_2$ [Abbatt & Molina, 1992] or HOCl [Scwell et al. 2000] or HOBr [Waschewsky & Abbatt, 1999; Hanson & Ravishankara, 1995] to produce Cl_2 or BrCl gas. The Cl_2 and BrCl gas molecules are then photolyzed by sunrays into chlorine radicals that catalyze ozone destruction [Tolbert et al. 1987] & [De More, 1991]. The following reactions show the influence of HCl gas in the stratosphere to form the ozone hole:

$$HCl + ClONO_2 \longrightarrow Cl_2 + HNO_3$$

$$HCl + HOCl \longrightarrow Cl_2 + H_2O$$

$$HCl + HOBr \longrightarrow BrCl + H_2O$$

$$Cl_2 + h\nu \longrightarrow 2Cl$$

$$Cl + O_3 \longrightarrow OCl + O_2$$

These reactions can be limited by reducing the HCl solubility in the aerosol. Recent studies indicate that HCl gas molecules remain in molecular form in the gas phase. In contrast, in the liquid phase, the value of the dissociation constant is sufficient high to produce ions completely [Ardura & Donaldson, 2009]. In addition, the HCl solubility increases with the concentration of sulphuric acid in the aerosol at supercooled temperatures [Tabzadeh et al. 1994] and [Carslaw et al. 1995].

In fact, the kinetics of transport of gas molecules at the interface liquid- gas can be determined if these reactions take place either on the surface or in the bulk of the aerosol droplets. If the reactions occur on the surface of the liquid, the transfer of the molecules needs a short time, rather than the reactions take place in the bulk of the

liquid. Therefore, these kinetics of transfer of gas molecules have been studied using several experimental techniques such as droplet train flow reactor [Worsnop et al. 1989], wetted wall flow reactor [Brown, 1978] and Knudsen cell reactor [Caloz et al. 1997].

The measurements using the droplet train flow reactor reveal that the solubility of HCl gas molecules in the stratospheric aerosol increases with the concentration of sulphuric acid above 69 wt% [Robinson et al. 1998]. Using the wetted flow reactor, the measured values of the HOCl solubility are higher than expected in the concentration range of 62.5- 70 wt% of the sulphuric acid solution at a temperature of 250 K [Donaldson et al. 1997]. Further, the results from the experimental data of the wetted flow reactor demonstrate that the solubility of HCl in the sulphuric acid solution increase with a decrease in temperature for a given acid content and decrease with increasing acid content at a given temperature [Zhang et al. 1994]. Furthermore, at a concentration of the sulphuric acid solution below 61 wt%, the measurements of HCl and HOCl solubilities are in very good agreement with the calculated values for HCl and HOCl based on Carslaw et al. 1995 and Huthwelker et al. 1995 models, respectively [Hanson & Lovejoy, 1996].

Hurlbut and Beck developed first an experimental method to provide important physical and chemical information about gas-liquid surface interactions. This experimental method is named the atomic and molecular beam scattering technique [Hurlbut & Beck, 1959]. This technique was applied to measure the directions and velocities of Ne, Ar and Xe atoms scattering from perfluorinated polyether and squalane ($C_{14}H_{29}$) which have very low vapour pressure [King et al. 1993]. After that, these processes were observed both, direct inelastic scattering and trapping desorption, when gases such as Ne, CH_4, NH_3 and D_2O strike the liquid surface of glycerol or squalane [Seacker & Nathanson, 1993]. The first scattering experiments using the liquid surface of sulphuric acid solutions at supercooled temperatures were reported in 2000 by the Nathanson group [Moris et al. 2000]. These experiments explored the collisions and interactions of the strong acid HCl with the sulphuric acid solutions. A detailed description of gas- liquid collisions and reactions can be achieved by quantitatively determining the fraction of acid molecules that undergo: trapping, direct scattering, interface dissociation or reaction, bulk solvation and

desorption. Moreover, the sulphuric acid content becomes higher by the evaporation of water through the high vacuum of this experiment. As a result, the mass accommodation of HCl gas onto the surface of the sulphuric acid solution and the time of the solubility of HCl in the liquid bulk of the sulphuric acid solution (residence time) can be measured in different concentrations of this solution.

However, the molecular beam technique recorded the residence time of HCl molecules in the deuterated sulphuric acid solution at temperature 213 K. It is found that the time of the solubility of HCl increases with an increase of the concentration of sulphuric acid solution in the range concentration above 65 wt% [Behr et al. 2001]. The measured proton exchange of HCl molecules indicates that these values decrease with increasing concentration of sulphuric acid solution [Behr et al. 2001].

The molecular beam technique is used in this work to investigate the proton exchange of HCl and the lifetime with respect to solubility as it interacts with the bare deuterated sulphuric acid solution at temperatures of 213, 218 and 228 K. In addition, this technique is also used to monitor the kinetics of desorption of water from the liquid [Samuel et al. 2006] and solid surface of this solution at supercooled temperatures.

In the case of the desorption of water from the liquid surface, several experimental techniques were applied in order to understand the kinetics of the evaporation of the water molecules from a liquid surface. Some of these techniques are the evaporation apparatus [Ward et al. 2004], Raman thermometry and the molecular beam technique.

The evaporation apparatus from [Ward et al. 2004] indicates that the liquid surface is the coldest place at the gas-liquid interface during the evaporation. Raman thermometry is used to measure the temperatures of the rapidly evaporating liquid water droplet injected into the vacuum. The results indicate that the evaporation of water molecules may occur through geometric requirements [Smith et al. 2006]. Using the coupled liquid water jet source and the molecular beam apparatus, the time of flight spectra reveals that the velocity distribution of the molecules which evaporate from liquid surface shifts from the Maxwellian velocity distribution [Faubel

et al. 1988]. From recent observations of the velocity distribution of desorbing water from the liquid surface are not consistent with the Maxwell-Boltzmann distribution at the supercooled temperature [Brastad & Nathanson, 2011].

The adsorption of atmospheric trace gases on the solid surface can often be well described by simple Langmuir or BET isotherms. In addition, the dissolution of the gas molecules in the bulk of solid or of primary liquid can be determined by a Henry's law solubility constant [Kolb et al. 2010]. In fact, the adsorption, desorption and the solubility of the gas molecules on the ice surface depend dramatically on the ice microstructure [Sadtchenko et al. 2000a] and [Bar-Nun & Owen, 1998] such as: an amorphous phase (Ia), crystalline cubic form (Ic) and hexagonal phase (Ih) [Hobbs, 1974] and [Eizenberg & Kauzmann, 1969]. Using temperature programmed desorption mass spectrometry, the measurements demonstrate that the HCl uptake molecules depend on the ice microstructure which depends dramatically on the preparation conditions of these experiments [Sadtchenko et al. 2000b].

On the other hand, the adsorptions of the trace gases on the surface of a liquid as well as the dissolution of these gases in the bulk of binary aqueous solution need significant assumptions in order to describe these processes. In the case of liquid surface, these processes depend on the physical properties of the liquid absorber such as viscosity, surface tension, density, etc.
In the case of the adsorption and the solubility of gas molecules in the aqueous solutions, the viscosity of the liquid might be important in order to determine the kinetics of the transfer of the molecule from the gas phase to the liquid phase at the interface gas- liquid as well as the decay time of the gas molecule in the bulk of liquid. The surface tension plays perhaps a significant role to determine the adsorption of the gas molecule onto the surface of the liquid and the desorption of water molecules from the surface. Indeed, the surface tension may influence the directions of the recoiling atoms from the liquid surface. The specular intensities change weakly for inert gas molecules scattering from the liquid metal surfaces which have the high surface tensions [Ronk et al. 1996].

As presented above, the sulphuric aerosols play an important role in the photochemical reactions in the atmosphere. The sulphuric aerosols in the mid-latitude stratosphere can be produced by subsequent oxidation of the sulphur dioxide to form the sulphuric acid solution [Deshler et al. 1992]. The aqueous solutions of the sulphuric acid are concentrated under very low temperatures in the stratospheric layer to obtain the supercooled and highly concentrated sulphuric acid solution [Bianco & Hynes, 2006]. The sulphuric acid content increases with increasing diameter of the aerosol [Baron & Willeke, 2001].

Several theories are represented in this thesis to describe the heterogeneous reactions as well as the desorption water from the liquid surface. One of these theories is the capillary wave theory. This theory attempts to describe the results of the accommodation coefficient and the unexpected measurements of the residence time of HCl gas in the whole range of concentrations of sulphuric acid solution. This theory may also explain the kinetics of the desorption of water from the liquid surface of the sulphuric acid solution at supercooled temperatures. Many studies [Knox & Phillips, 1998], [Phillips, 1997, 2000, 2001 b, 2004 a, b, 2005] and [Packwood & Phillips, 2009] described that the surface of the liquid is not planar but is an elastic membrane and the vibration of the surface molecules is similar to the wave motion. This motion is named capillary waves, which are produced in different wave lengths by the surface tension (restoring force).

The motivation of this thesis gives the best explanation in more depth to describe the unexpected experimental results which were measured by using the molecular beam scattering techniques. However, these experimental measurements consist of the velocity distribution of water molecules which are desorbing from solid surface and liquid surface of the sulphuric acid solution at supercooled temperatures. Furthermore, the mass accommodation coefficient of HCl onto the surface of the sulphuric acid solution as well as the residence time of HCl in the liquid bulk of the sulphuric acid solution at very low temperatures can be described quantitatively by using the calculations according to the capillary wave theory.

1. Experimental setup

1.1 Overview

This chapter describes the molecular beam machine. It is used to identify the effects between the gas molecules and the liquid molecules at the interface region. It can be analysed by the energy distribution, the density distribution of the desorbing molecules from the surface liquid and the residence time of the gas molecules in the liquid.

The molecular beam scattering apparatus consists of five different chambers:

1- Molecular beam source chamber which creates the molecular beams.
2- Source differential chamber, where the effusive flux entering the scattering chamber is reduced.
3- Scattering chamber, where the liquid reservoir is located in its centre.
4- Detector- differential chamber that decreases the background signal entering to the detector chamber
5- Detector chamber, which consists of the quadruple mass spectrometer.

The details of each chamber will be described later. Fig (1.1) is schematic of the scattering apparatus.

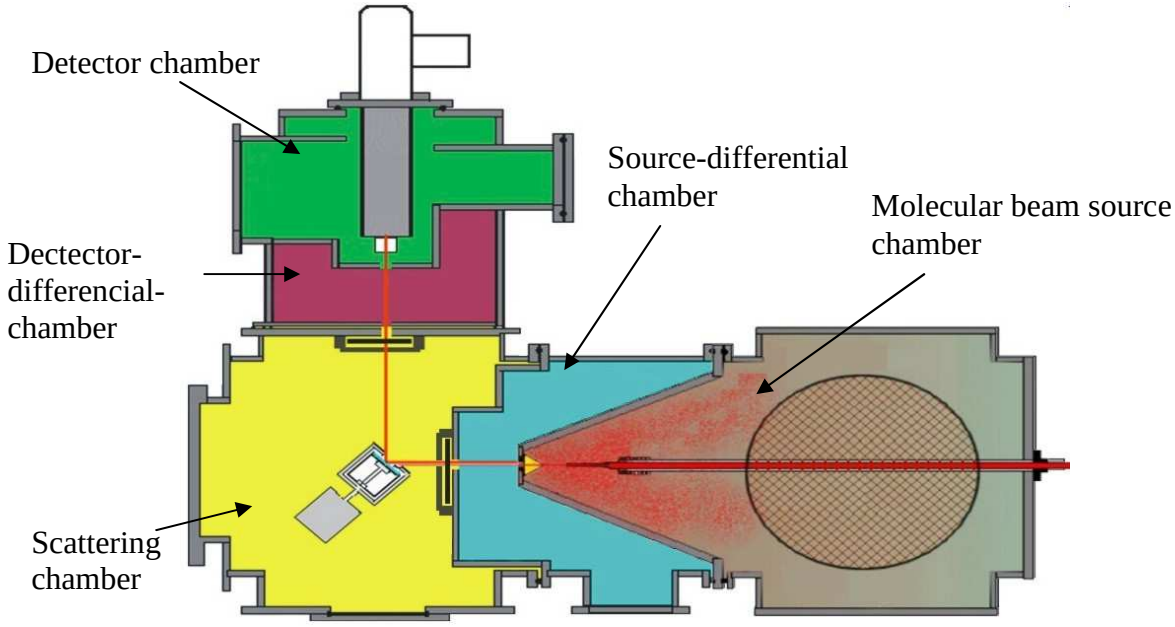

Figure (1.1) Molecular beam apparatus

Molecular beams are formed in the molecular beam source chamber by adiabatic expansion. After expansion, only one of them is passing throw the skimmer, source differential chamber to the scattering chamber. In the scattering chamber, this beam strikes the surface of a liquid film, which is produced by rotating a glass wheel through the liquid in a reservoir. The beam scatters from the surface into the vacuum. The exiting scattering beam is monitored by using a mass spectrometer in the detector chamber. The mass spectrometer detects the intensity of desorbing molecules versus time of flight between it and the chopper wheel. In the scattering chamber two different choppers are found either before the liquid reservoir (pre-chopper) or after it (post- chopper). The kinetic energy is measured by chopping the exiting molecules into short pulses with the post chopper wheel. The residence time of molecules in a solution is also measured by using the pre chopper wheel.
The scattering machine is controlled by the flux and pressure sensors in order to protect it from the damage. If any problem occurs, it switches off automatically, such as a low vacuum of ~ 10 mbar in the source beam chamber or in the case of emergency electricity blackout.

1.2 Molecular beam chamber

Molecular beams are formed in this chamber by pressurizing a nozzle consisting of a 5 mm diameter glass tube that is sealed at one end with 100 µm diameter aperture. Two steel collars, each one consists of four screws, which are used to secure the nozzle in the stainless steel cylindrical holder and a heater at the end of this holder. The distance is set at 6 cm. The flux of entering the source differential chamber can be reduced by increasing the nozzle- skimmer distance. The glass nozzle is needed to limit the corrosion and contamination inside it. The pressure of the gas is between 2- 5 bar inside the nozzle and it is 3. 10^{-3} mbar in this chamber, due to the molecular beams that are produced by adiabatic expansion. We have used lower pressures for beams 2% of HCl in H_2 while higher pressures have been used for pure HCl. The nozzle can be heated from 26℃-140℃ by copper wir e (Lack draht CUL 200, 1,0 mm O.D., 20 m long, resistance of 2,6 Ohms) to increase the kinetic energy of the

exiting molecules from the aperture and to reduce the concentration of dimers. The temperature is measured and controlled by the bang- bang controller (GIR 2000 PT).

The following figure (Fig 1.2) shows the molecular beam source chamber:

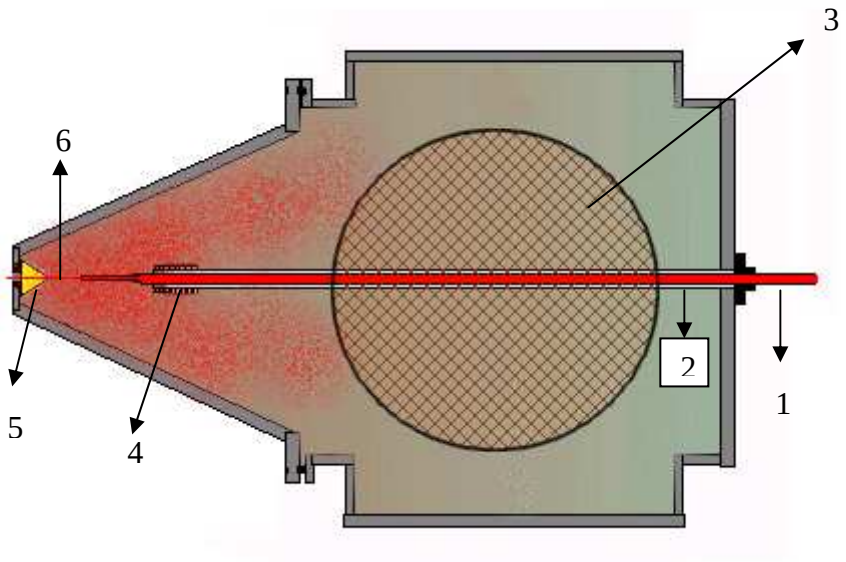

Figure (1.2) Scheme of the molecular beam chamber: 1. glass nozzle, 2. stainless steel holder, 3. diffusion oil pump, 4. heater, 5. skimmer, 6. molecular beam

The skimmer is made from gold to prevent corrosion and contamination, which are formed by using the molecular beam from aggressive gases. This contamination does not allow the molecular beam to pass through the skimmer vent (diameter of 1 mm) parallel from the molecular beam chamber to the source- differential chamber. The skimming of the molecular beam is used to reduce the pressure in other chambers and to block the molecules, which have non mono kinetic energy. Other gas molecules, that are not passing through the skimmer must be pumped out from this chamber by using a diffusion oil pump (Pfeiffer 6000) with pumping speed of 4000 $l.s^{-1}$. If corrosive gas is used in this experiment, a liquid nitrogen trap is needed to condense it and to block it to reach the pre- pumps system. Figure (1.3) shows the diffusion oil pump and pre-pumps system.

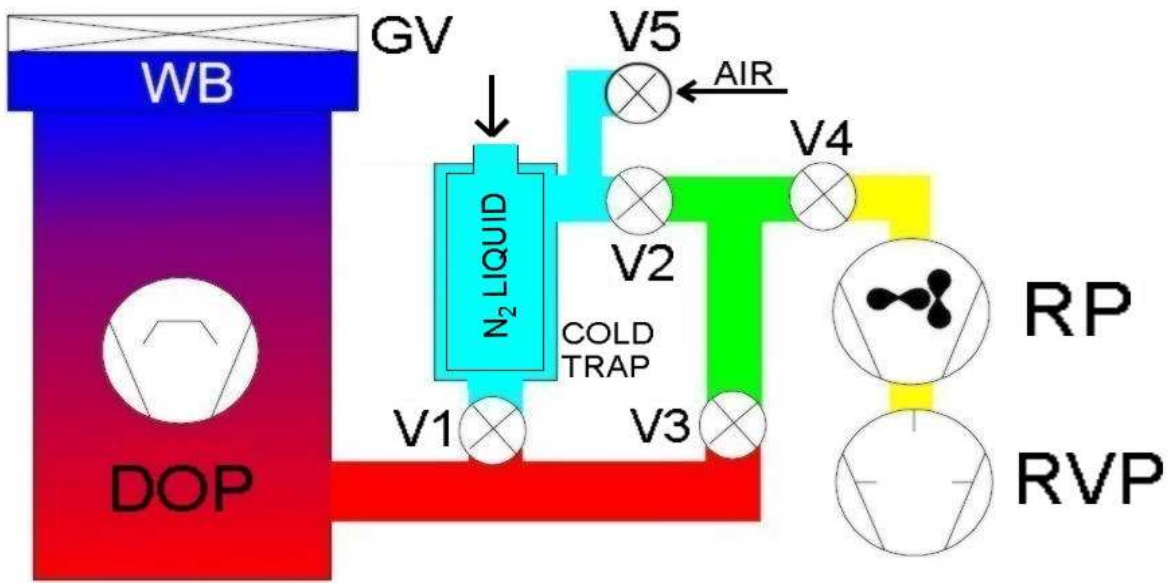

Figure (1.3) Diffusion oil pump, pre-pumps and valves system

The oil diffusion pump, roots pump and rotary vane pump are connected respectively. The pressure between the diffusion pump and the pre- pumps are measured by the pressure sensor (Active Pirani Transmitter Pfeiffer 1000- 1.10^{-4} mbar). When the rotary vane pump is switched on, the pressure is reduced to about 5 mbar if both pre- pumps are turned on, this pressure is reduced to 2.10^{-2} mbar. The liquid nitrogen cooling trap is connected between diffusion oil pump and the pre-pumps system in order to protect the pre- pumps system from the corrosive gases. The pre- pumps are filled with special oil (Androl 555). This oil resists the aggressive gases such as HCl and HBr. The oil diffusion pump and the baffle on the top of this pump are cooled by a water line. The temperature in this pump is controlled by thermo- sensor. The chamber is saved from the trace of oil by this cooling system. Figure (1.3) will define the work of this vacuum system in two cases:

1- Rare gas such as Argon.
2- Aggressive or corrosive gases such as HCl or HBr.

In the first case, the cooling trap is separated. That means valves (V1) and (V2) are closed. The valves (V3) and (V4) are opened. In this case the gas pumped away from the chamber direct to pre-pumps system without passing the cooling trap.

In the second case, the cooling trap is necessary to save the pre- pumps system from the damage of aggressive gases. The valves (V1), (V2) and (V4) are open. The valve (V3) and vent- valve are closed. In this way the gas is pumped out from the chamber and is passing throw the cooling trap. The corrosive gas condenses on the inside surface of the double jacket of cooling trap. This trap is cooled by the liquid nitrogen to reach the condensation temperature of HCl gas. Thus the pre- pumps system is saved from the damage of aggressive gases. After the experiment is completed, the valves (V1) and (V2) are closed since the valve (V3) has been opened. After that the vent valve is opened to sublimate the corrosive gas and let them escape form the cooling trap.

1.3 Source differential chamber

This chamber is located behind the source main chamber and is used to reduce the effusive flux of the molecular beam to the next chamber (scattering chamber). The molecular beam, which is passing from the hole of the skimmer to the blend (1), must be parallel to flow out from blend (1) (diameter 2 mm) to the scattering chamber. The distance is about 10 cm between the skimmer and blend (1). The molecules, which are not passing throw blend (1), must be pumped away from this chamber to keep the pressure at about 10^{-4}- 10^{-5} mbar. Therefore the turbo- molecular pump Leybold vacuum (TMP 600 C) with pumping speed of 650 $dm^3.s^{-1}$ as well as the pre- pump Leybold TRIVAC (D65 B CS) with pumping speed of 65 $m^3.h^{-1}$ were used. In this chamber we use only one turbo- molecular pump which is enough in the experiment, because the pumping speed of this pump is satisfactory to reach this vacuum.
This blend (1) is closed in the water evaporation experiment because the nozzle is not required in this experiment. Thus the scattering chamber is separated from the two previous chambers which are described above. In figure (1.4) is schematic diagram of the source differential chamber.

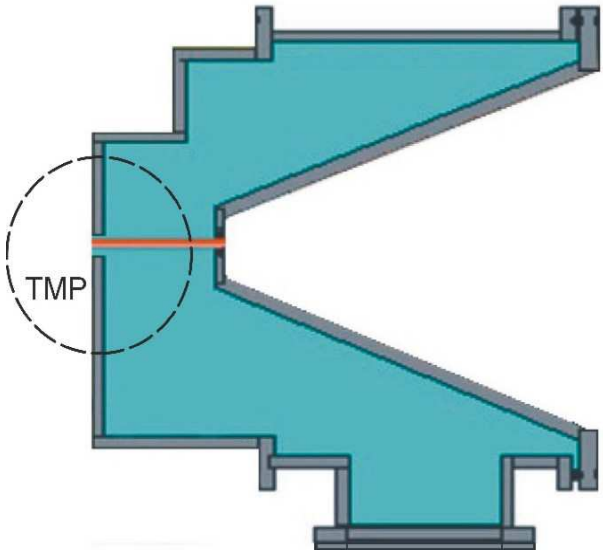

Figure (1.4) Scheme of source differential chamber

1.4 Scattering chamber

The second main chamber in this apparatus is the scattering chamber. The effects or reactions between gas molecules and liquid molecules whether on the surface or in the bulk of liquid occurs in this chamber. This chamber consists of:

1- pre- chopper, 2- liquid reservoir, 3- post- chopper

After the molecular beam was exiting from the blend (1). It passes through the slot of pre- chopper which is located directly in front of the blend (1). Then this beam strikes the surface of the liquid, which was formed on the surface of wheel in the liquid reservoir, at incident angle and final angle are equal to 45°. The molecules of this beam are scattering in different directions from the liquid surface in this chamber. One trajection of scattering molecules is passing through the slot of the post-chopper. After that the scattering molecules are leaving this chamber through blend (2), which exists directly behind of the post- chopper. Figure (1.5) shows, how the molecular beam is entering and leaving the scattering chamber.

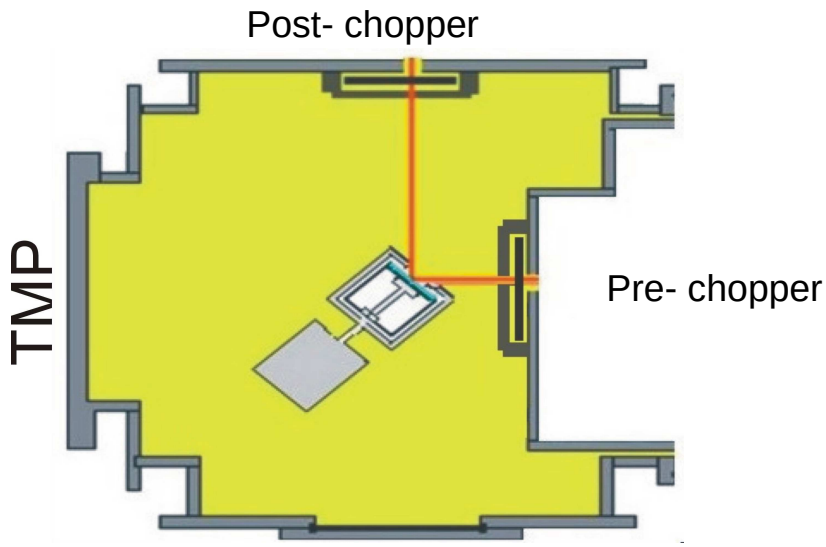

Figure (1.5) Schematic of a scattering chamber with the locations of pre- chopper, liquid reservoir and post- chopper, respectively.

1.4.1 Pre- chopper

The time of flight spectra for a modulated molecular beam (before the liquid reservoir) can be recorded in this experiment by using the pre- chopper. The pre-chopper is a metallic disk with two slots (diameter 2 mm), which were cut out of the end of the disk on opposite sides. The distance between the pre- chopper and the surface of the wheel in liquid reservoir is 7 cm. The pulses of molecular beam can be formed by the rotation of the disk. The rotation frequency of the pre- chopper, which can be controlled out side the scattering chamber and varied between 150 Hz and 230 Hz, determines the width of pulses. In our work, the rotation frequency is 150 Hz and it creates 70 µs parcels of the gas.

1.4.2 Liquid reservoir

The position of liquid reservoir is at the centre inside the scattering chamber. The liquid reservoir consists from outside to inside: metal reservoir, teflon reservoir and the glass wheel. A continuously renewed film of sulphuric acid solution is produced by rotating a 4.5 cm diameter glass wheel throw 15 ml of deuterated sulphuric acid solution in the teflon reservoir at temperature T_{liq} 213, 218 and 228K. The metal reservoir is made from Titanium because this metal is: corrosion- resistant and

lightweight. The teflon reservoir has a resistance from the acidity of sulphuric acid and serves as an isolator from the liquid evaporation in the vacuum chamber. The gold plated wheel was used in this experiment because the reflection of laser from the gold surface is better than the glass wheel to draw the trajectory of the reservoir [Behr et al. 2009 a]. The gold wheel is not used anymore because the protective coating form gold is not fixable on the surface of wheel and it is more expensive than the glass one. The problem of the clearly reflection is solved by using a glass wheel, which is in the front of the surface of this wheel is slick and the behind surface is rigid. This glass wheel is fixed with the teflon axis by using three screws. This axis is attached tightly with the motor axis behind the liquid reservoir. The motor frequency will be changed from 5 – 35 Hz and translating that into glass wheel speeds. As the wheel rotates, the liquid film is exposed to the molecular beam through a 11mm x 3 mm rectangular opening in the front of the liquid reservoir. The beam interaction time with the liquid surface (t_{exp}) can be calculated using this following equation:

$$t_{\exp} = \frac{d}{2\pi rf} \qquad \text{Equation (1.4.1)}$$

d: is the diameter of the beam spot. r: is the distance from the centre of the wheel to the centre of beam. f: is the wheel frequency.

The exposure time is listed in the table (1.1)

Frequency of the motor (Hz)	Exposure time (s)
5	0,93
10	0,50
15	0,32
20	0,24
25	0,19
30	0,16
35	0,14

The sulphuric acid solution is cooled by using the cooling coil, which is isolated by the coating teflon that is fixed tightly on the surface of the cooler. This coating Teflon is very necessary to protect the cooling coil from the corrosion by the sulphuric acid. This cooler is used to keep the temperature constant in the solution in order to reduce the vapour pressure of water in the scattering chamber. A manipulator is connected through the moveable piece, which allows the liquid reservoir to move forward and backward from the centre of the rotation axis of the manipulator, to the top of this liquid reservoir. The desorbing molecules from the liquid surface are better measured by using the moveable piece in different spectral angles. This will be discussed in section (3.1.2). Figure (1.6) shows the schematic of the liquid reservoir with the move piece and the cooling tubs.

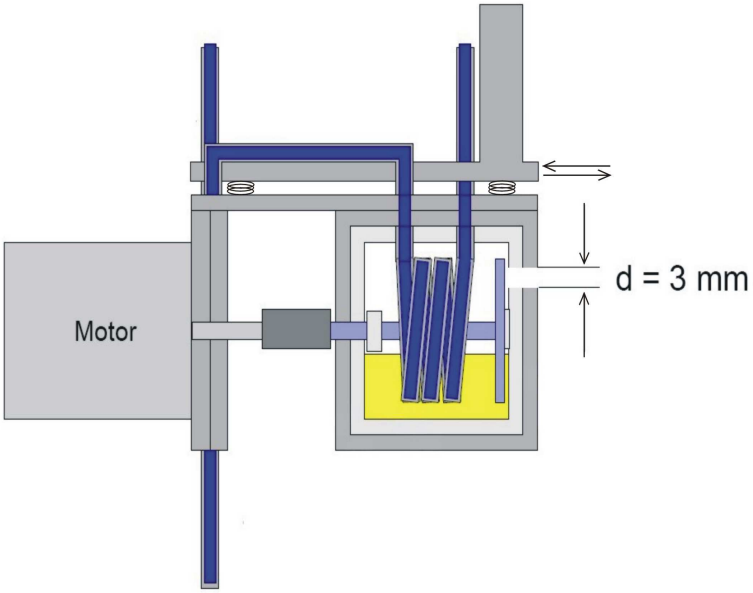

Figure (1.6) Moveable liquid reservoir

1.4.3 Post- chopper

The post- chopper is a wheel with two slots (diameter 4 mm), which are drilled out at the edge of it in the opposite side. The centre of it is fixed tightly with the motor axis by three screws. Gas pulses of 50 µs are produced by using a motor frequency of 200 Hz. This chopper is placed after the surface of the liquid wheel at the distance 13 cm and directly before the blend (2) (diameter 4 mm). The energy distribution of the desorbing molecules from the surface of the liquid can be determined by chopping the continuous molecular beams after their striking the liquid surface.

1.5 Detector- differential chamber

The number of evaporation molecules from the liquid surface is very high. It must be reduced by installing the detector- differential chamber, in order to decrease the back- ground signal. The molecular beam is passing through this chamber from blend (2) (diameter 4 mm) to the blend (3) (diameter 5 mm). The pressure in this chamber is about 10^{-7}- 10^{-8} mbar, thus it is equipped with a turbo molecular pump (TMU521P Pfeiffer) and a pre- pump (DUO 016 B, Pfeiffer) with pumping speed of 521 $l.s^{-1}$ and 16 $m^3.h^{-1}$, respectively. Figure (1.7) shows the molecular beam in this chamber as well as the location of the turbo molecular pump.

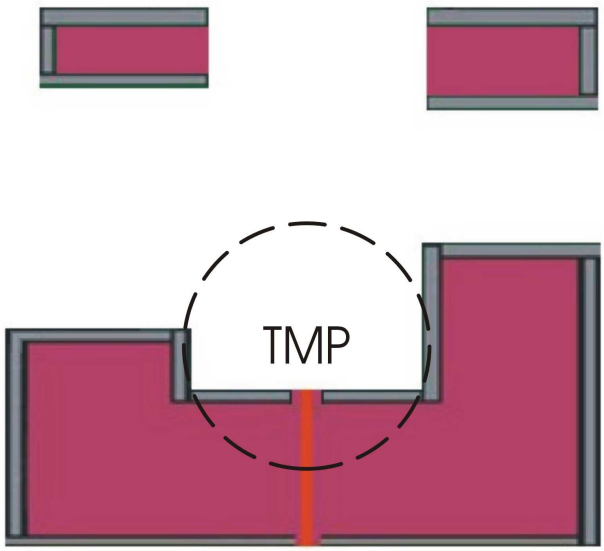

Figure (1.7) Schematic of the detector differential chamber

1.6 Detector chamber

The third main chamber in this apparatus is the detector chamber. The molecular beam enters this chamber from blend (3) (diameter 5 mm) to the ionization field of the mass spectrometer. The pressure in this chamber is about 10^{-8}- 10^{-9} mbar by

using the turbo molecular pump (Pfeiffer TMU 521P) with pumping velocity (520 $l.s^{-1}$) and pre- pump without oil (Varian Triscroll 300) with pumping speed (210 $l.s^{-1}$). A schematic diagram of the detector chamber is shown in Figure (1.8).

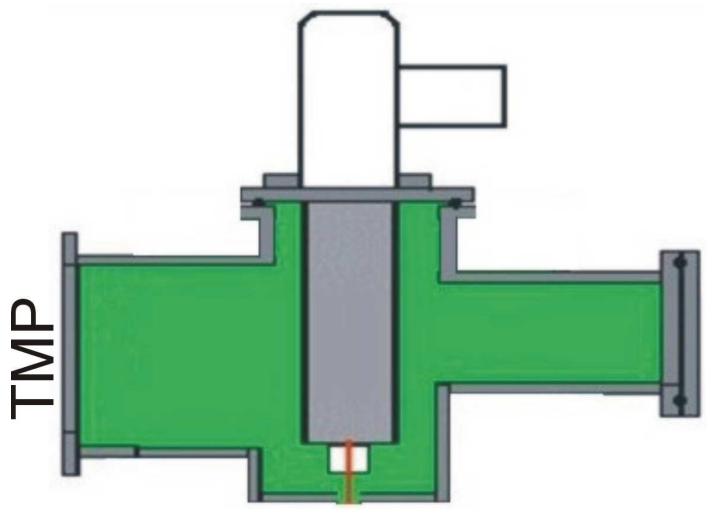

Figure (1.8) Schematic diagram of detector chamber and molecular beam as a red line

The quadrupole mass spectrometer (Pfeiffer QMG 422) is the detector and is used to monitor the densities and arrival times of the particles, which are scattering and desorbing from the liquid film. The QMS consists of three components:

1- Ionizer, where the molecules and atoms are ionized and focused into the quadrupole rods.
2- Quadrupole rods, which select the ions with a specific mass- to- charge ratio (m/z); m: is their mass and z: is their electric charge.
3- SEV (secondary electron amplifier), which improves the resolution of the signal.

The molecules are ionized to positive ions in the ionization field with different masses. The positive ions are filtered to one selected mass- to- charge by passing parallel through the quadrupole rods. They are accelerated to the ion- electron conversion plate and striking it to produce secondary electrons, which are amplified by a series of metallic dynodes. Besides, these secondary electrons are converted then into an electron pulse. The output current of the SEV is then the number of

density of scattering or desorbing molecules at the selected (m/z) as a function of arrival time (µs). The schematic view of this system is shown in figure (1.9).

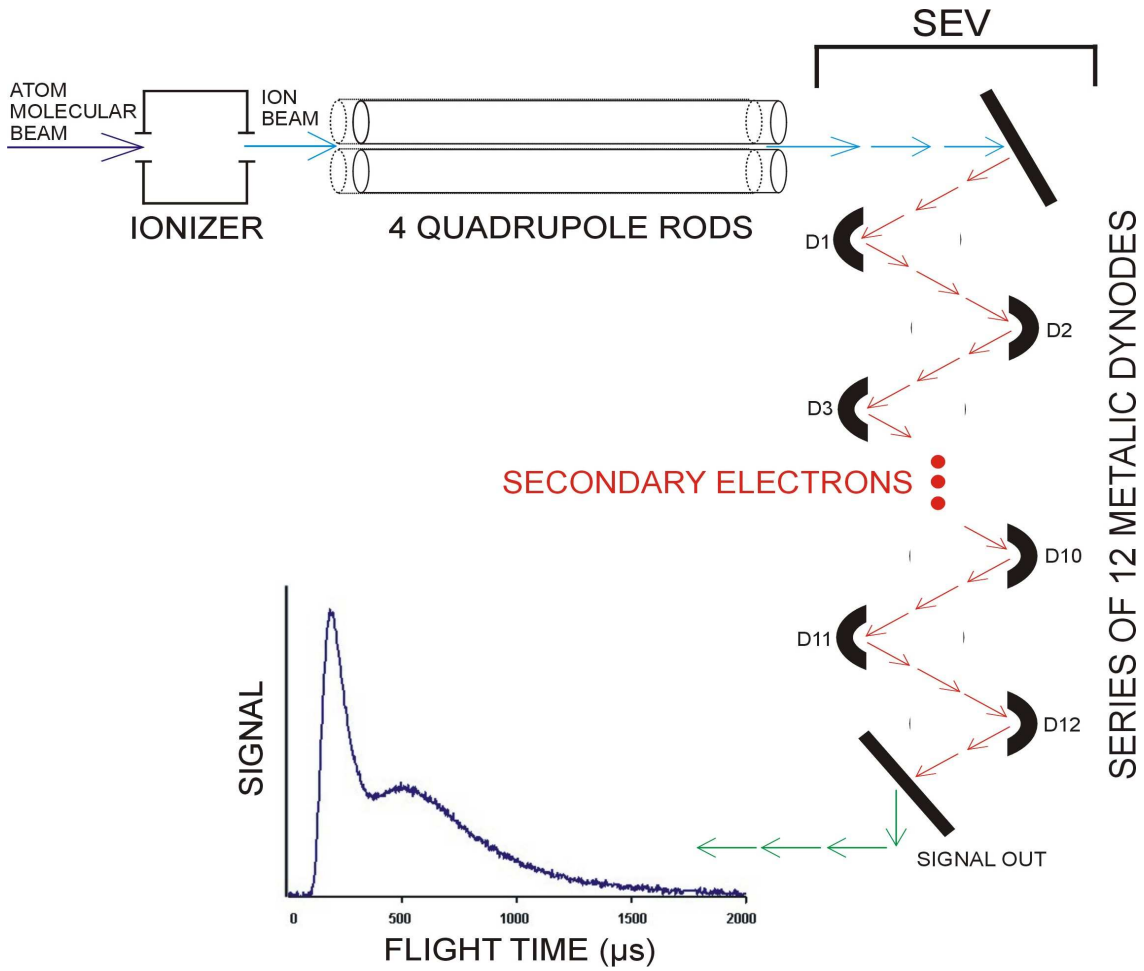

Figure (1.9) Schematic view of the QMS and SEV

1.7 Chemicals

The gas tanks which are used in this work are as following:

1- Argon pure (Air Liquid 4.6), the packing pressure inside the nozzle is 6 bar, the incident energy is 6 $kJ.mol^{-1}$.

2- Hydrogen chloride (Air Liquid 4.6), the packing pressure inside the nozzle is 6 bar, the incident energy is 6 $kJ.mol^{-1}$.

3- Hydrogen chloride (Air Liquid 2,8) 2% mixed with H_2 (Air Liquid 3.0) 98% , the packing pressure inside the nozzle is 2 bar, the incident energy is 140 kJ.mol^{-1}.

The solution of D_2SO_4 / D_2O is produced, as follows:

10 ml D_2SO_4 (99,9 wt% D_2SO_4 98,9 atom %D Aldrich) was diluted with 15 ml of deuterium oxide (Deuterium oxide 99,9 atom %D) in the ice bath in order to reduce the evaporation of deuterium oxide by dilution and to keep the concentration of this solution constant. We prepared the deuterated sulphuric acid solution in concentration of 52 wt%. This solution was poured in the Teflon reservoir by using a glass syringe (Poulet and Graf GmbH). Before the scattering apparatus set up, the sulphuric acid solution is concentrated by the evaporation of D_2O through the high vacuum in the scattering chamber.

The titration method of the sulphuric acid solution:

The sulphuric acid solution is titrated by using sodium hydroxide (1 mol.l^{-1} Waldeck) and indicator phenolphthalein. 1 ml of the solution is weighted to determine its density (d_{D2SO4}), diluted with distillated water and poured two or three droplet from the indicator. Then it is titrated with NaOH (V_{NaOH}). The concentration in weight per cent is calculated by the equation as following:

$$D_2SO_4 wt\% = \frac{100{,}09 \cdot V_{NaOH}}{20 \cdot d_{D2SO4}} \qquad \text{Equation (1.7.1)}$$

2. Data evaluation and analysis

2.1 Determination the incident beam energy

The translation energy of the molecular beam which occurs before striking the surface of the liquid, can be measured when the angle between the source chamber and the detector chamber is 180°. That means, the m olecular beam flows in straight line from the aperture of the nozzle to the ionization field of the mass spectrometer. The liquid reservoir must be removed from the scattering chamber. One chopper is used to produce the gas pulses. Figure (2.1) shows this setup.

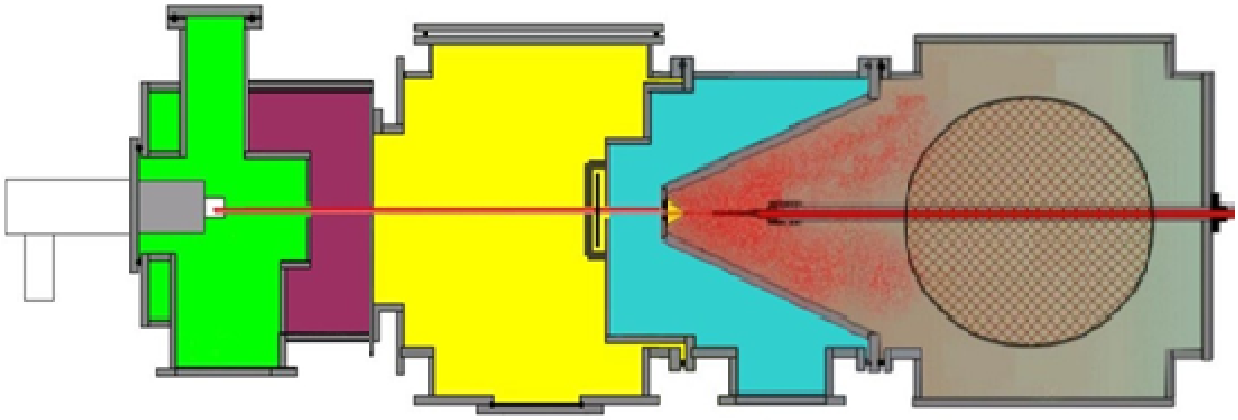

Figure (2.1) The linear experiment setup

This method is necessary to determine the incident energy of each gas, which will be used later in the scattering technique. The mass spectrometer measures the density number of gas N(t) as a function of flight time, as shown in figure (2.2).

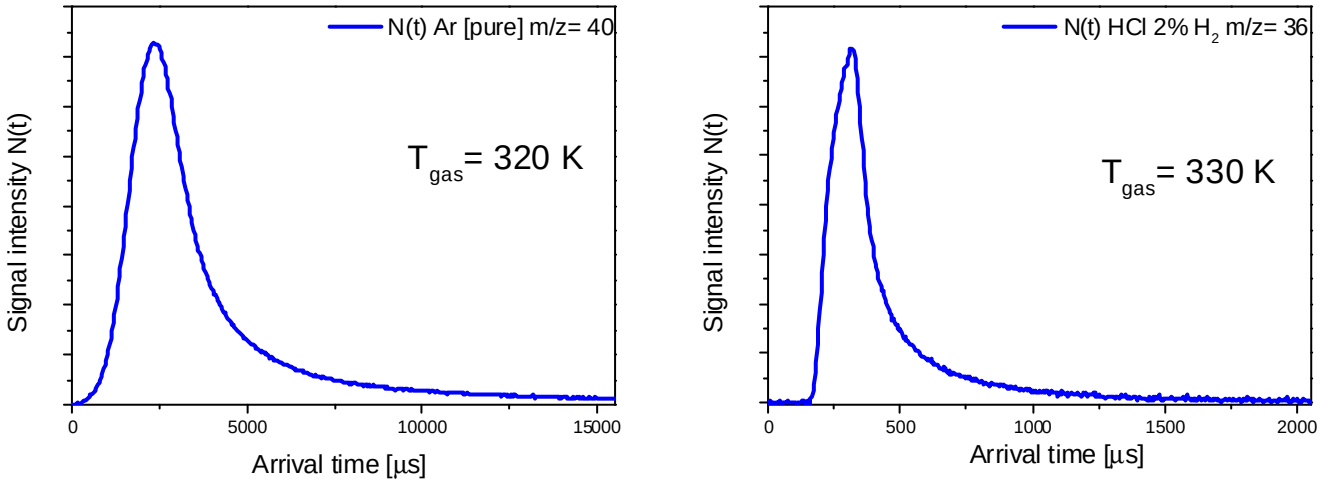

Figure (2.2) The density number of gases versus TOF for Ar and 2% HCl in H_2

The relative flux or the probability $P(E_{inc})$ depends on the density number N(t) and is calculated by equation:

$$P(E_{inc}) \propto N(t) \cdot t^2 \qquad \text{Equation (2.1.1)}$$

The incident energy E_{inc} is:

$$E_{inc} = \frac{1}{2} m_g \cdot \left(\frac{L}{t}\right)^2 \qquad \text{Equation (2.1.2)}$$

m_g: is the mass of the gas

L : is the flight pass for the pulses of molecules (49 cm)

t : is the arrival time of pulse

Thus the incident energy can be computed from the relation between $P(E_{inc})$ and the energy (kJ) and extracted from the diagrams in figure (2.3).

The incident energy of the 2% of HCl in H_2 is: E_{inc}= 140 kJ.mol^{-1}

The incident energy of pure Ar and pure HCl are: E_{inc}= 6 kJ.mol^{-1}

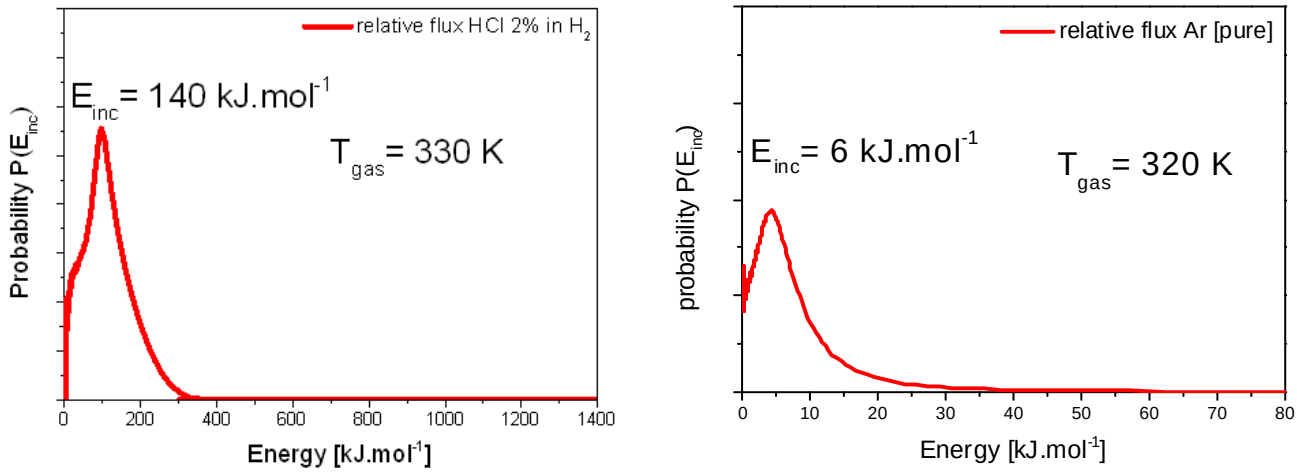

Figure (2.3) The relative flux versus energy for Ar and HCl 2% in H_2

2.2 TOF post- chopper arrangement

The energy distribution of the scattering and desorbing particles is detected by using the post- chopper spectra, which are plotted as the number density N (t) versus arrival time. The start time of post- chopper spectra is after the molecules scatter or desorb from the liquid surface. The arrival time of post- chopper accounts for the flight of time of scattering and desorbing particles at the distance before the ionizer of mass spectrometer about 27 cm. the location of post- chopper is shown in figure (2.4). The arrival time using post- chopper continuous molecular beam is:

$$t_{arrival}(post) = \frac{d_{post}}{v_{fin}} \qquad \text{Equation (2.2.1)}$$

d_{post}= 27 cm v_{fin} : the velocity of molecules after scattering or desorption from liquid

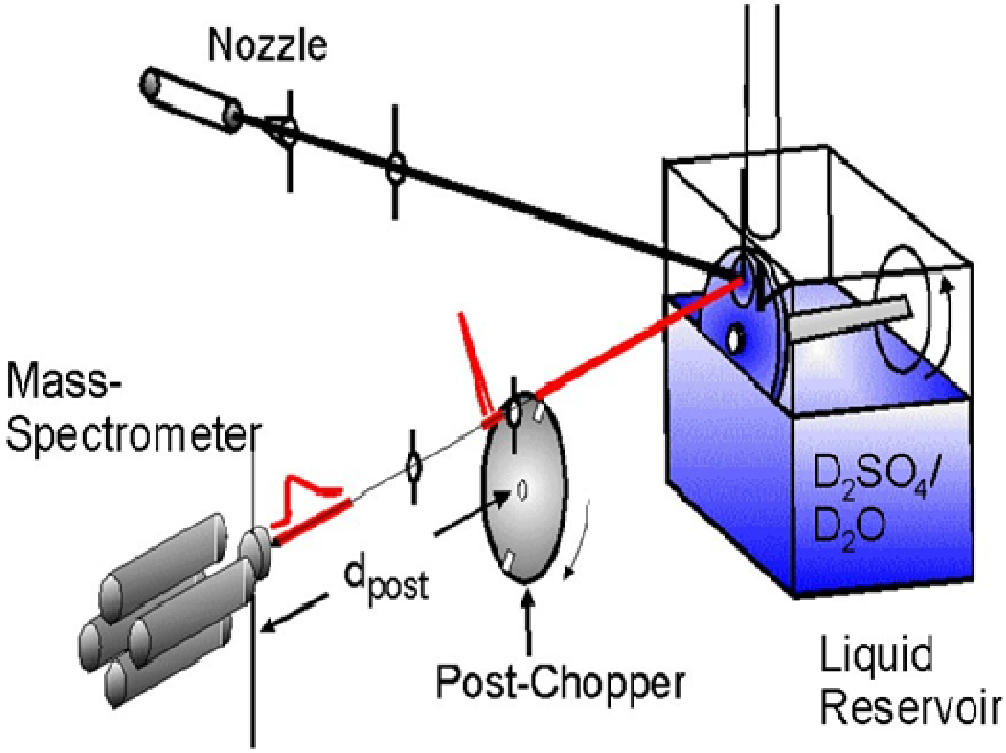

Figure (2.4) Schematic view of the location of post- chopper in the scattering technique

The true arrival time is a result from the correction of observed arrival time with experimental offset. These offsets are: the electronic offset, forward and backward offset and the ion flight time offset.

2.2.1 The electronic offset

This offset corrects the time delay between the amount of time, which the pulse takes to travel from the post- chopper to the ionization field of mass spectrometer, and the time needed for the wheel slot to rotate fully in front of the blend (3) behind the post-chopper. This time is the half of the pulse width: $t_{eo} = 20\,\mu s$.

2.2.2 Forward and backward time offset

This time offset can be measured by taking half of the difference between the peak arrival times for clockwise and counter clockwise wheel rotation

$$t_{FBO} = \left(\frac{t_{FO} - t_{BO}}{2} \right)$$ Equation (2.2.2)

2.2.3 The ion flight time offset

This offset depends on the mass spectrometer, which is used in the experiment. The ion takes a time to travel through the quadrupole rods to the ion detector (or exactly to the ion- electron conversation plate).

$$t_{ion-flight} = \alpha \cdot \sqrt{m_{ion}}$$ Equation (2.2.3)

α: this value in our work is “5”.

m_{ion}: the mass of ion.

The true arrival time for post- chopper TOF is then given by:

$$t_{true}^{post} = t_{observed} - t_{eo}^{post} \mp t_{FBO}^{post} - (\alpha \cdot \sqrt{m_{ion}})$$ Equation (2.2.4)

Figure (2.5) shows a timing pulse train and TOF spectrum of post- chopper.

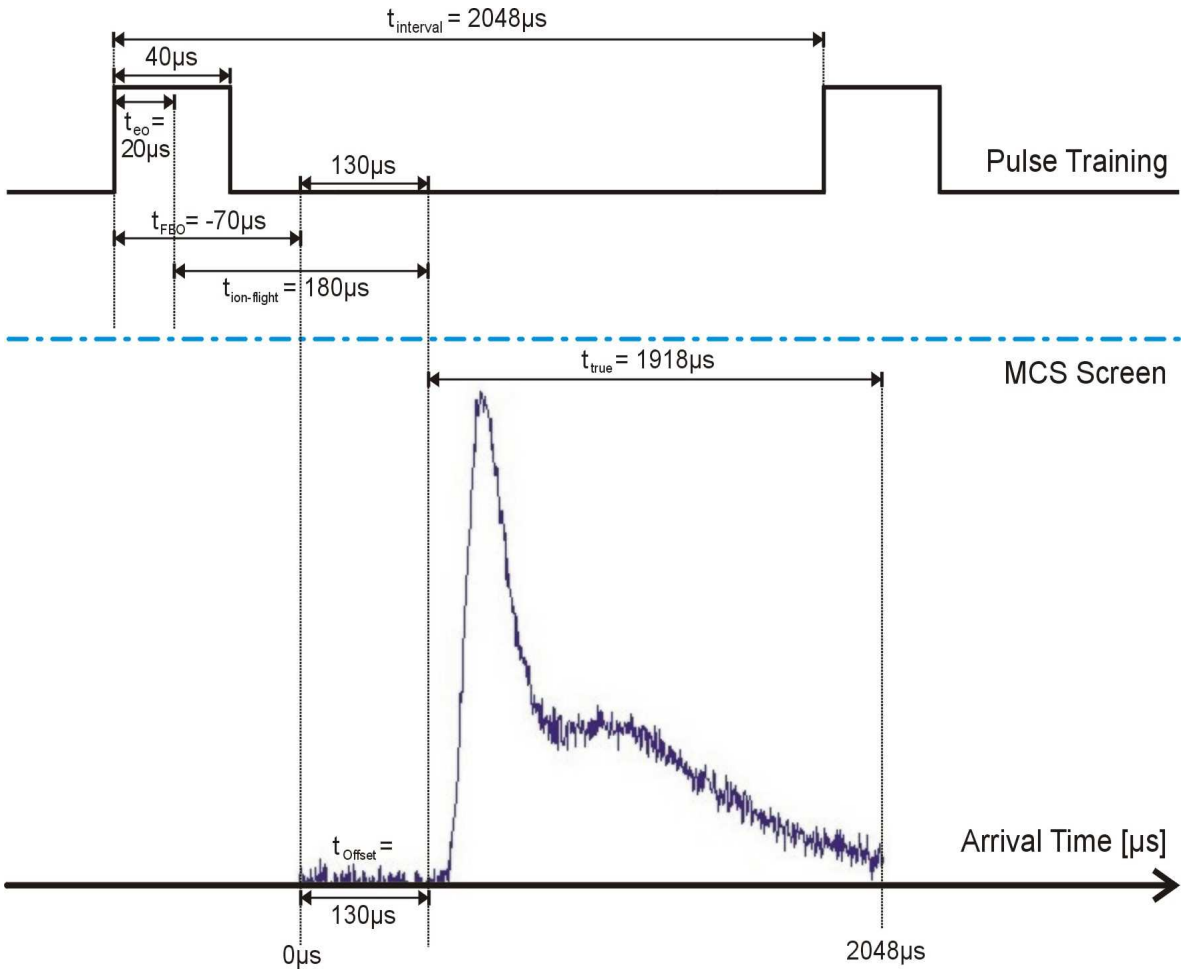

Figure (2.5) Timing diagram for a post- chopper wheel speed of 200 Hz

2.3 TOF pre- chopper arrangement

The TOF spectra of the pre- chopper are plotted as the number density N(t) versus arrival time the time which is needed for the molecules to dissolve and desorb from the liquid. The start time of the pre- chopper is before the molecules strike the liquid surface. Figure (2.6) shows the location of pre- chopper and the distance between pre- chopper and ionizer of the mass spectrometer. The arrival time using the pre-chopper modulated molecular beam is:

$$t_{arrival}(pre) = \frac{d_{inc}}{v_{inc}} + \tau + \frac{d_{pre}}{v_{fin}}$$ Equation (2.3.1)

where:

d_{inc}: is the distance from the pre- chopper to the liquid surface (12 cm)

d_{pre}: is the distance from the liquid surface to the ionizer of mass spectrometer (36 cm)

v_{inc}: is the velocity of the molecular beam before striking the surface. This velocity can be calculated from the translation energy (that is described previous in section 2.1).

τ : is the residence time that the molecules spend in contact with the liquid before desorbing. It will be described later.

v_{fin}: is the velocity of molecules after striking or desorbing from the liquid surface.

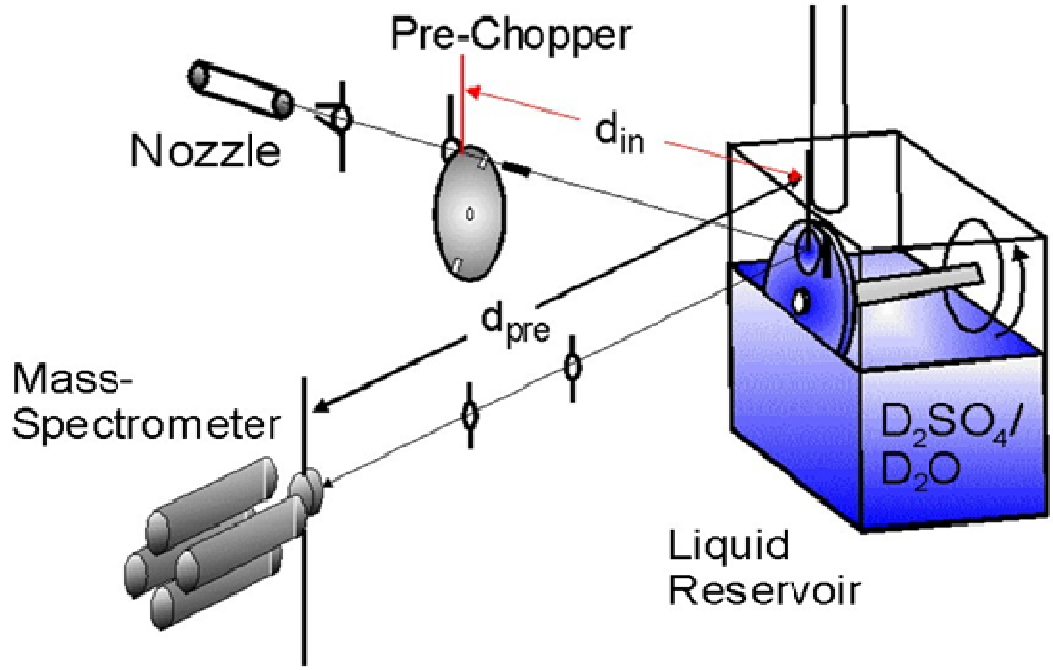

Figure (2.6) Scheme of the pre- chopper and the distance

The pre- chopper spectrum has a wrap- around effect, which is formed through the overlapping of the previous spectrum with the next spectrum.

The wrap- around of pre- chopper spectrum is larger than the one of the post-chopper because the arrival time accounts for the flight time and the gas residence time in the solution. The true arrival time for the pre- chopper time of flight is given by:

$$t_{true}^{pre} = t_{observed} - t_{eo}^{pre} \mp t_{FBO}^{pre} - (\alpha \cdot \sqrt{m_{ion}}) - \frac{d_{inc}}{v_{inc}}$$ Equation (2.3.2)

t_{FBO}^{pre} = 800 µs (the forward / backward offset for the pre chopper is larger than that by post- chopper and is t_{eo}^{pre} = 30 µs.

2.4 Extraction of the residence time from TOF spectra

The residence time of the molecules in the bulk liquid can be revealed from the comparison between both pre- and post- chopper spectra. The time of flight spectra of post- and pre- chopper have two components, namely inelastic scattering and thermal desorption. The inelastic scattering molecules arrive earlier at the ionization field of mass spectrometer, because they have a high energy. Thermal desorbing molecules reach to the ionizer of the mass spectrometer later, because they dissipate their energy at the surface of liquid before desorbing from it. These two components can be found separated for the molecular beam, which has high incident energy. But for the molecular beam, which has low incident energy, is very difficult to recognize these two components.

The residence time can be extracted by comparing pre- and post- chopper spectra. Both spectra must be corrected before the comparison using two steps.

First, the post- chopper path length (2048 µs) is shorter than the pre- chopper flight bath (3072 µs). The arrival times in the pre- chopper spectrum must be decreased by multiplying the ratio of flight path distances, as in equation:

$$t_{currect}^{pre} = t_{true}^{pre}\left(\frac{d_{post-ionizer}}{d_{liquid-ionizer}}\right)$$ Equation (2.3.3)

Second, the arrival time for both spectra must be also corrected by using the time offsets for pre- and post- chopper, as they have been outlined above.

In the case for the high incident energy of the molecular beam can be easier compared through the overlapping the inelastic scattering peaks of pre- and post-

chopper spectra, because the residence time for the inelastically scattered molecules is equal to zero. In contrast, the molecular beam with low incident energy has not a separated inelastic scattering component. In this case, it is difficult to determine the exact offsets in the arrival time between both spectra. But this problem can be vanished by using a rare gas, which has identical incident energy. The differences in arrival times and intensities between pre- and post- chopper spectra of this gas disappear. That means that the curve of the pre- chopper spectra is aligned with one of the post- chopper spectra.

After achieving these two steps for the studying gases, any remaining differences in arrival times and intensities of thermal desorbing molecules in the pre- and post-chopper spectra are owing to the residence times of molecules in contact with the liquid. Figure (2.7) shows the difference between pre- and post- chopper time of flight spectra.

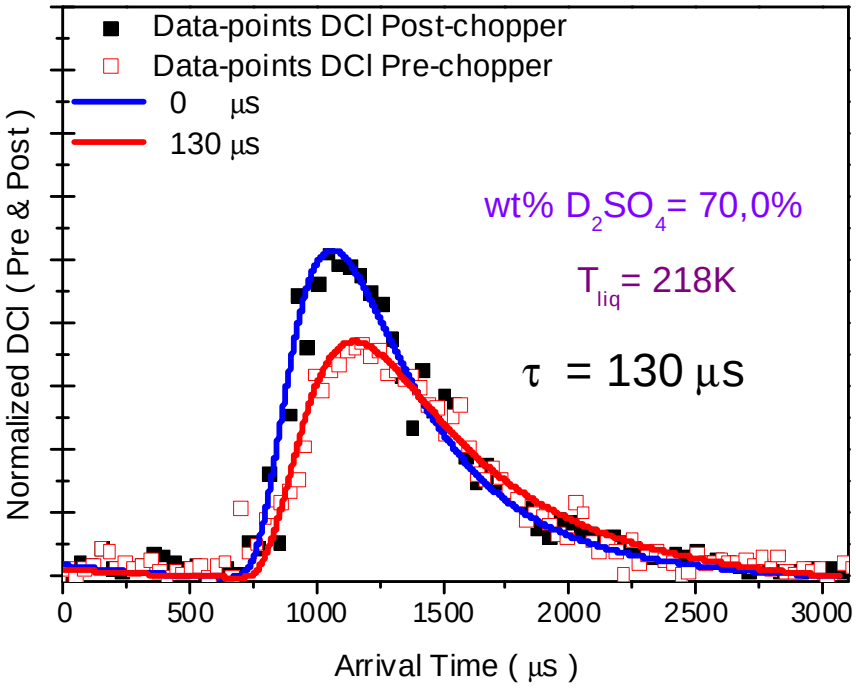

Figure (2.7) Pre- and post- chopper spectra for HCl E_{inc}= 6 kJ.mol^{-1}

2.5 Calculation of the residence time

When the gas molecules come onto the surface of the liquid, a fraction of them will trap at the liquid surface, diffuse in the bulk and solvate in the bulk before they

desorb from the surface. That means that the gas molecules spend some time on the liquid surface and in the bulk before they desorb from it. This delay in time is defined as a residence time τ. The residence time can be obtained by the equalization between the net uptake gas flux into the liquid and the diffusive flux on the liquid side. The net uptake gas flux into liquid is calculated by using Flick's first law in one dimension (x). This is measured in an inward direction along the normal to the surface.

The net uptake gas flux is extracted from the difference between two fluxes F_{in} and F_{des} (t):

$$F_{net} = F_{in} - F_{des}(t) \qquad \text{Equation (2.5.1)}$$

F_{in} : is the flux gas entering the liquid, which is defined as:

$$F_{in} = \alpha_{th} \cdot F_{hit} \qquad \text{Equation (2.5.2)}$$

F_{hit} : is the flux of the solute molecules coming on the liquid surface defined as:

$$F_{hit} = \frac{n_g \cdot \bar{v}}{4} \qquad \text{Equation (2.5.3)}$$

n_g : is the number of gas molecules in the gas bulk.

This flux will be rewritten by applying Henry's law as:

$$F_{hit} = \frac{c_l^{\circ} \cdot \bar{v}}{4HRT} \qquad \text{Equation (2.5.4)}$$

α_{th} : is the thermal accommodation coefficient

$$\alpha_{th} = \frac{N_{enter}}{N_{TD}} \qquad \text{Equation (2.5.5)}$$

N_{enter} : is the number of molecules that enter the liquid

N_{TD} : is the number of molecules that strike the liquid from thermal desorption

$\bar{v}$: is the average velocity of the gas molecules (= incident and exiting gas molecules)

Then the incident flux is:

$$F_{in} = \frac{c_l^{\circ} \cdot \alpha_{th} \cdot \bar{v}}{4HRT} \qquad \text{Equation (2.5.6)}$$

The flux of desorbing molecules from the surface of liquid after (t) time is:

$$F_{des}(t) = \frac{n_g^* \cdot \alpha_{th} \cdot \bar{v}}{4}$$ Equation (2.5.7)

And by applying Henry's law can be rewritten as:

$$F_{des}(t) = \frac{c_g^* \cdot \alpha_{th} \cdot \bar{v}}{4HRT}$$ Equation (2.5.8)

The net flux of solute molecules sticking on the liquid surface or dissolving in the bulk liquid is:

$$F_{net} = F_{in} - F_{des}(t) = \frac{\alpha_{th} \cdot \bar{v}}{4HRT}\left(c_l^0 - c_l^*\right)$$ Equation (2.5.9)

c_l^0 : is the concentration of gas molecules in the gas phase or before striking on the liquid surface ($x = -\infty, t = 0$)

c_l^* : is the concentration of gas molecules after desorbing from the surface liquid ($x = 0, t = t$).

Thus the mass conversion is imposed across the interface at x= 0 by:

$$-D\left.\frac{\partial c}{\partial x}\right|_{x=0} = F_{net}$$ Equation (2.5.10)

And from the equation the net flux can be written:

$$-D\left.\frac{\partial c}{\partial x}\right|_{x=0} = \frac{\alpha_{th}\bar{v}}{4HRT} \cdot \left(c_l^0 - c_l^*\right)_{x=0}$$ Equation (2.5.11)

The gas transport in the liquid film is assumed that the gas- liquid interface is a boundary of zero thickness separating bulk gas and bulk liquid phases, (x=0).

$$-D\left.\frac{\partial c}{\partial x}\right|_{x=0} = \sqrt{\frac{D}{\tau}} \cdot \left(c_l^0 - c_l^*\right)_{x=0}$$ Equation (2.5.12)

Thus the residence time can be extracted by equalizing equation (2.5.11) with equation (2.5.12):

$$\tau = D \cdot \left(\frac{4HRT}{\alpha_{th} \cdot \bar{v}} \right)^2$$ Equation (2.5.13)

D: is the diffusion coefficient in the liquid phase ($cm^2.s^{-1}$)

H: is the solubility of the gas molecules in the liquid ($mol.l^{-1}.atm^{-1}$)

R: is the gas constant ($atm.l.mol^{-1}.K^{-1}$)

T: is the temperature of the liquid (K)

The residence time is the time required for the desorption flux to reach 57% of the entering flux. The desorbing flux decreases every time when the entering flux is decreased and the lifetimes of molecules, which enter the liquid, must be increased to reduce the desorption rate. However, the desorption probability depends on the solvation or residence time of the gas molecules dissolving in the liquid. The diagram (2.8) shows, that desorption probability curves rise (in the beam on) and drop sharply (in the beam off) by different residence time in the solution.

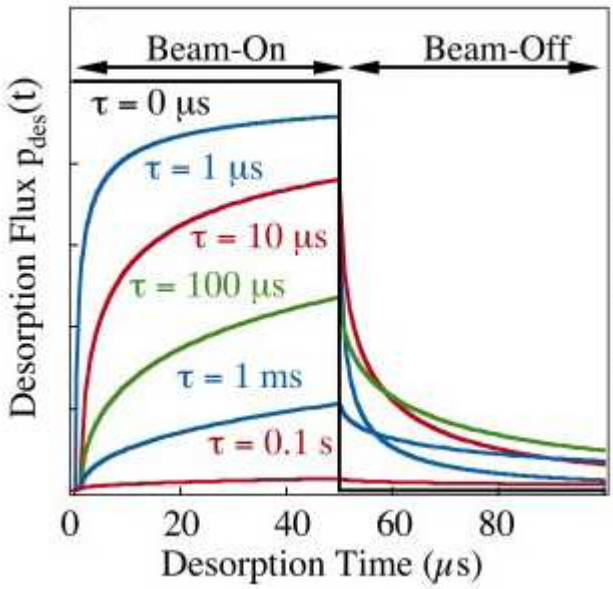

Figure (2.8) Desorption probability versus the desorption time [Nathanson, 2004]

The desorption flux during the pulse of the impinging gas rises with the time until at 50 μs it reaches to a maximum. At this time the surface is saturated from the solute. Over 50 μs desorption flux drops sharply, because there are no impinging gas molecules to replenish those that desorb. The desorption flux at the beam off depends only on the desorbing molecules from the liquid. For longer residence time,

the curves rise and fall less sharply, because the gas molecules with larger value of residence times diffuse deeper into the liquid and desorb more slowly in both (beam on and off). The areas under each curve are equal, because the equal number of gas molecules that are uptaken into the liquid and desorb from it.

Thus the per- chopper spectra can be simulated by convoluting the Maxwell-Boltzmann distribution $N_{MB}(t)$ with the desorption probability at the time τ $P_{des}(\tau)$ [Morris et al. 2000]. The convolution is:

$$N_{fit}(t_{arrival}) = \int_0^{t_{arrival}} P_{des}(\tau) \cdot N_{MB}(t).dt \quad \text{Equation (2.5.14)}$$

The simulated pre- chopper TOF spectra is shown in figure (2.9). It shows that the peak intensities decrease and shift to longer times with increasing residence time.

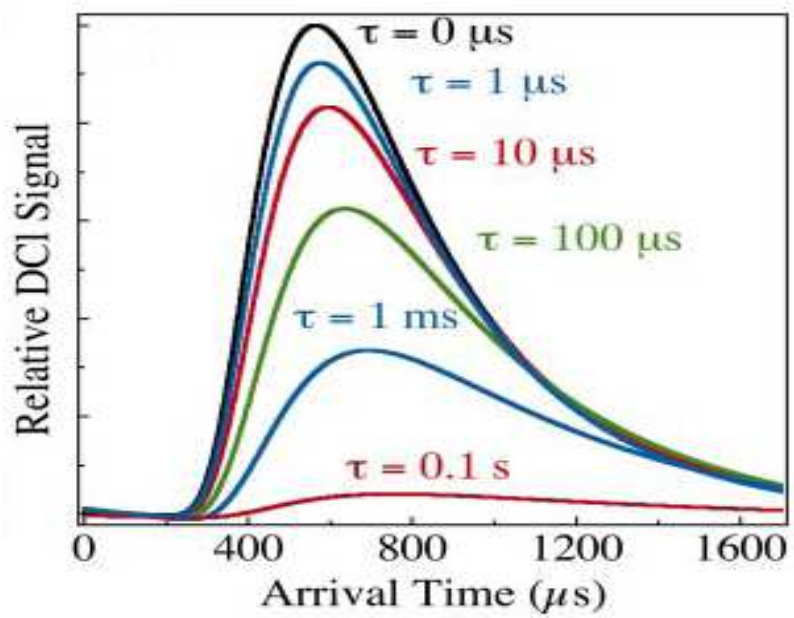

Figure (2.9) Convolution of P_{des} (t) with Maxwell-Boltzmann distribution [Nathanson, 2004]

3. Water desorption from a D_2SO_4 / D_2O surface

The kinetics of desorbing water play a significant role in determining the lifetime of changing sulfuric acid concentration in the aerosols. The change in concentration has an effect on the behavior of gas uptake and gas solution dynamic on the surface and in the bulk of aerosol particle. Furthermore, the heterogeneous reactions for the stratospheric ozone depletion depend on the concentration of sulfuric acid in aerosol. First, we will present the experimental results of D_2O molecules desorbing from a solid and liquid surface of deuterated sulphuric acid solution using post chopper spectra. These data will be compared with theories classical kinetic theory [Scharge, 1953], statistical rate theory [Ward & Fang, 1999] and transition state theory [Nagayama et al. 2003]. Thereafter it will be pointed out in more details the capillary wave theory, in order to describe the different behaviors of D_2O molecules desorbing from solid as well as from liquid surface.

3.1 Experimental results

Vacuum evaporation experiments have been used to monitor the loss of deuterium oxide from the solid and liquid surface of deuterated sulphuric acid solution at temperatures of 213, 218 and 228K. In addition, the intensity of escaping D_2O from ice and liquid surface is observed with different concentration of D_2SO_4 and different spectral angles in the range from 0°to 65°.

The vacuum evaporation technique consists of three chambers, which are the scattering chamber, the differential detector chamber and the detector chamber. The liquid reservoir is located at the centre of the scattering chamber. The differential detector chamber is used here to reduce the background of the time of flight spectra. In addition, the quadrapole mass spectrometer detects the density of desorbing D_2O molecules from the liquid surface of sulphuric acid solution. The details of this technique can be shown in figure (3.1). The spectral angle is equal to zero ($\Phi = 0°$).

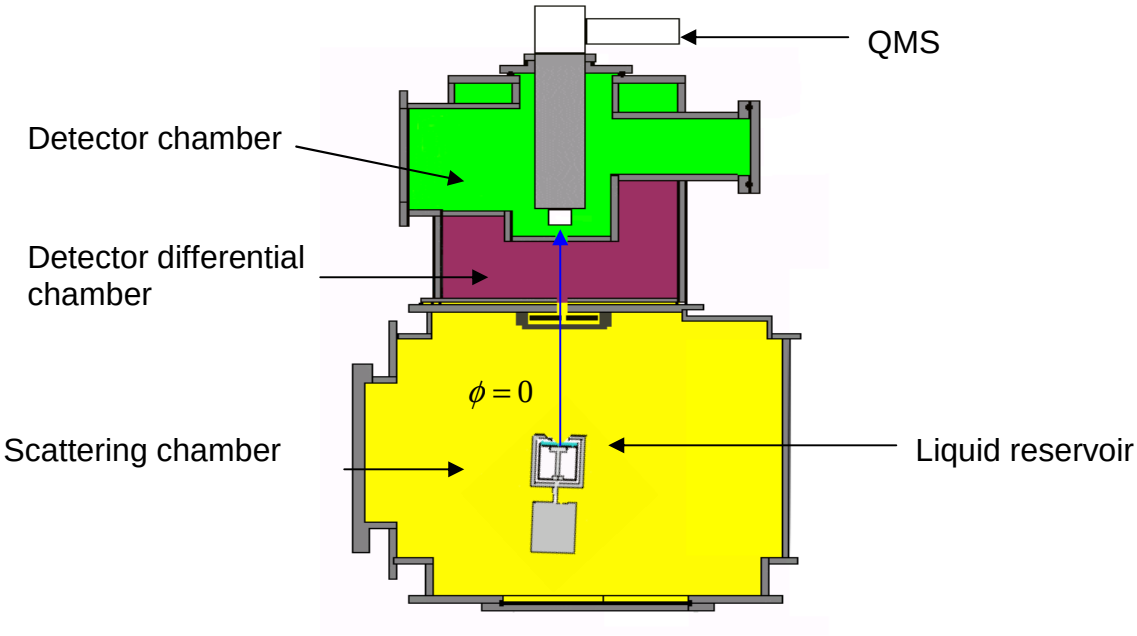

Figure (3.1) Schematic view of the vacuum evaporation technique at zero spectral angle

In the case of the spectral angle being higher than zero, it is placed between “N” and “D” where “N” is the normal to the whole liquid reservoir and “D” is the straight distance between the surface of liquid and the ionization field of the mass spectrometer, as illustrated in the figure (3.2).

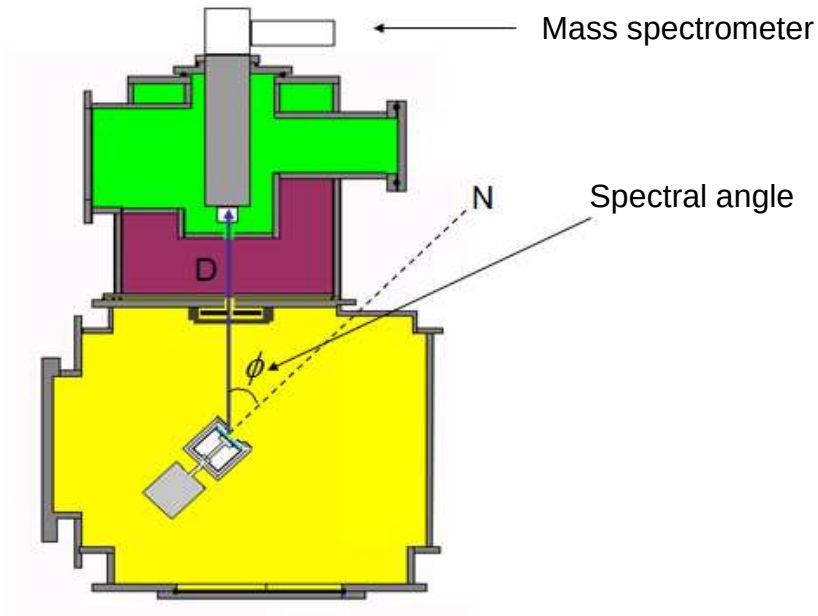

Figure (3.2) Scheme of the variation of the spectral angle (Φ)

The liquid reservoir can be adjusted using the manipulator, which is fixed on the top of it. The continuously renewed film is created by rotating the glass wheel in the sulphuric acid solution. The heavy water molecules desorb from the surface under the vacuum in the scattering chamber. As a result, the concentration of sulphuric acid solution increases as the technique operates longer time. At the high concentration of the sulphuric acid solution, this solution changes from the liquid phase to the solid phase. In the case of solid surface, the glass wheel has no ability to rotate. In this condition, we will observe D_2O molecules desorbing from the solid surface. According to the sulphuric acid water phase diagram [Giauque et al. 1960] this indicates that the solid surface consists of the mono- and dihydrate sulphuric acid (MSA) & (DSM) at the concentration of 78 wt%. The kinetic energy is measured by chopping the D_2O molecules desorbing from liquid surface or solid surface into the short continuously pulses with the post chopper disk, as shown in figure (3.3).

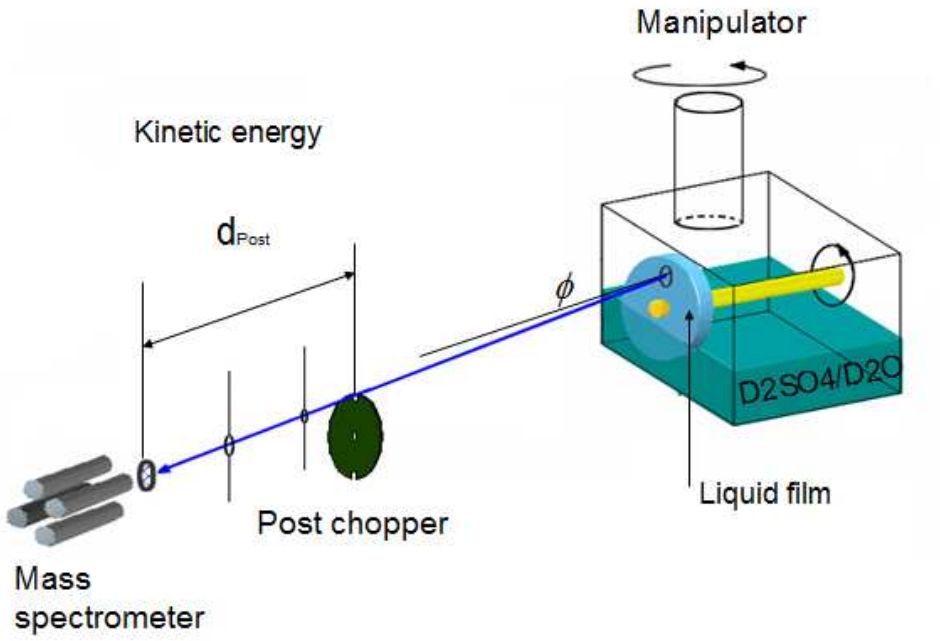

Figure (3.3) Schematic view of the location of post chopper in the vacuum evaporation experiment

3.1.1 Desorption from a solid surface

The experiment analyses the density of desorbing molecules from the surface as a function of time, which is needed to travel from the observed solid surface to the ionizer field of mass spectrometer.

The experimental signal is named the time of flight (TOF) spectrum. The signal of TOF depends on the detector. The mass spectrometer is sensitive to the density of molecules [Scoles et al 1988]. Therefore, the density distribution of desorbing molecules from the surface is extracted based on the velocity distribution using the following equation:

$$N(t) \propto \frac{1}{t}.f(v) \qquad \text{Equation (3.1.1)}$$

Where:

$N(t)$: is the number density of arrived molecules to mass spectrometer from observed surface as a function of time.

$f(v)$: is the velocity distribution of the escaping molecules from the surface.

The Maxwell- Boltzmann velocity distribution is given as [Knox & Phillips, 1998]:

$$f(v) = \frac{1}{2\pi}\left(\frac{M}{RT}\right)^2 \cdot v^3 \cos\phi \cdot \exp\left[\frac{-E_{tot}}{RT}\right] \qquad \text{Equation (3.1.2)}$$

Combining these tow equations above, the number of density distribution of TOF spectra is formed as:

$$N(t) \propto \frac{1}{2\pi}\cdot\frac{1}{t}\left(\frac{M}{RT}\right)^2 \cdot v^3 \cos\phi \cdot \exp\left[\frac{-Mv^2}{2RT}\right] \qquad \text{Equation (3.1.3)}$$

This distribution is named a Maxwell-Boltzmann density distribution of desorbing molecules from the surface. As a result, this equation outlines that the desorbing molecules from the surface have a velocity distribution which accords with the Maxwell-Boltzmann velocity distribution.

Figure (3.4) shows the number density of desorbing molecules D_2O from a solid surface as a function of the arrival time in (μs). The temperature of the surface of the mixture of the mono- and dihydrate sulphuric acid is equal to 213 K. The green curve is calculated based on the equation (3.1.3).
The post- chopper spectrum illustrates that the velocity distribution of desorbing molecules fits with Maxwell-Boltzmann distribution at the temperature of the solid surface 213 K.

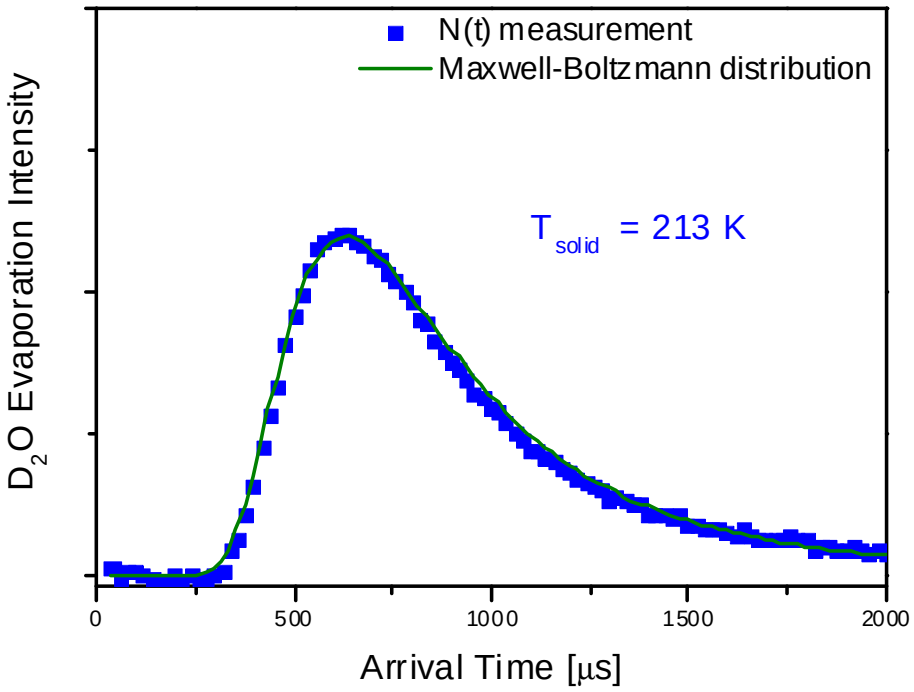

Figure (3.4) TOF spectrum of desorbing D_2O molecules from solid surface at 213K, the green curve is a Maxwell- Boltzmann density distribution

This result accords with the classical kinetic theory, which assumes that the velocity distribution for molecules desorbing far away from the interface is the Maxwell-Boltzmann velocity distribution [Fowler, 1965]. Furthermore, this theory supposes that the temperature in the exponent in the equation of the velocity distribution is equal to the temperature at the interface.

Figure (3.5) demonstrates the TOF spectra of D_2O escaping molecules from the solid surface of sulphuric acid at super cold temperature 213 K and in at a concentration of sulphuric acid of 78 wt% for different spectral angles of 0°, 5°, 30°, 40°, 55°, 60° and 65°. The measurements illustrate that the density distribution of emitting D_2O molecules from the solid surface is equal to the calculated density distribution according to the Maxwell-Boltzmann velocity distribution. The concentration of sulphuric acid during the experiment is constant. Hence, the decreasing intensity signal for D_2O desorbing does not ascribe correspond to the increase the concentration of sulphuric acid.

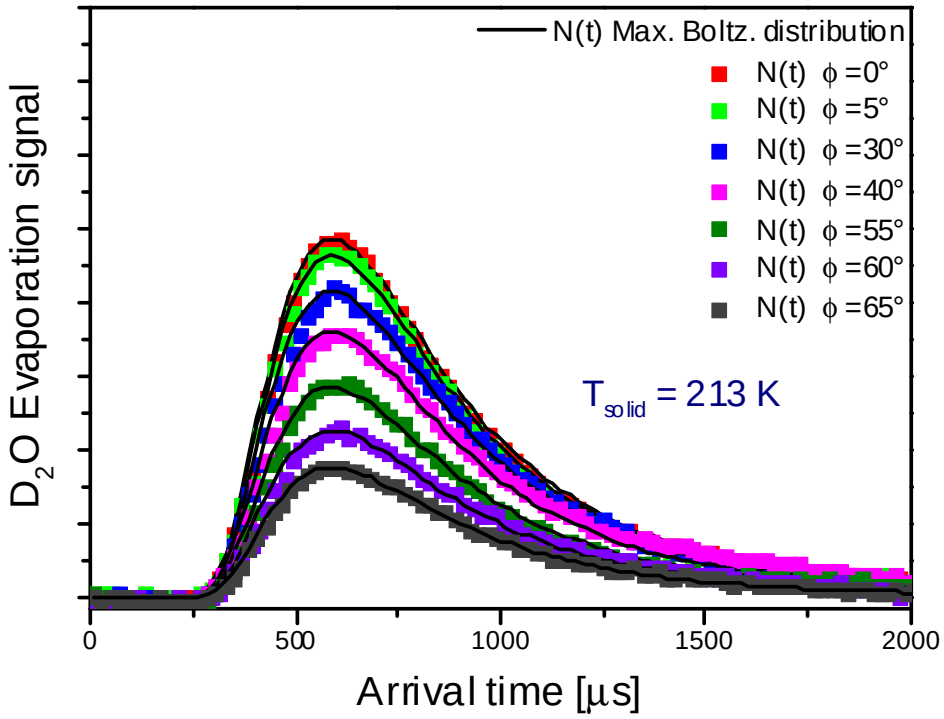

Figure (3.5) TOF spectra of D_2O desorbing from a solid surface at 213 K and a concentration of D_2SO_4 of 78 wt% for spectral angles of 0°, 5°, 30°, 40°, 55°, 60° and 65° (Maxwell-Boltzmann distribution)

However, the measurements present that the change in spectral angle does not influence the velocity distribution of emitting D_2O molecules. In contrast, the intensity signal of escaping D_2O molecules decreases with increasing spectral angle. In other word, the molecules escape from the solid surface to the gas phase with the total kinetic energy, as shown in the figure (3.6).

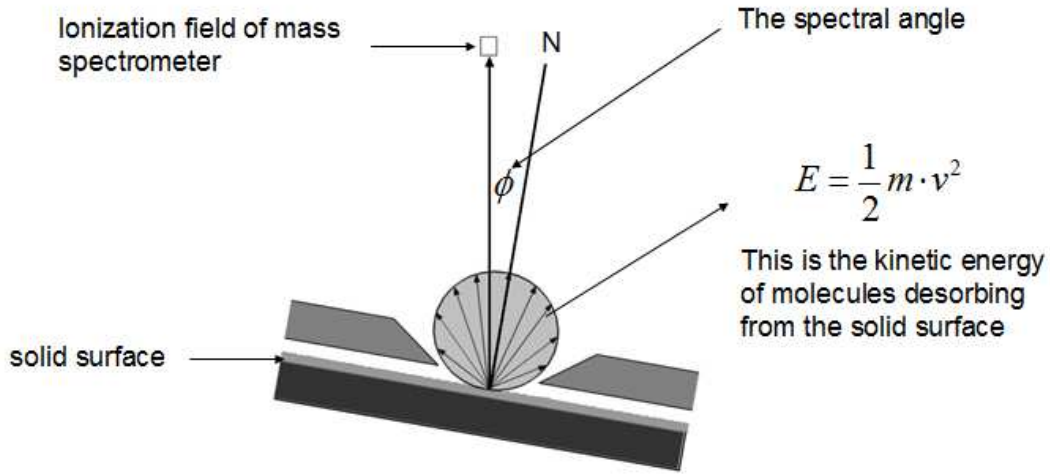

Figure (3.6) Schematic view of the difference between the spectral angle and the kinetic energy of desorption (solid surface)

3.1.2 Desorption from a liquid surface

In case of a fluid surface, the post- chopper spectra indicate that the Maxwell-Boltzmann density distribution is broader than the experimental density distribution, as presented in figure (3.7). This observation points out that the velocity distribution of the desorbing D_2O molecules from a liquid surface is different from the velocity distribution of escaping D_2O molecules from a solid surface. Additionally, the difference of experimental data and Maxwell-Boltzmann density distribution decreases, when the value of the temperature of the liquid surface becomes higher.

In fact, the statistical rate theory suggests that the velocity distribution of the emitted molecules from the liquid surface has a Maxwell-Boltzmann distribution but with higher temperature than from the surface of the liquid. The difference in temperature in the gas phase and on the surface is approximately about 7 K [Ward & Fang, 1998]. Nevertheless, the results of the vacuum evaporation experiment are not associated with the calculation based on the statistical rate theory, because the deviation from this theory is more than 20 K.

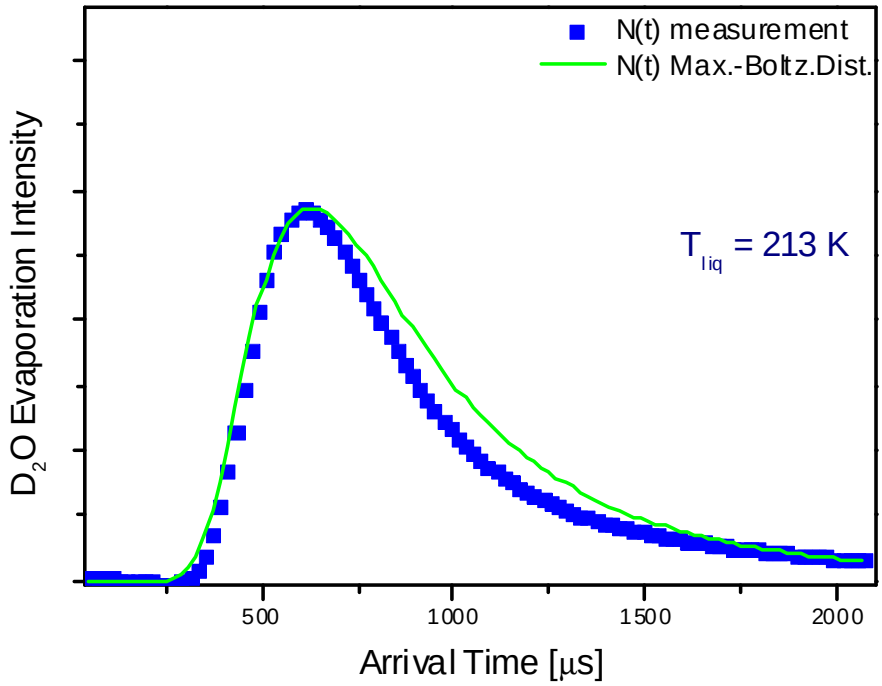

Figure (3.7) TOF spectrum of desorbing D_2O from the liquid surface of sulphuric acid solution at 213 K

The temperature of the liquid surface is reduced by the evaporative cooling at the liquid- gas interface [Ward & Duan, 2004]. This means, when the evaporation occurred, the desorbing molecules from the liquid surface need some of the energy. The surface of liquid supplies the energy to the desorbing molecules. Thus, the gas-liquid interface is the coldest place in the evaporating liquid [Rahimi & Ward, 2005].

One study has shown that the velocity distribution of the desorbing molecules corresponds to a Maxwellian distribution by using the temperature, which is found larger than the temperature at the liquid surface. In addition, it was inserted also a corrected velocity without being physically acceptable [Faubel, 1998].

The transition state theory assumes that the evaporation occurs only for those molecules, which have enough energy to pass the transition state barrier [Nagayama, 2002] and [Cheng, 2011]. In the case of the evaporation into vacuum, it might be impossible to calculate the velocity distribution of the molecules desorbing from the liquid surface by using the calculation from this theory.

Figure (3.8) is a plot of the density distribution of D_2O desorbing from liquid surface of sulphuric acid versus the arrival time in microsecond for a decreasing number of spectral angles from 0°, 10°, 30°, 40° to 65°. The measurements are recorded not only for a constant temperature of sulphuric acid of 213 K but also for a constant concentration of this liquid solution of 64 wt%, in order to prevent the effects of the temperature as well as the concentration on the intensity of D_2O desorbing molecules from the observed liquid surface. The experimental data show that the intensity of this kind of velocity distribution decreases as the value of spectral angle becomes higher.

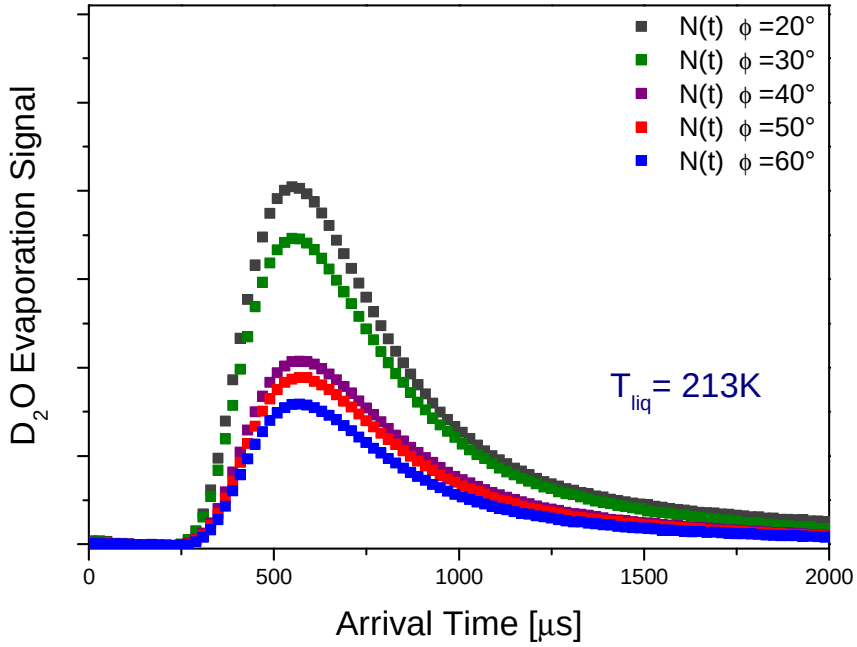

Figure (3.8) TOF spectra of D_2O desorbing from a liquid surface at 213 K in and a concentration of D_2SO_4 of 64 wt% for different spectral angles 0°, 10°, 2 0°, 30° and 65°

Overall, as illustrated in figures (3.5) and (3.8), the results demonstrate that the main probability emission of D_2O desorbing molecules from solid and liquid surface of sulphuric acid solution is normal to the observation surface.

In the next step, the evaporation rate of D_2O desorbing from the surface as a function of the spectral angle will be presented. This evaporation rate D_2O can be calculated by the integration of TOF spectrum for desorbing D_2O, as expressed by:

$$TD_{D_2O} = \int N(t)\,dt \qquad \text{Equation (3.1.4)}$$

A plot of the rate of desorption versus the spectral angle is presented in figure (3.9). The cosine function of spectral angle, its cosine square function and the measured desorption rate of D_2O escaping from the liquid surface of sulphuric acid in different concentration of D_2SO_4 are revealed also in this figure. The subscripts of “Ataya” and “Scharfenort” stand for Ataya (this work) and Scharfenort (Dissertation Essen, 2007) measurements, respectively.

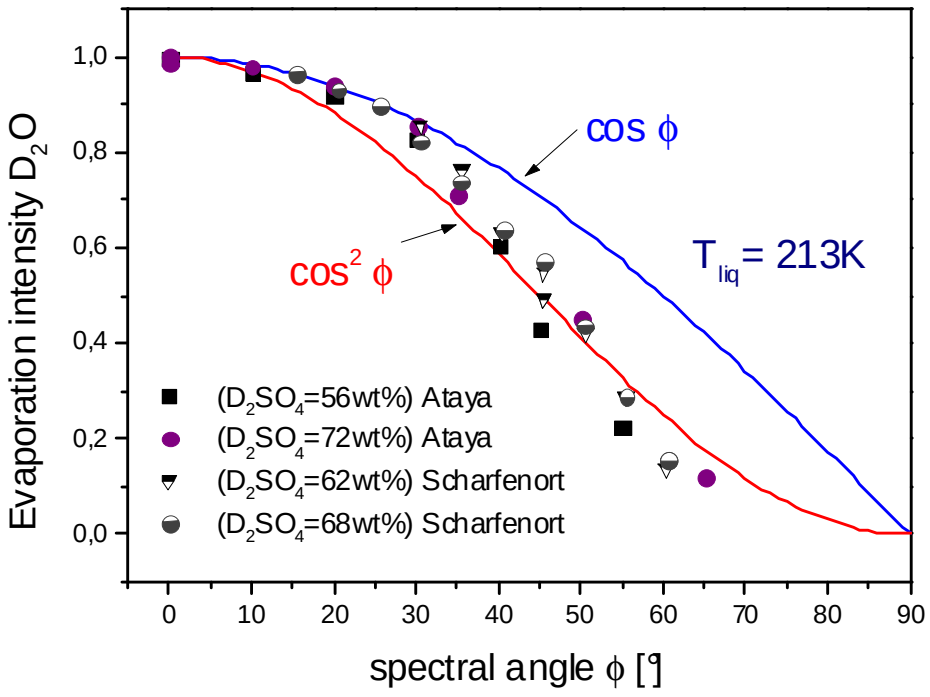

Figure (3.9) The evaporation rate of D_2O as a function of spectral angle for different concentrations of sulphuric acid (position of rotation axis in panel b)

Desorption rates are normalized to the highest value of the desorption rate at spectral angle ($\phi = 0°$) for each concentration of sulphuric acid solution. As shown in this figure, the measurements of desorption rate is associated with the cosine function of the spectral angle between (0°- 30°). A fter that, the deviation of the experimental desorption rate from the cosine function curve increases at spectral angles above 30°. Eventually, the reduction of deso rption rate can not be determined as a function of spectral angle. As expected, the normalized rate of desorption does not depend on the concentration of sulphuric acid.

In a previous study [Scharfenort, 2007] of the desorption rate for D_2O molecules from the liquid surface of D_2SO_4 it was shown that the reduction of the evaporation rate is expressed as a function of angular cosine square of the spectral angle (ϕ). The results of this study did not consider the decrease of the desorption rate which is affected by the geometrical liquid reservoir in the scattering chamber as well as by the acidity of the solution. The effect of the acidity of the solution on the evaporation rate can be vanished through the normalization of this rate as outlined above. Furthermore, the experimental measurements of the desorption rate can be recorded directly from the liquid surface without obstruction through the rotation of the liquid reservoir by using the moveable piece as expressed in section (1.4.2). Figure (3.10) illustrates that the position of the manipulator's rotation axis plays an important role in improving the measured rate of desorption at different values of spectral angle. This improvement can be shown in figure (3.10) in the panels (b), (c) and (d), where the field of the observed spectral angle is between (0°- 30°), (0°- 45°) and (0°- 65°), respectively. However, the foreside of the liquid reservoir is presented in figure (3.10a) and the rotation axis is drawn as a black circle in panels (b), (c) and (d) of the figure (3.10).

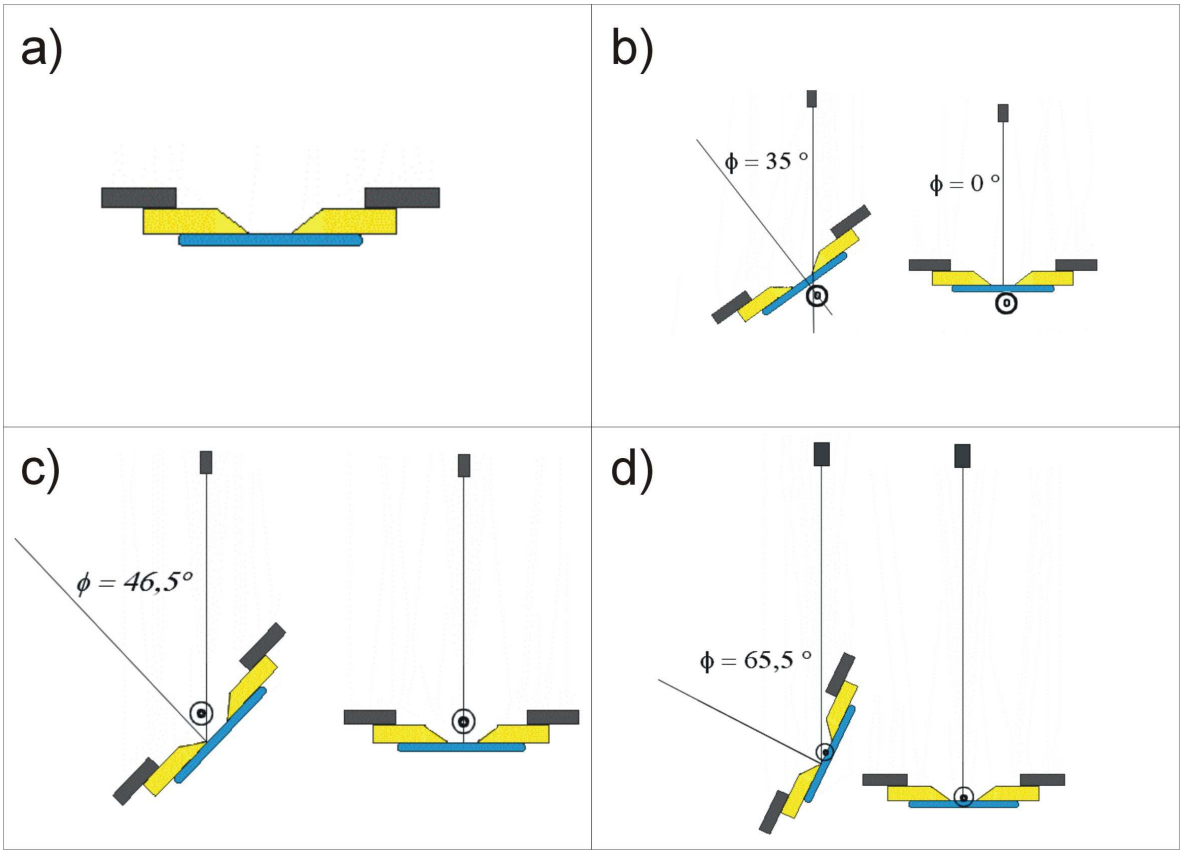

Figure (3.10) Schematic view for the improvement of the spectral angle

Figure (3.11) displays that the deviation between the measured rate of the desorption for escaping D_2O molecules from the liquid surface and the curve of the angular cosine function of the spectral angle decreases at spectral angles above 40° and 45°. Additionally, these measurements are in accord with the calculated values based on the cosine function of spectral angle, while the difference between the experimental data and the curve of the cosine function increases again at the observed angle above 45°. In this case, the position of the rotation axis of the manipulator was in front of the liquid reservoir, as illustrated in figure (3.10 c). As a result, the deviation between the measured rate of the evaporation and the cosine function of the spectral angle is caused by the prevention of the desorbed molecules from the liquid surface which depends on the geometrical liquid reservoir in the scattering chamber, as shown in figure (3.10 b).

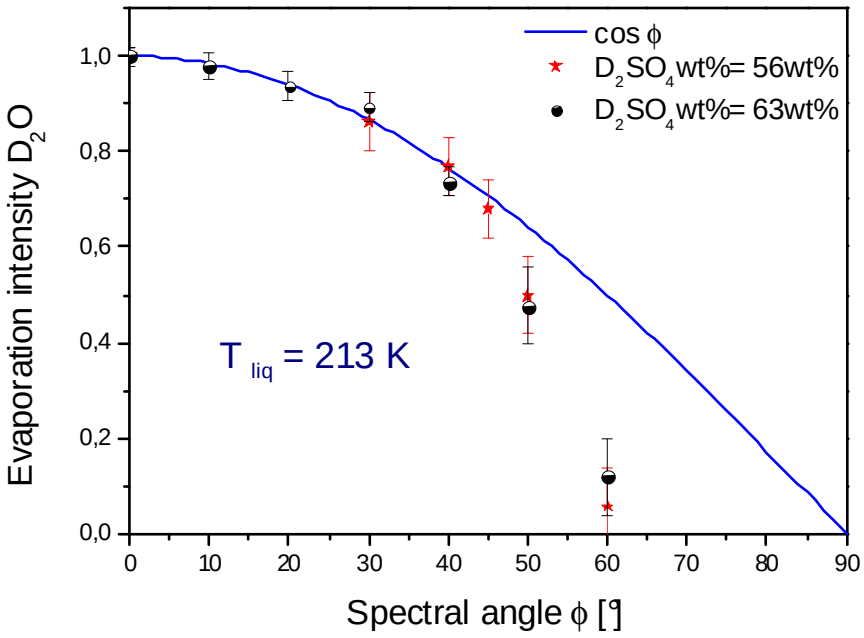

Figure (3.11) The evaporation rate of D_2O against the spectral angle (Position rotation axis in panel c)

The optimal position of the manipulator's rotation axis is presented in figure (3.10 d). In this case, the observed spectral angle changes from 45° to 65°. The change in intensity of D_2O desorbing from the liquid surface is not prevented by the experimental error. Therefore, the decrease in the measured rate of the evaporation is associated with the calculated value based on the angular cosine function of the spectral angle of between (0°- 65°), as shown in fi gure (3.12). The measurements are recorded at a concentration of lower than 76 wt% at a temperature of 213 K in order to ensure that the D_2O molecules escape from the liquid surface of the sulphuric acid solution. These results are in agreement with the cosine of the spectral angle at the pre- exponent in the velocity distribution of the desorbing molecules from the liquid surface, as will be expressed in the equation (3.2.12).

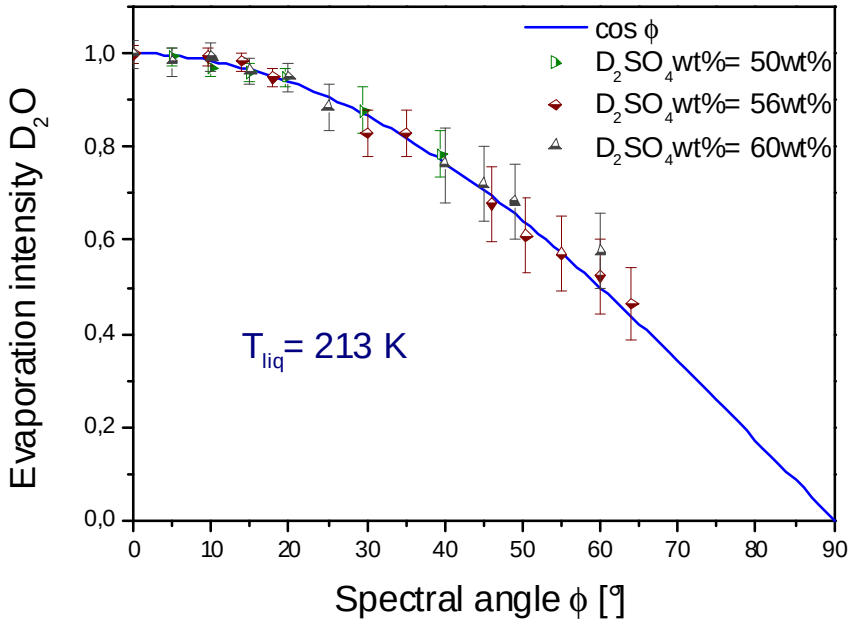

Figure (3.12) The evaporation rate of D_2O from the liquid surface versus the spectral angle (position of the rotation axis in panel d)

A plot of the D_2O evaporation rate against the spectral angle is outlined in figure (3.13). The measured values of the desorption rate of the escaping D_2O from the liquid surface and the solid surface of the sulphuric acid solution at the temperature of 213 K and at the concentrations of 54 wt% and 78 wt% are presented as a circles and triangles, respectively.

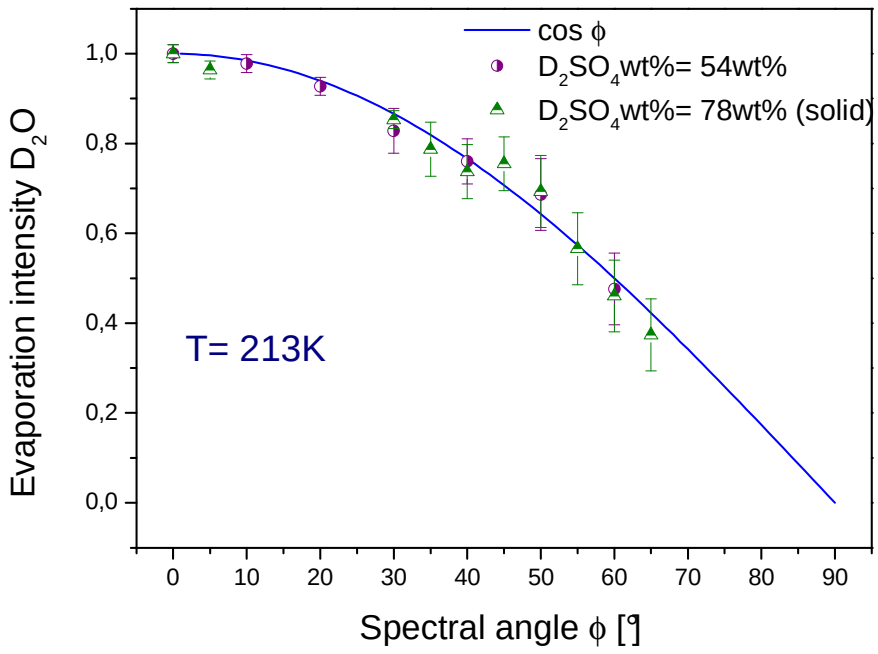

Figure (3.13) The desorption rate of the escaping molecules from the liquid and the solid surface as a function of the spectral angle

The experimental data associate with the cosine function of the spectral angle. This result ensures that the intensity of the Maxwell-Boltzmann velocity distribution in the pre- exponent varies as a cosine function of the spectral angle ($\cos\phi$).

3.1.3 Concentration dependence

Figure (3.14) displays two different TOF spectra for the desorbing D_2O molecules from the liquid surface of the deuterated sulphuric acid at two concentrations of 52 wt% and 69 wt% and at the temperature of 213 K. The intensity of the experimental density distribution of the emitting D_2O molecules decreases with increasing concentration of the sulphuric acid solution.

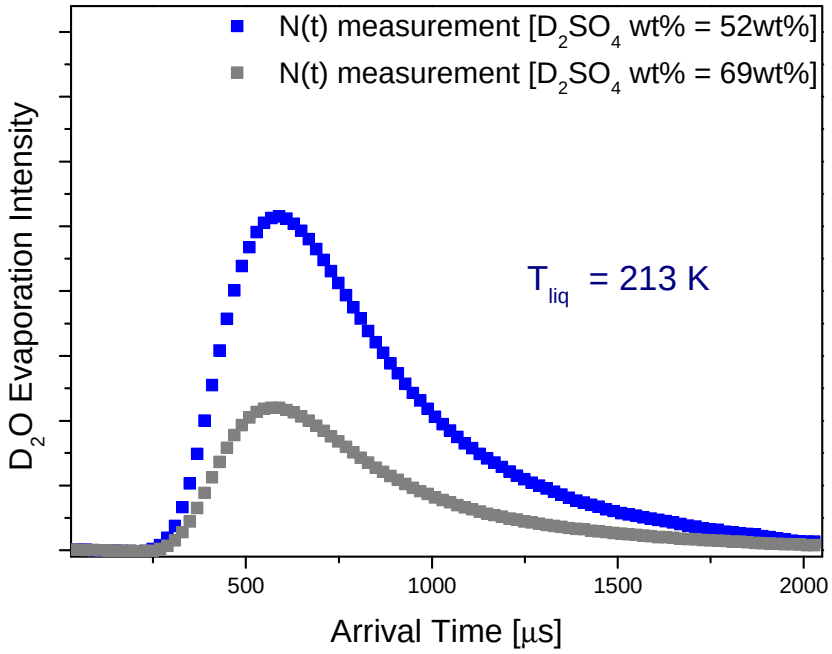

Figure (3.14) Post- chopper TOF spectra of the desorbing D_2O molecules from the liquid surface in the two different concentrations of 52 and 69 wt% at the temperature of 213 K

As a result, the intensity of the desorbing D_2O molecules from the liquid surface depends on the concentration of the sulphuric acid solution. The decrease in intensity may be described through the increasing viscosity of the sulphuric acid, where the viscosity of the sulphuric acid solution increases gradually as the concentration of the sulphuric acid solution increases.

This identification of this intensity is based on the ratio of the mole number of the heavy water and of the mole number of the deuterated sulphuric acid for each concentration of sulphuric acid solution in weight percent. Figure (3.15) is a plot of the relative D_2O evaporation versus the concentration of sulphuric acid. The blue line is the calculated ratio (D_2O:D_2SO_4) and the result is divided to the ratio of the first arbitrary concentration of 40 wt%, which is normalized to 1. For example, the ratio (D_2O:D_2SO_4) of the concentration of 40 wt% is (3: 0.4) = 7.5, the normalization = 1. And the ratio of the concentration of 60 wt% is (2: 0.6) = 3.33, the normalization = 3.33: 7.5 = 0.44

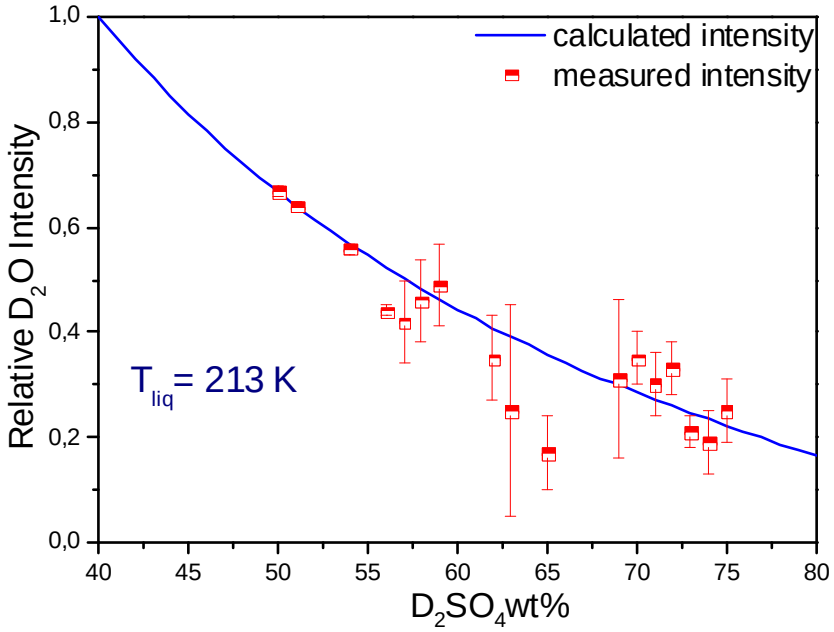

Figure (3.15) the relatively evaporation of D_2O as a function of the sulphuric acid concentration in weight percent

The D_2O desorption rate from the surface of the sulphuric acid corresponds with the calculated curve according to the ratio (D_2O: D_2SO_4). As a result, the intensity of the escaping D_2O molecules from the surface associates with the consistence of the heavy water in the sulphuric acid.

3.2 Theoretical analysis using the capillary wave theory

The capillary wave theory allows the interpretation of studies of the escaping molecules from both liquid and solid surface with taking into account the dynamic process on the surface.

Firstly, in the case of solid surface, the experimental data for the velocity distribution of the desorbing D_2O molecules from the solid surface of sulphuric acid solution at the super low temperature correspond exactly to the calculation based on the Maxwell- Boltzmann velocity distribution. These results were shown in figure (3.4).

The equilibrium distribution of the velocities and the kinetic energies of the leaving molecules from the surface are described by the Maxwell- Boltzmann velocity distribution and correspond to the surface temperature. The form of the distribution function of the molecular velocity is given as [Knox & Phillips, 1998]:

$$f(v) = \frac{1}{2\pi}\left(\frac{M}{RT}\right)^2 \cdot v^3 \cos\phi \cdot \exp\left[\frac{-E_{tot}}{RT}\right] \quad \text{Equation (3.2.1)}$$

Where:

v : is the velocity of the escaping molecules from the surface

M : is the molar mass of the escaping molecules

T : is the temperature of the surface

ϕ : is the spectral angle, which is observed by the vacuum evaporation experiment

E_{tot} : is the total kinetic energy of the leaving molecules from the surface

$$E_{tot} = \frac{1}{2} M \cdot v^2 \quad \text{Equation (3.2.2)}$$

Thus, the form of the velocity distribution can be rewritten as:

$$f(v) = \frac{1}{2\pi}\left(\frac{M}{RT}\right)^2 \cdot v^3 \cos\phi \cdot \exp\left[\frac{-Mv^2}{2RT}\right] \quad \text{Equation (3.2.3)}$$

This velocity distribution is in agreement with the speed of escaping molecules from the solid surface.

The molecules do not vibrate on the solid surface, because there does not exist any motion of the capillary waves. The surface is perfectly planar. The molecules escape from the surface with total kinetic energy and the molecules in the bulk of the solid are not able to replace the free location of the desorbing molecules. The velocity vector of the emitted molecules is perpendicular to the perfect planar solid surface. Figure (3.16) illustrates the kinetic of the escaping molecules from the solid surface.

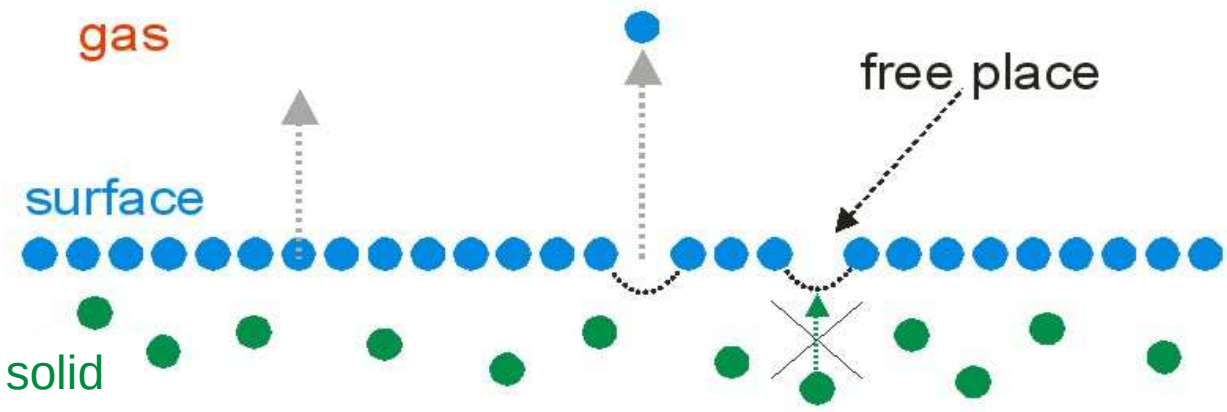

Figure (3.16) Schematic view of the escaping molecules from the solid surface

In the case of the fluid surface the Maxwell- Boltzmann distribution can not describe the kinetic energies and the average velocities of the molecules desorbing from the liquid surface, because the behaviour of the molecules on the surface of liquid is not in the same as that on the surface of a solid. Therefore, a different distribution to describe the desorbing molecules from the liquid surface will be needed. In fact, the capillary wave theory supposes that the surface of the liquid is not extremely planar. While the other three theories, which are outlined above, assume that the liquid surface is perfectly flat. However, the transition state theory suggests that the molecules in the liquid need sufficient energies in order to pass the thickness of energy barrier at the transition state and desorb from the liquid surface. The thickness of the energy barrier is identical to the dynamic surface which is expressed by capillary wave theory. Hence, the molecules can escape from the liquid phase to the gas phase only by passing through this dynamic surface. This dynamic surface can be described exactly by using the local mode of the capillary wave theory. This mode points out that the molecules are vibrating on the surface by the conjunction with the thermal motion of capillary waves. As a result, this oscillation of the surface molecules has an effect on the distribution of the velocities for the desorbing molecules from the liquid surface.

Based on this theory, the kinetic process of the escaping molecules from the liquid surface will be presented first, in order to understand the velocity distribution of these molecules. The kinetic process of the desorption has two extreme cases [Phillips 1997]. Figure (3.17) illustrates these two cases. In the first extreme case, the emitted molecules are lost from the tip of a sharp wavelet with the total kinetic energy and the velocity trajectory being at the right angle to the original surface. In the second extreme case, the molecules escape from the opposite side of the capillary wave and the root mean square displacement moment and the velocity trajectory are perpendicular to the mean surface.

The capillary waves oscillate over and under the planar surface. In the case of desorption, only the period and the location of the wave motion over the original surface are considered. The root mean square displacement moment is the average time of the duration of the downward motion of the capillary wave over the mean surface.

The super location of the desorbing molecules from the surface of the liquid is determined by extracting the tilt of the molecular liquid surface based on the calculation of the root mean square slope.

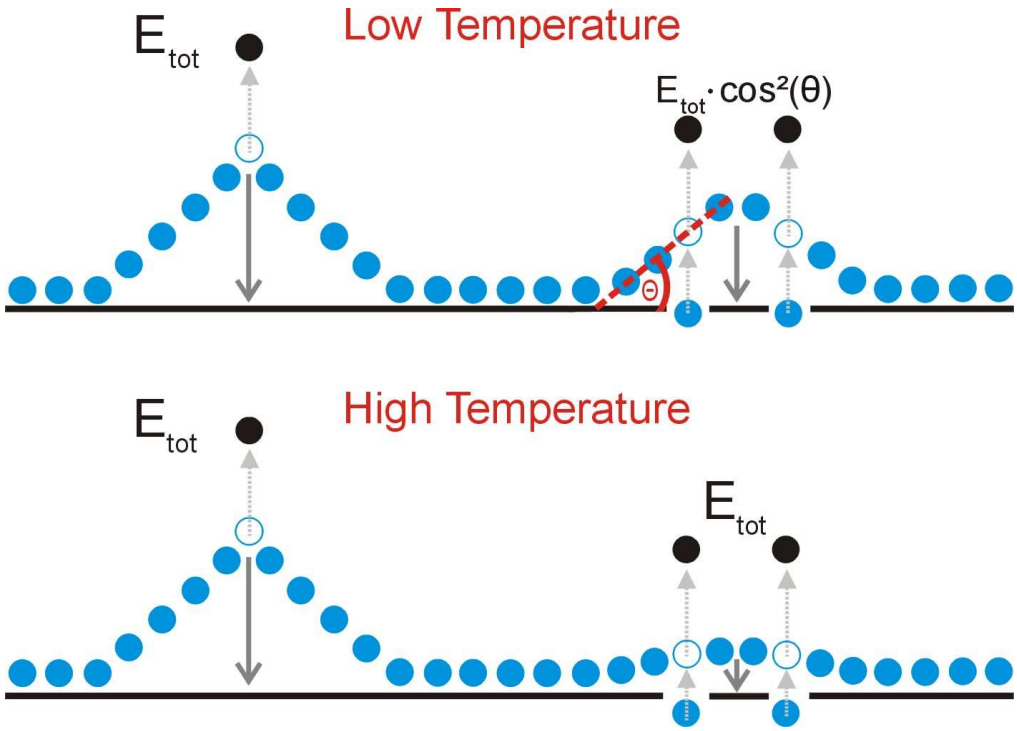

Figure (3.17) The kinetic process of desorbing molecules from the liquid surface

The form of the root mean square slope along x and y axis is given as [Phillips 1997, 2001a]:

$$\left(\frac{\partial \zeta}{\partial x}\right)_{rms} = \sqrt{\frac{\pi k_B T}{8\gamma\sigma^2}} \qquad \text{Equation (3.2.4)}$$

where:

k_B : is the Boltzmann constant ($g.cm^2.s^{-2}.K^{-1}$).

T : is the temperature of sulphuric acid solution (K).

γ : is the surface tension of sulphuric acid solution ($mN.cm^{-1}$).

σ : is the wave diameter, which depends on the temperature of liquid (cm).

ζ : is the vertical displacement of the molecules on the membrane of the capillary wave (cm).

The relationship between the vertical displacement and the amplitude of the capillary wave is given as [Phillips 1997]:

$$\zeta^2 = \frac{1}{2} \cdot a^2 \quad \text{Equation (3.2.5)}$$

The angle θ can be calculated by the arctangent of the root mean square slope as follows:

$$\tan\theta = \left(\frac{\partial \zeta}{\partial x} \right)_{rms} \quad \text{Equation (3.2.6)}$$

$$\theta = \arctan \left(\sqrt{\frac{\pi k_B T}{8 \gamma \sigma}} \right) \quad \text{Equation (3.2.7)}$$

The angle θ is located between the planar surface and the surface of one side of capillary wave during the desorption of the molecules from the same side.

The idea above reflects that the molecules are emitted from the surface of the capillary wave with other kinetic energy, because the velocity of the molecules which are desorbing from capillary wave is affected by the tilt of the capillary wave surface at the moment of the desorption. The kinetic energy is correlated with the root mean square displacement slope as illustrated in figure (3.18) below.

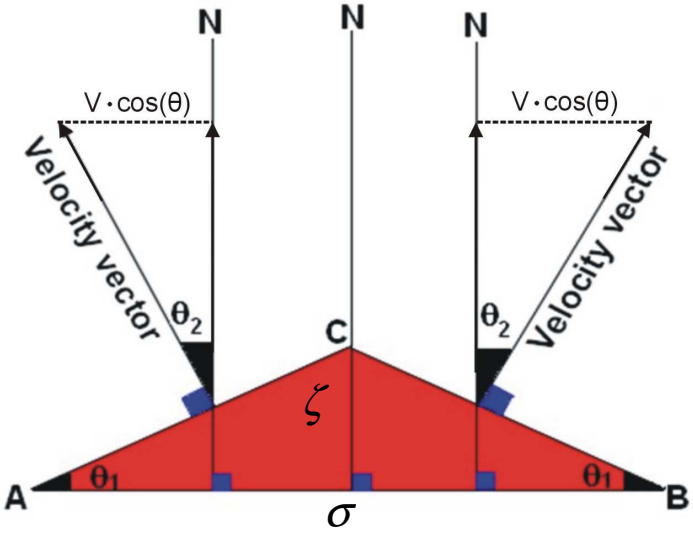

Figure (3.18) Schematic view of the desorbing molecules from the liquid surface at a very low temperature

The triangle points out of the capillary wave at the root mean square displacement in the positive amplitude (the location and the moment of the desorption). “N” is the normal to the mean surface (planar surface) of the liquid. The angle θ_1 is placed between one of both sides of the capillary wave at the moment of the root mean square displacement and the planar surface of the liquid. This angle is calculated as described above. The angle θ_2 is located between the pseudo velocity vector and the normal to the mean surface.

The deviation of the trajectory of pseudo velocity vector to the normal has the same slope of the tilting capillary wave at the moment of the root mean square displacement (at the moment of the escaping molecules). In the case of the desorbing molecules from the liquid surface, the velocity of the desorbing molecules is given as:

$$v_{real} = v \cdot \cos\theta \qquad \text{Equation (3.2.8)}$$

where:

v_{real} : is the real velocity of the molecules desorbing from the surface of capillary wave at the moment of desorption

v : is the velocity of the desorbing molecules from the flat liquid surface

Therefore, the kinetic energy of the escaping molecules from the liquid surface is given as:

$$E^{\theta} = \frac{1}{2} m \cdot v^2 \cdot \cos^2\theta \qquad \text{Equation (3.2.9)}$$

The kinetic energy theta of a desorbing molecule at the angle θ to the normal is equal to the total kinetic energy multiplied by $\cos^2\theta$ as [Phillips, 1997]:

$$E^{\theta} = E_{tot} \cdot \cos^2\theta \qquad \text{Equation (3.2.10)}$$

From the formula arises the velocity distribution of the desorbing molecules from the surface of the liquid:

$$f(v) = \frac{1}{2\pi}\left(\frac{M}{RT}\right)^2 \cdot v^3 \cdot \cos\phi \cdot \exp\left(\frac{-E^{\theta}}{RT}\right) \qquad \text{Equation (3.2.11)}$$

Combining equations (3.2.10) and (3.2.11) gives:

$$f(v) = \frac{1}{2\pi}\left(\frac{M}{RT}\right)^2 \cdot v^3 \cdot \cos\phi \cdot \exp\left(\frac{-Mv^2\cos^2\theta}{RT}\right) \qquad \text{Equation (3.2.12)}$$

This formula is used to describe the velocity distribution for molecules which desorb from the liquid surface. The essential difference from the Maxwellian velocity distribution is the angular cosine square factor ($\cos^2\theta$) in the exponential factor. Henceforth, the velocity distribution of molecules which are emitted from the liquid surface is named non-Maxwell-Boltzmann velocity distribution.

The figure (3.19) is the post- chopper signal of D_2O molecules which desorb from the liquid surface of deuterated sulphuric acid solution at temperature of 213 K. The red curve shows the density distribution according to a non-Maxwell-Boltzmann velocity distribution. This density distribution is extracted by combining equations (3.1.1) and (3.2.12):

$$N(t) \propto \frac{1}{2\pi} \cdot \frac{1}{t}\left(\frac{M}{RT}\right)^2 \cdot v^3 \cos\phi \cdot \exp\left[\frac{-Mv^2\cos^2\theta}{2RT}\right] \qquad \text{Equation (3.2.13)}$$

In order to bring the experimental data in accordance with the calculated density distribution, the angular cosine square factor is inserted as a corrector factor in this equation (3.2.13). The experimental measurements correspond with the non-Maxwell- Boltzmann density distribution where the value of theta is equal to 33.5° and the diameter of the capillary wave is taken as (σ = 2.16 X 10^{-8} cm) at the temperature of the liquid of 213 K.

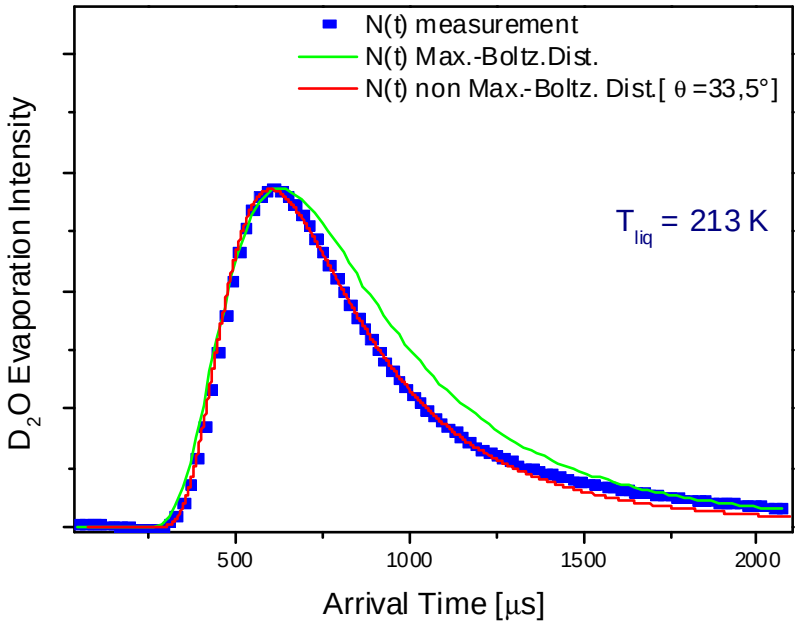

Figure (3.19) TOF spectrum of desorbing D_2O from the fluid surface of sulphuric acid solution at 213 K. The red curve presents a non-Maxwell-Boltzmann distribution

The figure (3.20) shows the post- chopper TOF spectra of D_2O desorbing from the liquid surface of sulphuric acid with different values of spectral angles in the range from 0°, 10°, 30°, 40° to 65°. The measurements are recorded at the constant temperature of sulphuric acid of 213 K. In the case of a liquid surface, the density distribution of D_2O escaping molecules is associated with the computed density distribution, which is based on the non-Maxwell-Boltzmann velocity distribution. However, the spectral angle has no effect on the energy distribution of escaping D_2O molecules in exponential forms of non-Maxwell-Boltzmann velocity distribution form. This result corresponds with the result that has already been indicated in the case of the solid surface.

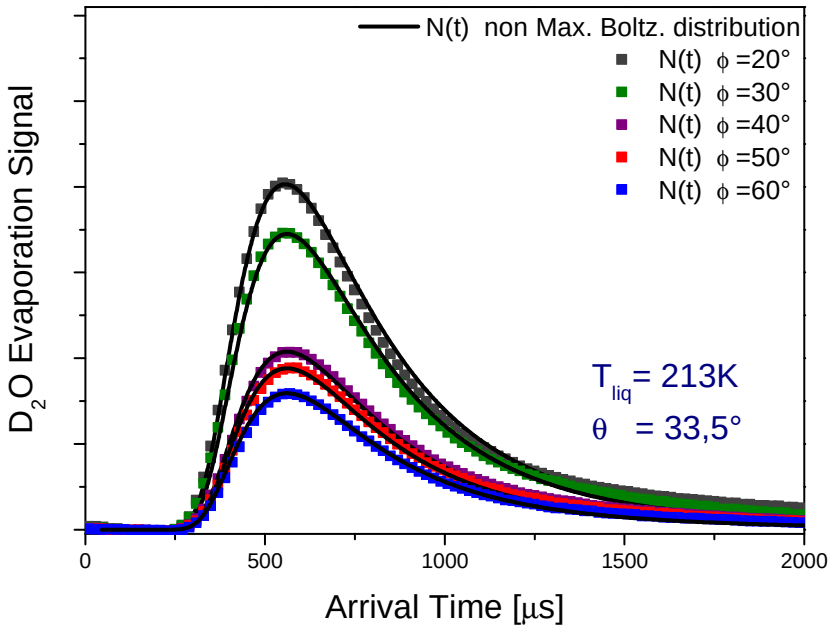

Figure (3.20) TOF spectra of D_2O desorbing from liquid surface at 213 K in the concentration of 64 wt% for different spectral angles 0°, 10°, 20°, 30° and 65° (Non-Maxwell-Boltzmann distribution)

The experimental data indicate that the change in spectral angle does not influence the velocity distribution of emitting D_2O molecules, whereas the intensity signal of escaping D_2O molecules gradually decreases as the spectral angle increases. In other words, the molecules desorb from the liquid surface to the gas phase with the theta-dependent kinetic energy, as illustrated in the figure (3.21) below.

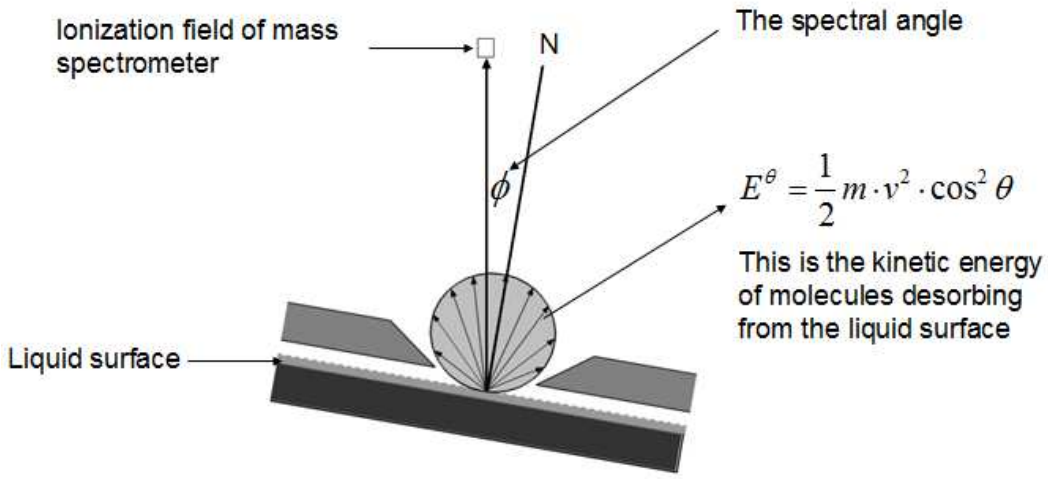

Figure (3.21) Schematic view of the difference between the spectral angle and the kinetic energy of the desorption (liquid surface)

In fact, the experimental observations show that the concentration of the binary acid solution has only a small effect on the tilting of the capillary wave on the surface of liquid. In contrast, the equation (3.2.7) outlines that there must be a relationship between the surface tension of the sulphuric acid solution and theta factor. Moreover, the surface tension of sulphuric acid solution decreases with the increase of the sulphuric acid concentration, as shown in Myher's model (1998). Figure (3.22) displays two different post- chopper TOF spectra of D_2O molecules escaping from the liquid surface of D_2SO_4 / D_2O solution in two concentrations of 52 and 69 wt% at the temperature of solution of 213 K. The experimental density distribution of emitting D_2O molecules fits with the computed density distributions regarding to non-Maxwell-Boltzmann velocity distribution with the angular cosine square factor at ($\theta = 33.5°$).

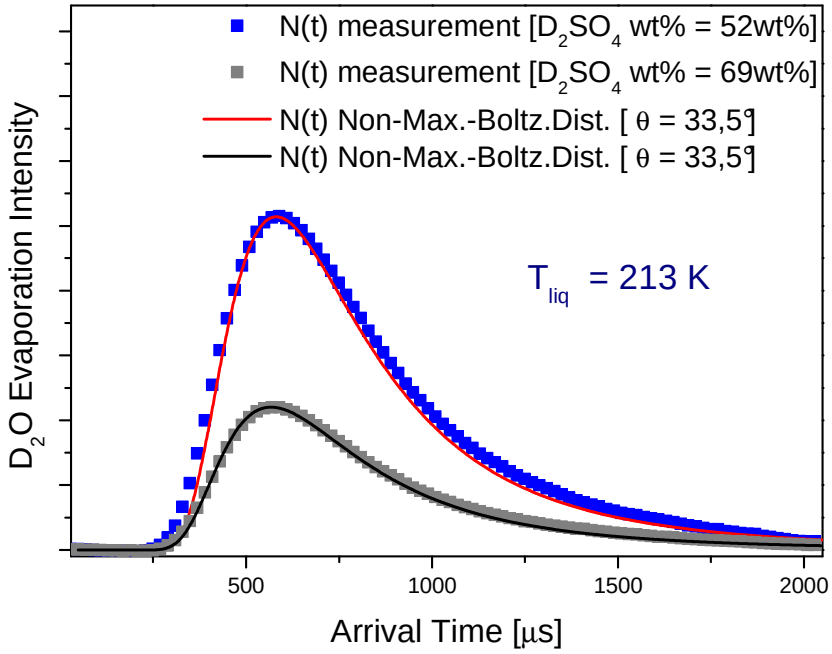

Figure (3.22) Post- chopper TOF spectra of desorbing D_2O molecules from liquid surface at two different concentrations of 52 and 69 wt% at temperature of 213 K

As a result, the changeable values of the surface tension play a negligible role in the slope of the capillary wave at the moment of the D_2O molecules desorb from the liquid surface. However, these results support that the evaporation takes place in the local mode of the capillary wave theory. Where the harmonic oscillation of the capillary wave converses into an anharmonic oscillation at a short wavelength and

the influence of the surface tension is vanishing in this case [Phillips 2004a, 2004b, 2005].

The angular cosine square factor depends on the temperature of the liquid surface. The diameter of the capillary wave increases with the increase of the temperature, because the number of molecules that form the capillary wave becomes higher [Phillips 2000]. This increase in the diameter of the capillary wave drives from the expansion of the surface with increasing temperature. The figure (3.23) below shows that the theta decreases with an increase of the temperature of the liquid surface.

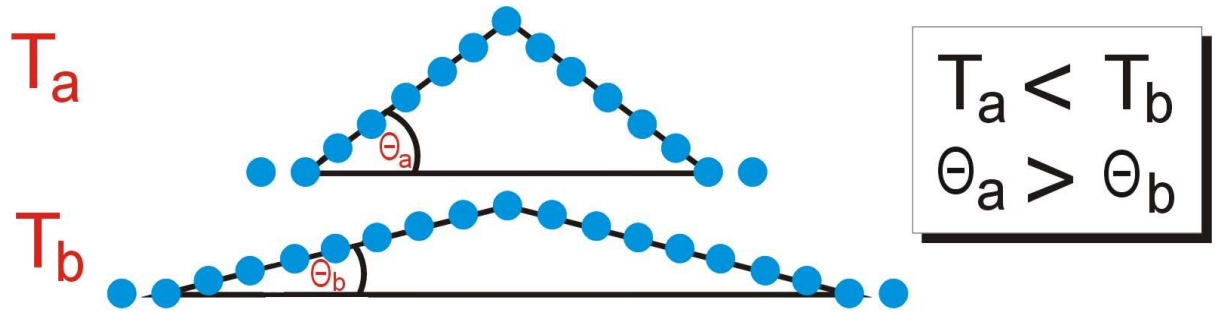

Figure (3.23) Schematic view of the correlation of the root mean square slope with the temperature of the liquid

The local mode of the capillary wave theory supposes that evaporation takes place if the wave vector is at its maximum value. The harmonic motion of the capillary wave changes to anharmonic oscillation by the loss of molecules from the surface to the gas phase at the positive amplitude. This maximum value is associated with the decreasing roughness of the wave surface with the increasing temperature of the liquid [Mora et al. 2003] and [Aarts et al. 2004]. Therefore, the molecules escape from the surface of the wave at a lower root mean square displacement slope, as well as lower amplitude with increasing the temperature of liquid surface.

The molecules emit from the planar surface of the liquid at a very high temperature. In this case, the velocity distribution of the desorbing molecules from the liquid

surface corresponds to the Maxwell-Boltzmann velocity distribution, as described in figure (3.17)

As analyzed in figure (3.19), the value of theta is equal to 33.5° at the temperature of the liquid surface of 213 K. Increasing the temperature of the surface liquid provokes an ascent of the number of the surface molecules, which contribute to the development of the capillary wave. The diameter of the capillary wave decreases with the falling temperature of the liquid surface. The TOF spectrum of D_2O molecules from the liquid surface of the D_2SO_4 reveals that theta is equal to 32° at the temperature of 218 K, as outlined in figure (3.24). The diameter of the capillary wave is equal to 2.20 X 10^{-8} cm. Hence, the value of the capillary wave tilt depends on the temperature of the liquid surface. This result has been found through the correspondence of the measurement of the density distribution to the calculated density distribution based on the non Maxwell-Boltzmann distribution.

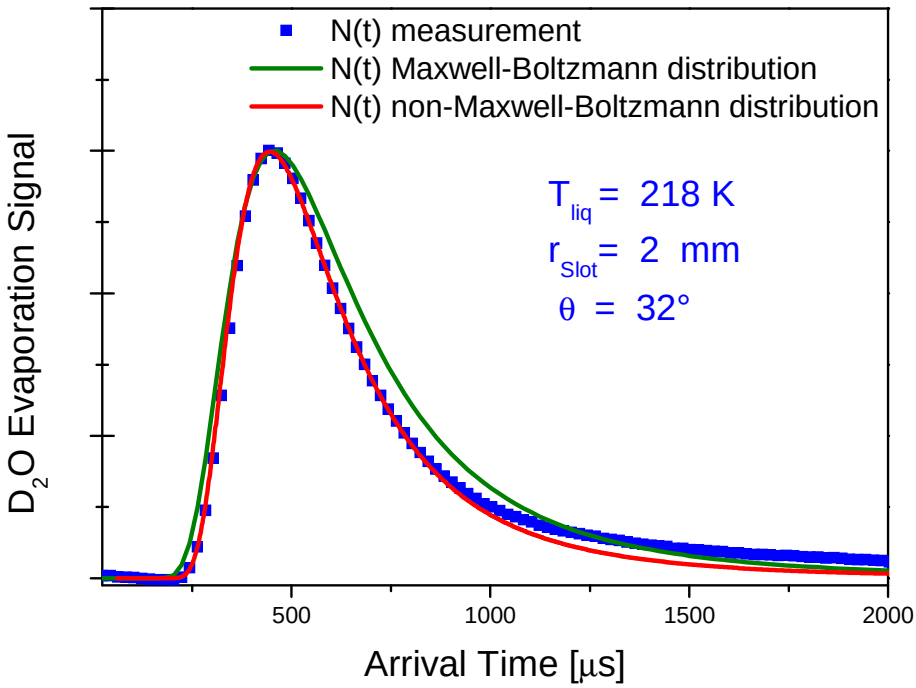

Figure (3.24) TOF spectrum of desorbing D_2O molecules from the liquid surface at 218 K, non-Maxwell-Boltzmann distribution in rms slope of 32°

Figure (3.25) shows that the calculated non-Maxwell-Boltzmann density distribution fits with the experimental data of the escaping D_2O molecules from the liquid surface at 228 K. This density distribution is computed with the diameter of the capillary wave ($\sigma = 2.57 \times 10^{-8} cm$) and the angular cosine square factor ($\theta = 29°$).

These results assure that the surface of the capillary wave expands when the temperature of the liquid surface increases. Furthermore, the results support the idea of the existence of capillary waves on the liquid surface and the continuous motion of the molecules on the surface affects the behaviour of the desorbing molecules from the surface liquid.

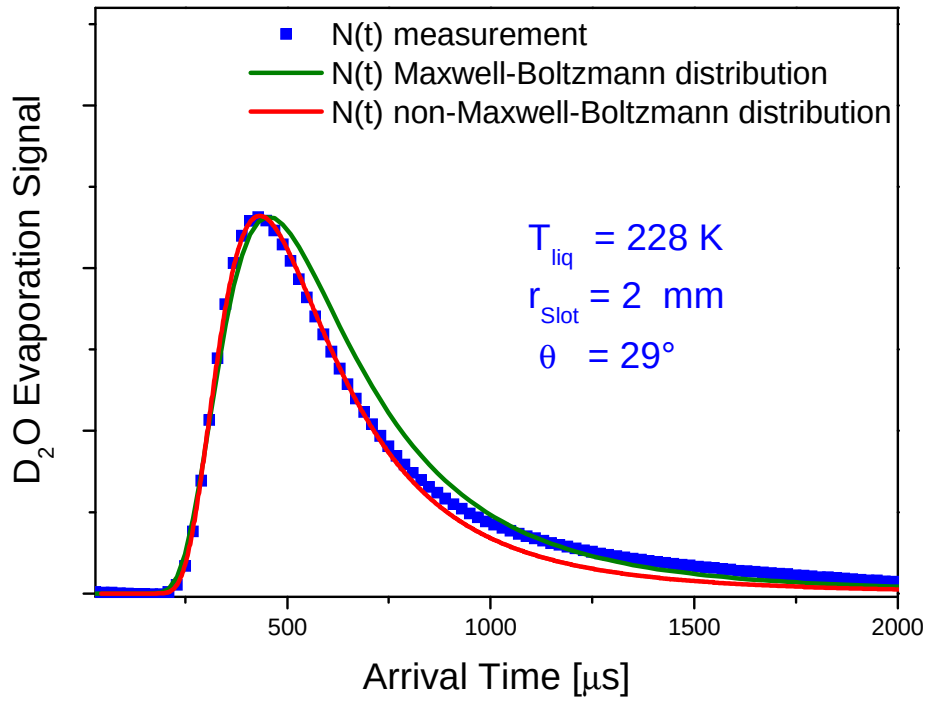

Figure (4.4) TOF spectrum of desorbing D_2O molecules from the liquid surface at 228 K, the root mean square slope is equal to 29°

Overall and as a result, the diameters of the capillary wave at the temperatures of 213, 218 and 228 K are σ = 2.16 X 10^{-8}, 2.20 X 10^{-8} and 2.57 X 10^{-8} cm, because the calculated density distributions fit the measured density distribution of the evaporating molecules at the angular cosine square factor θ = 33.5°, 32° and 29°, respectively.

To conclude, the intensity of the velocity distribution for escaping molecules from the liquid surface and the solid surface depends on the angular cosine factor ($\cos\phi$). This angle is located between the normal to the whole surface (surface of liquid wheel) and the distance, which is between the whole surface and the ionization field of the mass spectrometer. This spectral angle (Φ) has no effect on the kinetic energy of the desorbing molecules from either the solid surface or the liquid surface.

The intensity of the desorbing molecules from the liquid surface decreases with the increase of the concentration of the sulphuric acid. That may occur by reducing the velocity of the oscillation molecules at the local mode for capillary waves, because the created capillary waves need to create more time after desorption with high concentration than those with low concentration of sulphuric acid. Thus the delay time to reform the oscillation motion has an effect on the intensity of desorbing molecules from the liquid surface. However, the number of water molecules on the surface becomes smaller with higher concentration of the sulphuric acid solution. Therefore the intensity of the desorbing molecules from the surface is associated with the number of the water molecules on the surface.

The surface tension decreases with the increase of the concentration of the sulphuric acid solution, while the value of the viscosity becomes higher with increasing concentration of sulphuric acid in solution. This change in the values of the viscosity and the surface tension has an insufficient effect on the kinetic energies, which are needed to escape from the solid surface or the liquid surface by desorbing molecules.

In contrast, the kinetic energy depends only on the temperature of the liquid surface, because the root mean square slope (in molecular scale) decreases with the increase of the temperature of the liquid surface.

4. The accommodation coefficient of HCl on a D_2SO_4/ D_2O surface

The accommodation coefficient of HCl gas onto surface of D_2SO_4/ D_2O solution from a comparison between the post chopper TOF spectra before and after the exchange reaction ($H \rightarrow D$) will be determined first. The mass accommodation coefficient of HCl gas into a D_2SO_4/ D_2O surface can be then described by analysing three theories. The three mentioned theories are the following: the cavity theory [Pollack, 1991], transition state theory [Davidovits et al. 1995] & [Nathanson et al. 1996] and the capillary wave theory [Behr et al. 2009].

In the case of the transition state theory more details of the mechanism of the uptake of HCl gas on the deuterated sulphuric acid solution through the thermodynamic description will be presented. After that, the results are then compared with the calculated mass accommodation coefficient of HCl into the sulphuric acid solution according to the capillary wave theory.

4.1 Experimental data

The pathways for HCl molecules impinging to the liquid surface of the deuterated sulphuric acid solution at incident angle 45° will be described. The molecules collide with the liquid surface. Then, some of them scatter away from the surface with high energy (direct inelastic scattering). The others bounce and bind momentarily at the liquid surface and they dissipate their excess energy on the surface (trapping). These trapping molecules have two ways, either they desorb from the liquid surface before they undergo an exchange reaction (thermal desorption without exchange) or they penetrate in the bulk liquid, dissociate into H^+ and Cl^-, recombine with D^+ in the solution to produce DCl molecules, after that these molecules desorb from the liquid surface (thermal desorption after reaction). The pathways are illustrated in figure (4.1).

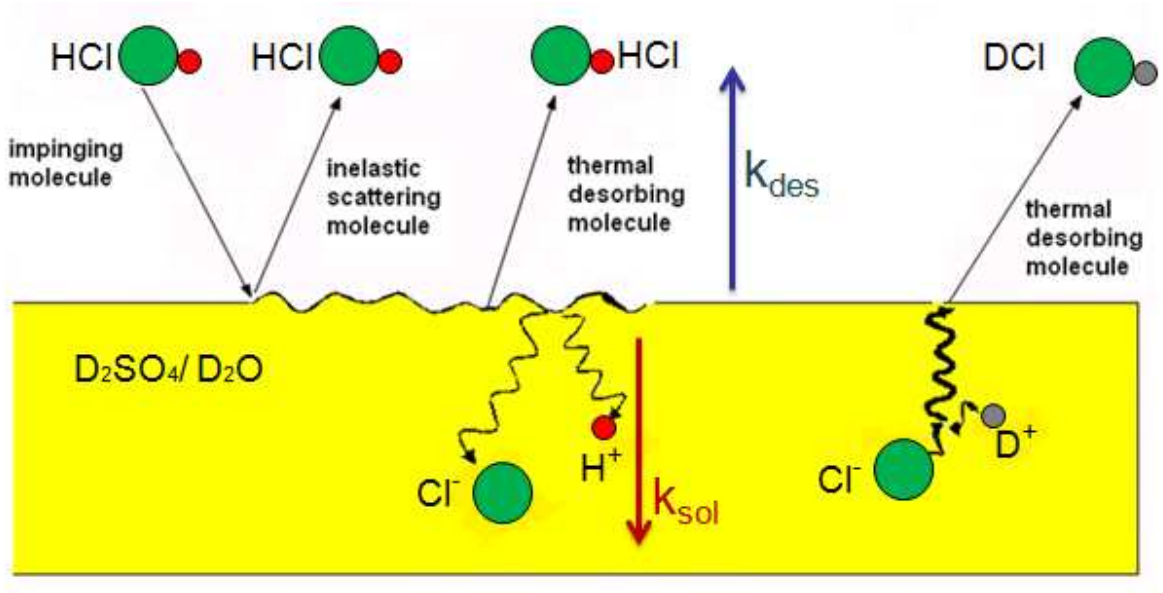

Figure (4.1) Observed pathways for HCl colliding with a deuterated sulphuric acid solution

The exiting molecules from these pathways are monitored by mass spectroscopy and the time of flight spectra analysis due to separate non- reactive collisions from those that involve ($H \rightarrow D$) exchange. The TOF spectra indicate that the HCl molecules have two components after collision with a high incident energy. The first component is the inelastic scattering (IS), which has a sharp peak at early arrival times. The second one is the thermal desorption (TD) at later arrival times, as shown in figure (4.2). In contrast, in the case of low incident energy, the inelastic scattering component does not appear separately in the TOF spectra which will be shown in the measurement such as the incident energy of HCl which is equal to 6 $kJ.mol^{-1}$, as presented in figure (4.5). In addition, the mass spectroscopy detects only the thermal desorption component in the TOF spectra for the molecules that have undergone ($H \rightarrow D$) exchange reaction such as DCl spectra.

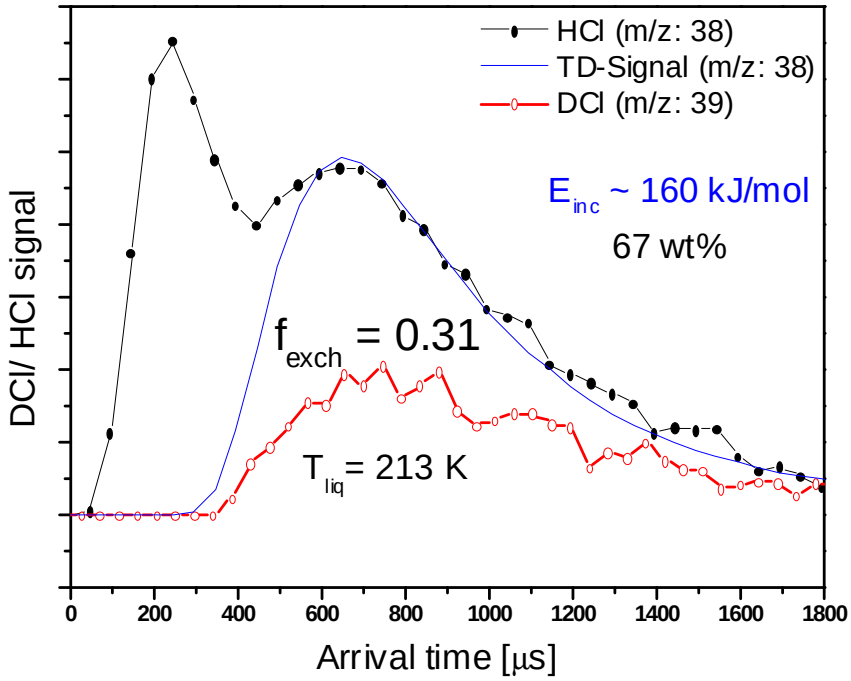

Figure (4.2) TOF spectra of HCl with incident energy of 140 kJ.mol^{-1} and DCl that is produced after the exchange reaction

The TOF spectra of HCl and DCl thermal desorption are used to determine the exchange fraction. The number of HCl molecules and also of DCl molecules that desorb thermally from the acid surface (TD_{HCl}, TD_{DCl}) are proportional to the integrated thermal desorption intensities for HCl and DCl signal. Then, the exchange fraction is the ratio of DCl to the sum of DCl and HCl thermal desorption intensities [Burden et al. 2009]. It is given experimentally as:

$$f_{exch} = \frac{TD(DCl)}{TD(HCl)+TD(DCl)} \qquad \text{Equation (4.1.1)}$$

The exchange fraction can be expressed as:

$$f_{exch} = \frac{k_{exch}}{k_{exch}+k_{des}} = \frac{k_{sol}}{k_{sol}+k_{des}} \qquad \text{Equation (4.1.2)}$$

The exchange reaction ($H \rightarrow D$) for the HCl molecules takes place in the bulk of the liquid. Thus, the exchange rate is equal to the solvation rate. Besides, the expression for the mass accommodation coefficient can be given as:

$$\alpha = \frac{k_{sol}}{k_{sol} + k_{des}} \qquad \text{Equation (4.1.3)}$$

Overall, the accommodation coefficient of HCl gas in the sulphuric acid at low temperature is equal to the exchange fraction ($\alpha = f_{exch}$) [Behr et al. 2009], [Morris et al. 2000].

Figure (4.3) below shows the post- chopper TOF spectra for the thermal desorption of HCl ($m/z = 38$) as a black signal and also the thermal of DCl ($m/z = 39$) as a red signal. The mass spectrometer detects these masses in order to reduce the contribution of Cl ($m/z = 37$) isotope in the TOF spectra. In this case, the incident energy of HCl molecules is 1.7 RT= 6 kJ.mol^{-1}. This means that all incoming molecules of HCl trap on the liquid surface of sulphuric acid. The intensity of DCl TOF spectrum is higher than that of HCl TOF spectrum at the concentration of sulphuric acid 52 wt% and temperature 228 K. The accommodation coefficient is 0.7, which has been observed above. This value illustrates that 7 molecules from each10 molecules which impinge on the liquid surface have undergone an ($H \rightarrow D$) exchange.

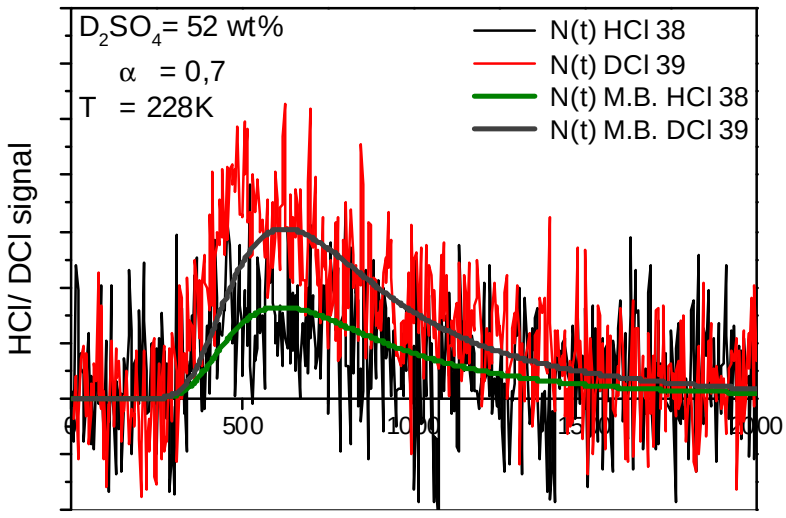

Figure (4.3) TOF spectra of HCl and DCl at the concentration of 52 wt% and the temperature of 228 K

The plots of mass spectroscopy signals of HCl and DCl against the arrival time in microsecond are represented in figure (4.4). The mass accommodation coefficient of HCl in sulphuric acid is (0.51) at the concentration of deuterated sulphuric acid of 62 wt% and the temperature of solution of 228 K.

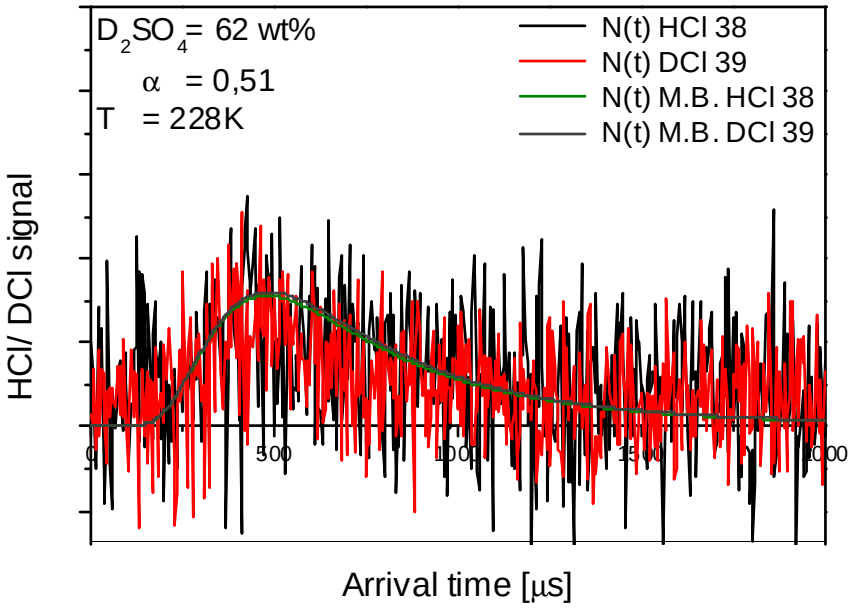

Figure (4.4) Post- chopper TOF spectra of HCl and DCl exiting from surface of sulphuric acid in concentration of 62 wt% and temperature of 228 K

In figure (4.5) illustrates that the ($H \rightarrow D$) exchange fraction is 0.31. As explained above, the accommodation coefficient is 0.31 at the concentration of 69 wt% and temperature of 228 K. At this concentration of sulphuric acid, only three molecules from each 10 molecules which are sticking on the liquid surface have the possibility to dissolve and dissociate in the liquid.

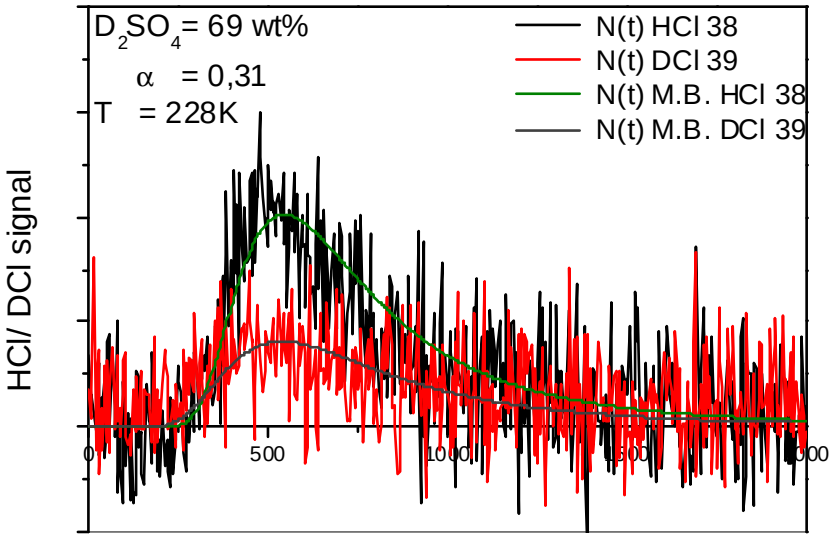

Figure (4.5) TOF spectra of HCl and DCl in the concentration of 69 wt% and temperature of 228 K

The post- chopper spectra in figures (4.3), (4.4) and (4.5) demonstrate that the ($H \rightarrow D$) exchange fraction depends on the concentration of the sulphuric acid, where the values of this fraction decrease with increasing concentration of sulphuric acid.

However, the relationship between the mass accommodation coefficient (α) and the concentration of solvent is represented in the following figure (4.6). This figure is a plot of the mass accommodation coefficient versus the concentration of sulphuric acid solution at the temperature of 218 K. The squares and triangles are the measured values of the mass accommodation coefficient of HCl with incident energy of 6 $kJ.mol^{-1}$ and 140 $kJ.mol^{-1}$, respectively. The results demonstrate that the values of the accommodation coefficient decrease as the concentration of the deuterated sulphuric acid solution increases.

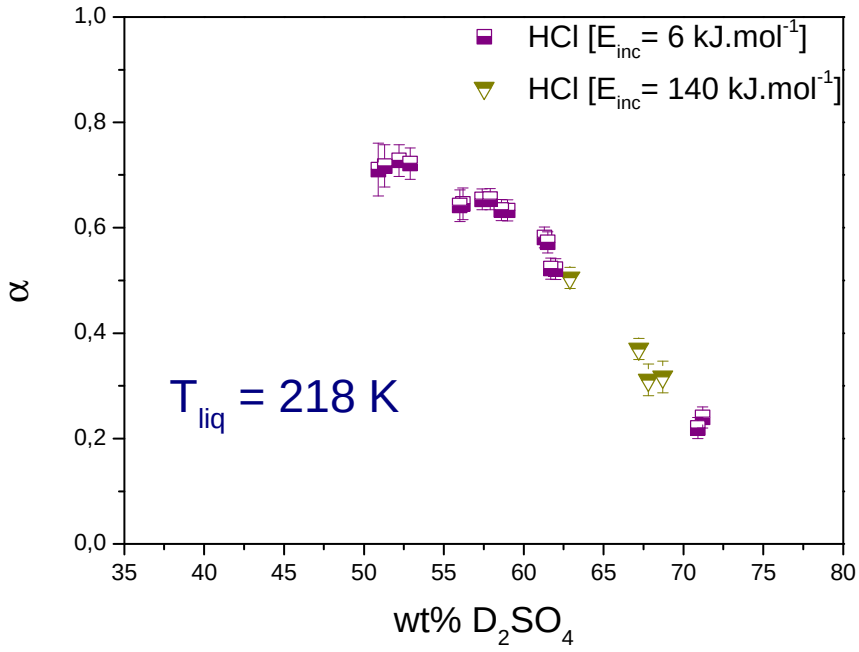

Figure (4.6) The mass accommodation coefficient of HCl as a function of the concentration of sulphuric acid solution in weight percent at 218 K

The figure (4.7) displays a plot of the accommodation coefficient against the concentration of the deuterated sulphuric acid solution in weight percent. The circles, yellow and red triangles are the measurements of the mass accommodation coefficient of HCl at the different temperatures of 213, 218 and 228 K, respectively.

The values of the measured mass accommodation coefficient decrease with increasing concentration of the sulphuric acid solution. Furthermore, there are two different behaviours of the HCl accommodated on the surface of a deuterated sulphuric acid solution. These behaviours are dependent on the concentration and temperature of the solution.

In D_2SO_4/ D_2O concentrations of 50- 65 wt %, the mass accommodation coefficient increases with falling temperature of the sulphuric acid solution. In contrast, the mass accommodation coefficient decreases as the temperature of the sulphuric acid solution becomes lower in the range of concentrations of D_2SO_4 / D_2O of over 65 wt%.

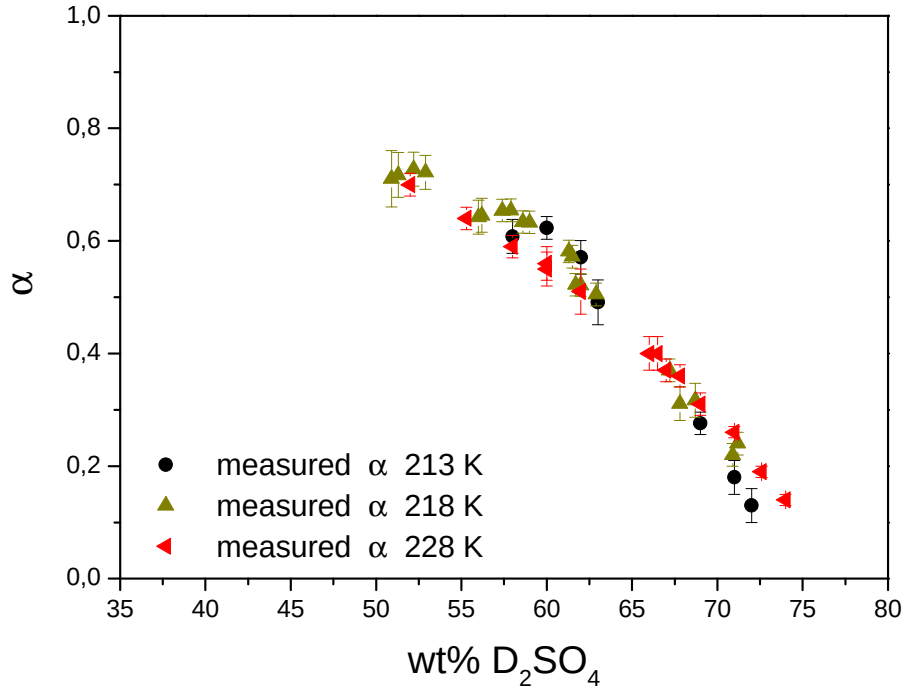

Figure (4.7) The measured mass accommodation coefficient of HCl versus the concentration of sulphuric acid solution in weight percent at 213, 218 and 228 K

4.2 Theoretical analysis using the cavity theory

The first model to describe the uptake of gases by liquids depends on the cavity theory [Pollack, 1991]. In the mid 1980s there was very little experimental information available to aid in the formulation of this model. The prevalent concept of the uptake process assumed that the impinging gas molecules must have sufficient kinetic energy to displace solvent molecules. Additionally, the gas molecules can enter the liquid, only if microscopic cavities of permissible sizes are compatible at the liquid surface near theirs locations. Figure (4.8) illustrates the uptake of HCl molecules by using the cavity model. The accommodation of HCl gas depends on the size of the molecule as well as the size of the cavity, where the uptake of the gas molecule occurs, as described in the figure.

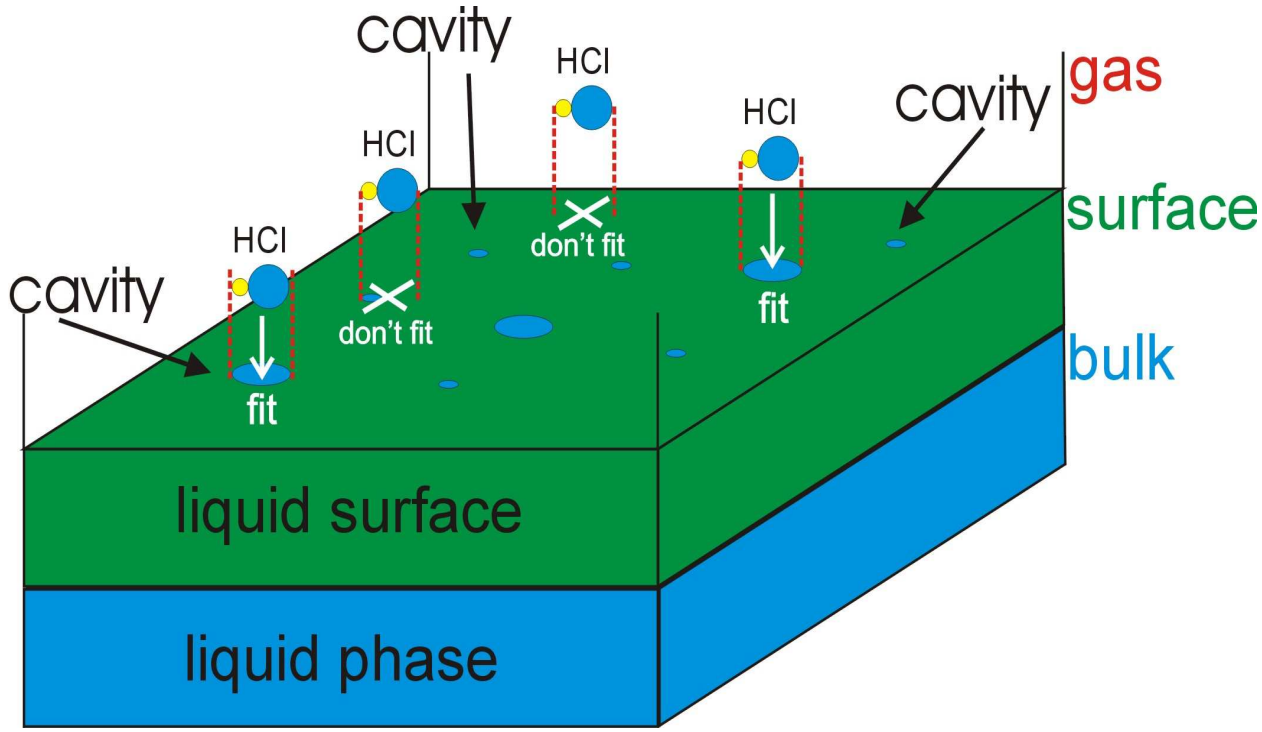

Figure (4.8) The cavity model for uptake gas molecules (HCl) on the liquid surface

Thus, to understand this model, the solvation rate is proportional to the probability of cavity formation, which is proportional to the exponent of the molar free energy of cavity formation in the liquid. This yields the equation:

$$k_{sol} = K \cdot \exp\left(\frac{-\Delta G_{cav}}{RT}\right) \quad \text{Equation (4.2.1)}$$

with:

$$\Delta G_{cav} = \Delta H_{cav} - T\Delta S_{cav} \quad \text{Equation (4.2.2)}$$

where:

ΔG_{cav} : is the molar Gibbs energy of cavity formation in the liquid

ΔH_{cav} : is the enthalpy of cavity formation in the liquid ($\Delta H_{cav} > 0$) [Reid & Sayer, 2003]

ΔS_{cav} : is the entropy of cavity formation in the liquid

The extracted desorption rate from the residence time of gas molecules on the liquid surface and their exit out of it in the gas phase are explained in the following equation:

$$k_{des} = K \cdot \exp\left(\frac{-\Delta G_{surf}}{RT}\right)$$ Equation (4.2.3)

where:

ΔG_{surf} : is the surface free energy of species

K : is the pre- exponential factor

The accommodation coefficient could be computed by the formulation of process as:

$$\frac{\alpha}{1-\alpha} = \frac{k_{sol}}{k_{des}} = \frac{K \cdot \exp\left(\frac{-\Delta G_{cav}}{RT}\right)}{K \cdot \exp\left(\frac{-\Delta G_{surf}}{RT}\right)}$$ Equation (4.2.4)

It will be rewritten as:

$$\frac{\alpha}{1-\alpha} = \exp\left(\frac{-\left(\Delta G_{cav} - \Delta G_{surf}\right)}{RT}\right)$$ Equation (4.2.5)

$$\frac{\alpha}{1-\alpha} = \exp\left(\frac{-\Delta G_{obs}}{RT}\right)$$ Equation (4.2.6)

This conforms with

$$\Delta H_{obs} = \Delta H_{cav} - \Delta H_{surf}$$ Equation (4.2.7)

and

$$\Delta S_{obs} = \Delta S_{cav} - \Delta S_{surf} \qquad \text{Equation (4.2.8)}$$

The calculations above are not suitable with the experimental results from Davidovitz et al. 1996, because the value of the observed enthalpy of the uptake of HCl gas in the sulphuric acid solution is ($\Delta H_{obs} = -58 kJ.mol^{-1}$); conversely, the computed enthalpy of uptake gas is a positive number in regard to the cavity theory.

In fact, this theory cannot describe the HCl gas molecules accommodated into the sulphuric acid solution, because the enthalpy of the cavity formation in the surface of liquid must be higher than zero [Reid & Sayer, 2003].

Therefore, Davidovitz and Nathanson have suggested another model. This model is called the cluster model. It depends on the transition state theory.

4.3 Theoretical analysis using transition state theory (Cluster model)

This theory suggests that the surface of the liquid represents a boundary of the transition region of the gas molecules to dissolve in the liquid by forming continually aggregates (cluster). The impinging gas molecule can be incorporated into the liquid bulk, which depends on the aggregation process with solvent molecules at the interface.

The trace gas reaches the surface of the solvent. Then, the molecules of the solvent form a cluster around the gas molecule. This cluster grows by adding the determining number of the solvent molecules until they form a critical cluster. After that, it merges into the adjacent bulk liquid. The number of molecules, which are required to form the critical cluster is the sum of the gas molecule and the additional number of the solvent molecules.

Thus, the number of the solvent molecules that have to aggregate with the trace gas molecule to form the critical cluster is (N*-1).

Based on the transition state theory, the solvation rate and the desorption rate can be expressed as:

$$k_{sol} = \frac{kT}{h}\exp\left(\frac{-\Delta G_{N*}}{RT}\right) \qquad \text{Equation (4.3.1)}$$

And

$$k_{des} = \frac{kT}{h}\sum_{N=1}^{N*-1}\exp\left(\frac{-\Delta G_{N}}{RT}\right) \qquad \text{Equation (4.3.2)}$$

Or the desorption rate can be written as:

$$k_{des} = \frac{kT}{h}\exp\left(\frac{-\Delta G_{vap}}{RT}\right) \qquad \text{Equation (4.3.3)}$$

Where:

k: is the Boltzmann constant

h: is the Planck constant

ΔG_{N*} : is the free energy which forms critical cluster

ΔG_{N} : is the free energy for each solvent molecule that formed a critical cluster.

ΔG_{vap} : is the free energy of the desorbing molecule from the liquid surface

Therefore, the mass accommodation coefficient may be computed as:

$$\frac{\alpha}{1-\alpha} = \frac{k_{sol}}{k_{des}} = \exp\left(\frac{-\left(\Delta G_{N*} - \Delta G_{vap}\right)}{RT}\right) \qquad \text{Equation (4.3.4)}$$

As a result, the observed free energy is given as:

$$\Delta G_{obs} = \Delta G_{N*} - \Delta G_{vap} \qquad \text{Equation (4.3.5)}$$

The observed Gibbs energy governing the mass accommodation is the difference between the free energy in critical cluster and the Gibbs energy of the vapour.

The observed entropy and enthalpy can be expressed then, respectively, as following:

$$\Delta S_{obs} = \Delta S_{N*} - \Delta S_{vap} \qquad \text{Equation (4.3.6)}$$

$$\Delta H_{obs} = \Delta H_{N*} - \Delta H_{vap} \qquad \text{Equation (4.3.7)}$$

The values of these enthalpies and entropies are always negative and the Gibbs energy barrier at the transition state theory is entropic in nature. The negative value of the entropy shows that the gas molecules dissolve into the liquid [Nathanson et al. 1996].

The figure (4.9) reveals the free energy diagram, which depends on transition state theory.

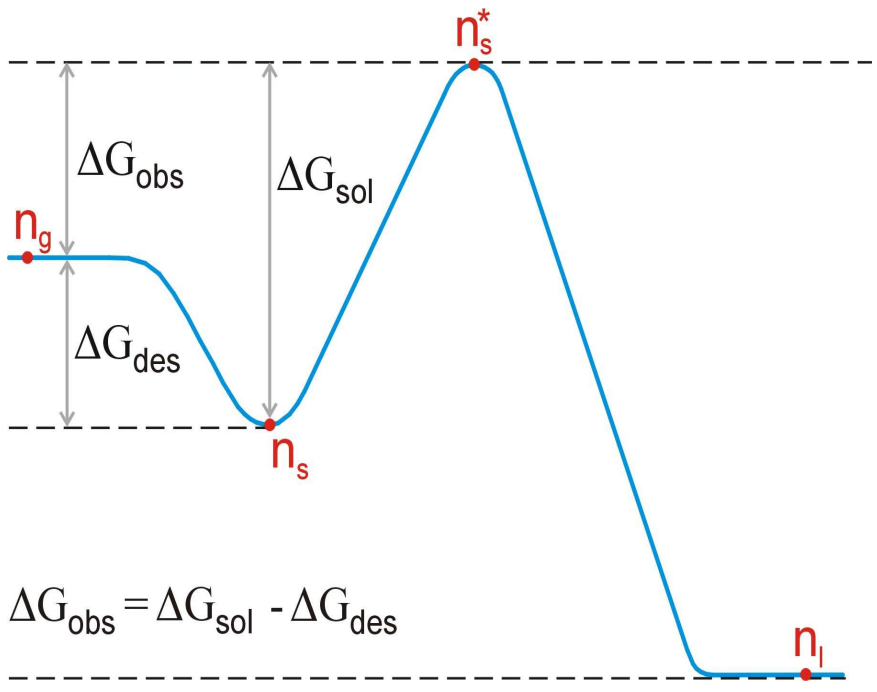

Figure (4.9) Free energy diagram of the critical cluster model

This Cluster model can be explained through two different mechanisms which are used to describe the transfer of the gas molecules from the gas phase to the condensed phase.

The first mechanism involves two stages of the uptake process, which are illustrated in this chemical equation [Davidovits et al. 1995]:

$$n_g \underset{k_{des}}{\overset{k_{ads}}{\rightleftharpoons}} n_s \xrightarrow{k_{sol}} n_l \qquad \text{Reaction (4.3.1)}$$

The gas molecule is first adsorbing at the surface of the liquid. The adsorbing molecule can either desorb from the interface and return back to the gas phase or transfer into the liquid phase.

k_{ads}: is the adsorption rate constant ($m.s^{-1}$)

k_{des}: is the desorption rate constant ($m.s^{-1}$)

k_{sol}: is the solvation constant (s^{-1})

Figure (4.10) illustrates the mechanism of the gas uptake in the liquid by using a two stages process. The adsorption and desorption as the first step and the solvation as the second step.

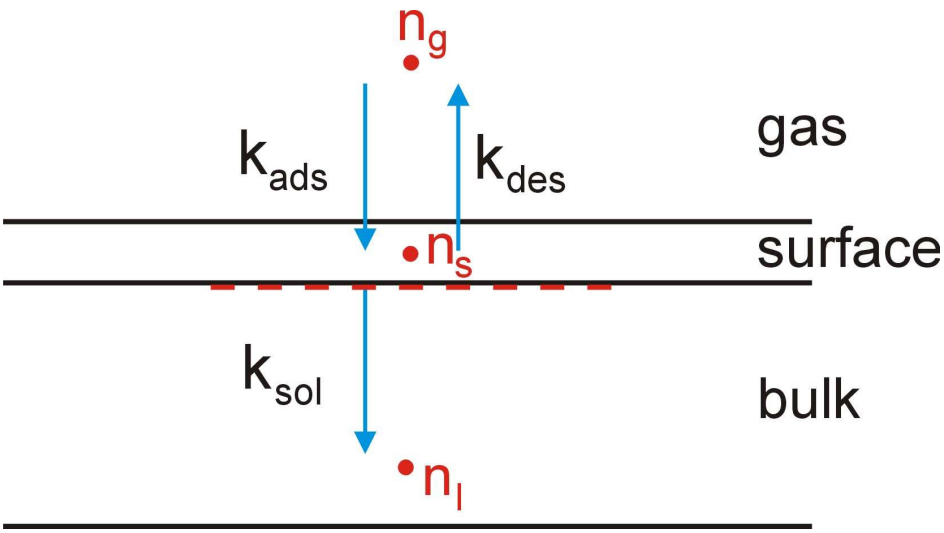

Figure (4.10) The mechanism with two stages uptake process

The maximum possible net flux of the gas molecules into the liquid is:

$$F_P = \frac{\alpha n_g \bar{v}}{4} \qquad \text{Equation (4.3.8)}$$

The net flux of incoming molecules on the surface is:

$$F_{net} = \frac{s n_g \bar{v}}{4} - k_{des} n_s \qquad \text{Equation (4.3.9)}$$

The solvation flux of adsorbing molecules into the bulk of the liquid:

$$F_{sol} = k_{sol} n_s \qquad \text{Equation (4.3.10)}$$

Considering the accommodation coefficient, the maximum possible net flux must be equal to the difference between the sticking flux on the surface and the desorbing flux from it, thus:

$$\frac{\alpha n_g \bar{v}}{4} = \frac{s n_g \bar{v}}{4} - k_{des} n_s \qquad \text{Equation (4.3.11)}$$

The maximum possibility net flux is also equal to the solvation flux in absence of the gas diffusion:

$$\frac{\alpha n_g \bar{v}}{4} = k_{sol} n_s \qquad \text{Equation (4.3.12)}$$

Combining these two equations above to eliminate n_g and n_s give:

$$\frac{\alpha}{s-\alpha} = \frac{k_{sol}}{k_{des}} \qquad \text{Equation (4.3.13)}$$

Under the atmospheric condition, the sticking coefficient is close to or equal to unity, thus:

$$\frac{\alpha}{1-\alpha} = \frac{k_{sol}}{k_{des}} \qquad \text{Equation (4.3.14)}$$

The rate constants are replaced by using the appropriate expression for Gibbs energy, as shown in the free energy diagram (4.11):

$$\frac{\alpha}{1-\alpha} = \frac{k_{sol}}{k_{des}} = \exp\left(\frac{-\Delta G_{sol}}{RT}\right) \Big/ \exp\left(\frac{-\Delta G_{des}}{RT}\right) = \exp\left(\frac{-\left(\Delta G_{sol} - \Delta G_{des}\right)}{RT}\right) \qquad \text{Equation (4.3.15)}$$

From this could be analyzed:

$$\frac{\alpha}{1-\alpha} = \exp\left(\frac{-\Delta G_{obs}}{RT}\right) \qquad \text{Equation (4.3.16)}$$

where:

The solvation Gibbs energy is equal to the free energy of the formation of a critical cluster size ($\Delta G_{sol} = \Delta G_{N^*}$).

The desorption free energy is equal to the sum of the free energy of each water molecule that is disintegrated from a gas molecule ($\Delta G_{des} = \Delta G_{vap} = \sum_{N=1}^{N^*-1} \Delta G_N$).

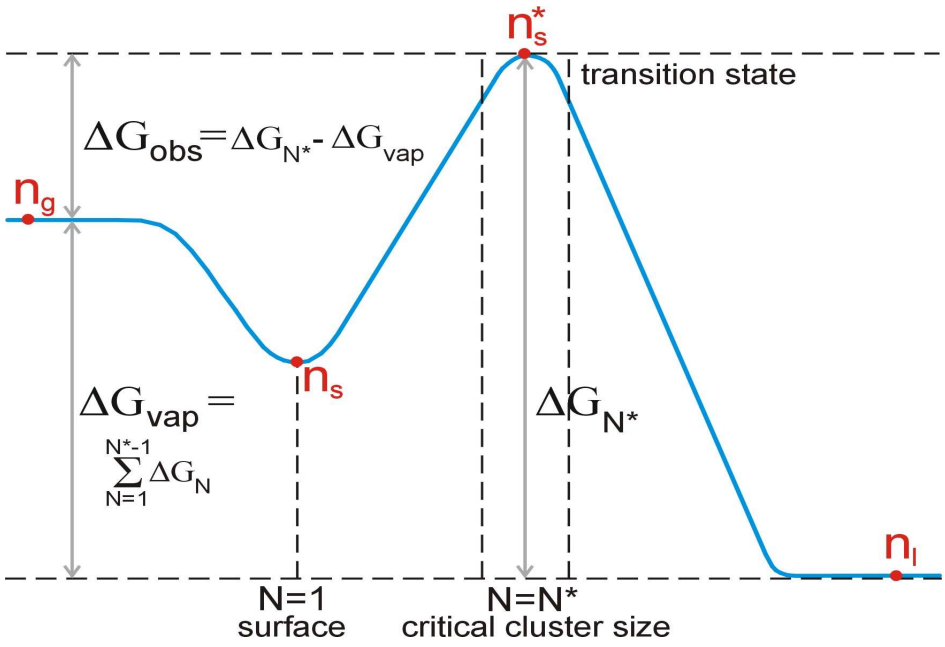

Figure (4.11) Free energy diagram two steps mechanism

The second mechanism involves a three- stages gas uptake process, it is similar to the first mechanism but it has an additional step, which is the formation of a critical cluster, that can be described in the following equation [Nathanson et al. 1996]:

$$n_g \underset{k_{des}}{\overset{k_{ads}}{\rightleftarrows}} n_s \underset{k_{vap,s}}{\overset{k_s}{\rightleftarrows}} n_s^* \xrightarrow{k_{sol}} n_l \qquad \text{Reaction (4.3.2)}$$

The gas molecule adsorbs on the surface of the liquid and then aggregates with water molecules to form the critical cluster, which can either be dissolved into a liquid bulk or disintegrated from the water molecules and desorb as a gas molecule. This mechanism will only be described the mechanism only by using the Gibbs energy to result from it the accommodation coefficient.

The rate of critical cluster formation at the interface is:

$$k_s = \frac{kT}{h} \exp\left(\frac{-\Delta G^*}{RT}\right) \qquad \text{Equation (4.3.17)}$$

where:

$$\Delta G^* = \Delta G_s^* - \Delta G_s$$ Equation (4.3.18)

ΔG_s^* : is the free energy of the dissolving critical cluster

ΔG_s : is the free energy of dissolving molecule from the surface into the liquid bulk

ΔG^* : is the free energy of the forming critical cluster with the adsorbing molecule on the surface.

The rate of the disintegration of the critical cluster at the interface is:

$$k_{vap,s} = \frac{kT}{h}\exp\left(\frac{-\Delta G_{vap,s}}{RT}\right)$$ Equation (4.3.19)

when:

$$\Delta G_{vap,s} = \Delta G_{vap} - \Delta G_s$$ Equation (4.3.20)

ΔG_{vap} : is the free energy of the evaporation from the liquid to the gas phase

$\Delta G_{vap,s}$: is the free energy of the gas phase molecules

The thickness of the interface is δ, in which the critical clusters are formed, as shown in the figure (4.12) below.

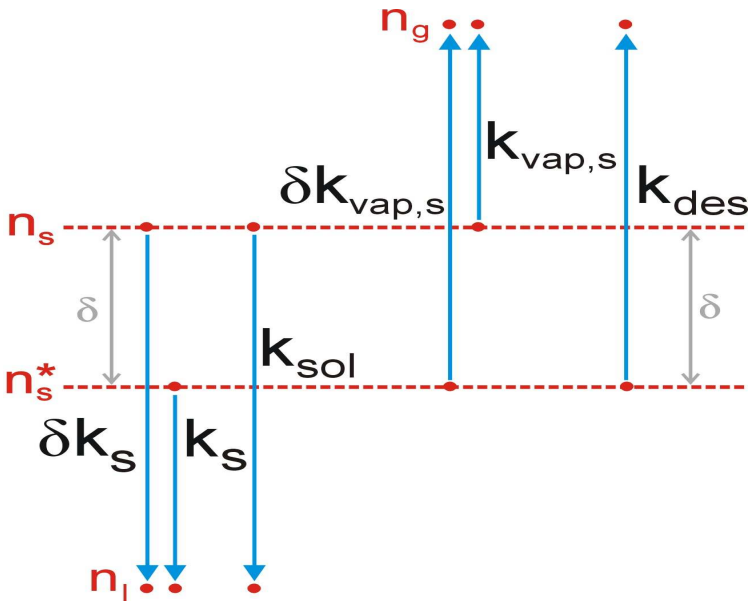

Figure (4.12) Schematic view of the adsorbing molecules from the critical cluster model

The rate of solvation of gas molecule through the formation of a critical cluster is:

$$k_{sol} = \delta.k_s = \delta.\frac{kT}{h}\exp\left(\frac{-\Delta G^*}{RT}\right)$$ Equation (4.3.21)

The rate of the desorbing gas molecule through disintegration of the critical cluster is:

$$k_{des} = \delta.k_{vap,s} = \delta.\frac{kT}{h}\exp\left(\frac{-\Delta G_{vap,s}}{RT}\right)$$ Equation (4.3.22)

The accommodation coefficient which depends on the critical cluster model can be extracted by calculating the ratio of the rate of the solvation constant and by dividing of the rate of the desorption constant:

$$\frac{\alpha}{1-\alpha} = \frac{k_{sol}}{k_{des}} = \exp\left(\frac{-\left(\Delta G^* - \Delta G_{vap,s}\right)}{RT}\right)$$ Equation (4.3.23)

The observed free energy can be determined from the equation:

$$\Delta G_{obs} = \Delta G^* - \Delta G_{vap,s}$$ Equation (4.3.24)

The diagram of the observed Gibbs energy in this model is illustrated in figure (4.13).

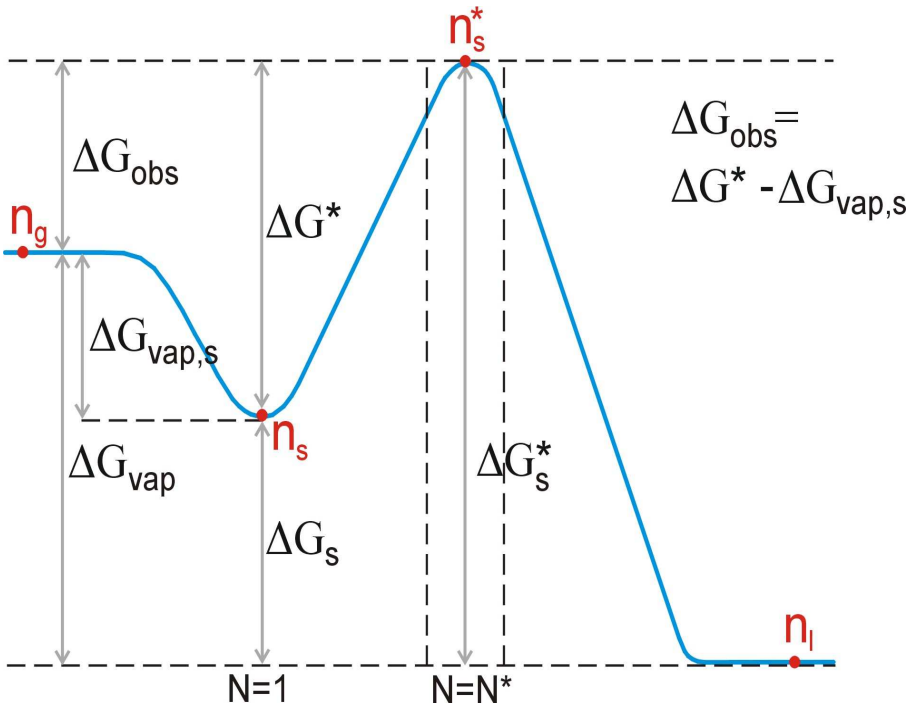

Figure (4.13) Diagram of free energy for a three steps mechanism

Hence, the experimental enthalpy and entropy can be described by using the critical cluster model. For example, HCl gas molecule aggregates at the surface with three or four molecules of water to form the critical cluster, which dissolves in the sulphuric acid solution.

As illustrated in figure (4.14), there are three cases of the mass accommodation coefficient of HCl in the sulphuric acid solution. These three cases depend on the value of the Gibbs free energy for the solvation of HCl in the sulphuric acid solution. In addition, the change in values of the Gibbs energy depends on the concentration of the sulphuric acid solution.

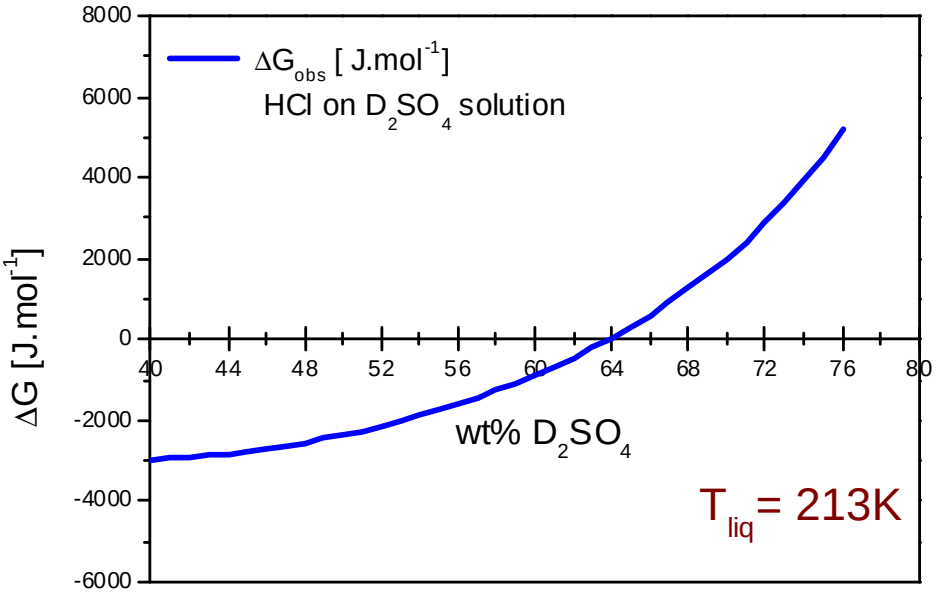

Figure (4.14) Diagram of Gibbs free energy versus the concentration of sulphuric acid

These three cases can be presented as follows:

At concentrations of the sulphuric acid solution between (40- 64 wt%), the free energy of HCl, which dissolves into the sulphuric acid solution is negative. This means that the solvation rate is higher than the desorption rate of HCl from the liquid surface.

At concentrations of the sulphuric acid solution equal to 64 wt%, the free energy of the HCl accommodated into the sulphuric acid solution is equal to zero, thus the solvation rate is equal to the desorption rate.

When the concentrations of the sulphuric acid solution are above of 65 wt%, the Gibbs energy of the HCl that dissolves in the sulphuric acid is positive. Therefore, the desorption rate is higher than the solvation rate of HCl in the bulk of the sulphuric acid solution.

The thermodynamic model can well explain the reduction of the mass accommodation coefficient of HCl as the concentration of sulphuric acid increases. This reduction is caused by the decreasing number of water molecules on the surface of the liquid with increasing concentration of a D_2SO_4/ D_2O solution. In other words, the number of the critical cluster depends on the number of water molecules on the liquid surface.

As described above, the ability to form the critical cluster reduces as the concentration of the sulphuric acid solution increases.

4.4 Theoretical analysis using the capillary wave theory

The capillary wave theory describes the thermodynamic model, which was suggested by Davidovitz and Nathanson, as a dynamic model depending on the transition state theory. The supposition of capillary wave theory is associated with the continuously thermal motion of surface molecules that is related with capillary waves.

The local mode gives an exact description of a sticking gas molecules on the surface of liquid as well as an immediate incorporation of these molecules into the under-layer at the surface level. The both processes of sticking and immediately solvation can perform the mass accommodation coefficient of the gas molecules at the interface gas- liquid [Behr et al. 2009].

In the first point, the dynamic process of the penetration of the gas molecule into the liquid according to the local mode capillary wave theory in order to understand the yield of the mass accommodation coefficient.

The progressive stages of the accommodation are explained from the adsorption to the solvation as following:

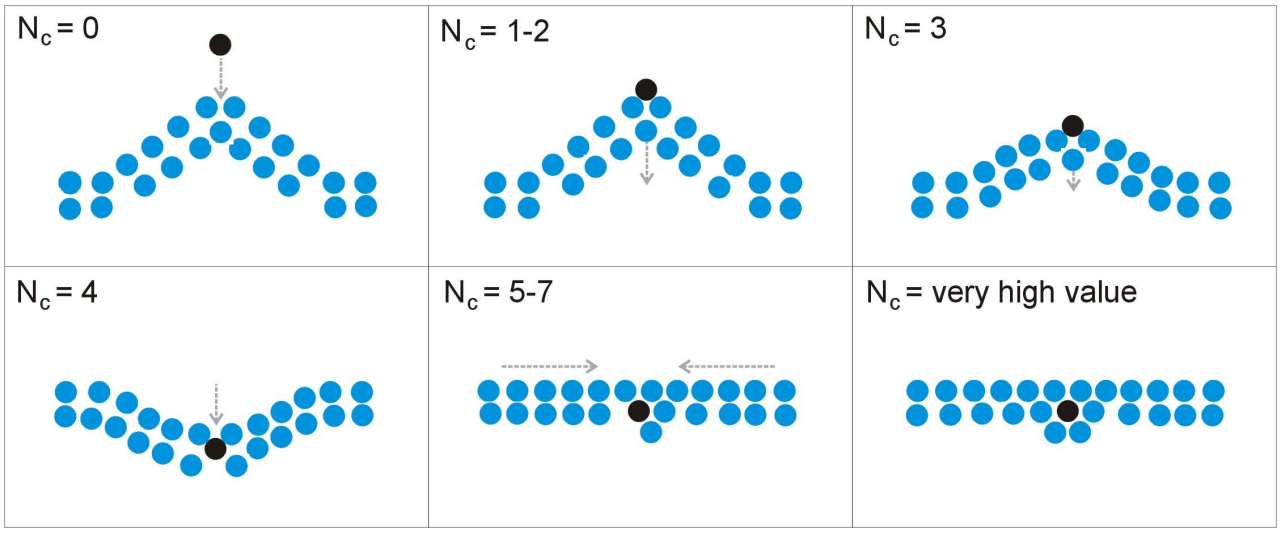

Figure (4.15) Scheme of the accommodation process depending on local mode capillary wave theory

The gas molecule sticks with the solvent molecule at the sharp- point wavelet, the coordinate number in this case is one or two. The gas molecule is pulled on the surface of the liquid by a downward motion of the capillary wave, the coordinate number increases to about three or four. Then the capillary wave is moving under the mean surface (planar surface) and taking the solute molecule into the under- layer of the liquid surface. In this case, the coordinate number has its maximum value. This progression from sticking on the surface to the solvation into the liquid body is the mass accommodation of the solute molecule in solvent condition.

The coordination number, as described in this theory, is equivalent to the number of liquid molecules that are surrounding and in contact with the gas molecule. The maximum value of the coordinate number points out that the solute molecule is

penetrated into the bulk liquid. Figure (4.15) shows an illustration of the progression from the adsorption to the solvation.

The local mode capillary wave theory describes the downward motion of the superposition local mode, which excites by thermal oscillation of the capillary wave. The solute molecules can penetrate into the solvent bulk at the width interface (capillary wave width) through the downward motion.

The local mode capillary wave model gives an excellent example of an investigation of reducing the mass accommodation coefficient of hydrogen chloride with increasing the concentration of super cold binary solution through the fall time of the capillary wave, which has a physical acceptability, as will be pointed out later.

The capillary wave spectrum in local mode is the product of the Bessel function with a time dependent function, which is given as [Phillips 2004a, 2004b, 2005]:

$$\zeta_l = A_l \cdot \left[1 - \exp\left(\frac{-t}{\tau_{rise}}\right)\right] \exp\left(\frac{-t}{\tau_{fall}}\right) \cdot J_0(kr) \quad \text{Equation (4.4.1)}$$

ζ_l: is the continuously displacement of the molecules on the membrane of the capillary wave

A_l: is the amplitude factor, in case of accommodation this value should be negative

τ_{fall}: is the fall time of capillary wave, which is given as:

$$\tau_{fall} = \frac{2\eta}{k\gamma} \quad \text{Equation (4.4.2)}$$

where:

η: is the viscosity coefficient [mPa.s]

k: is the wave vector [m^{-1}]

γ : is the surface tension [mN.m^{-1}]

τ_{rise} : is the rise time of capillary wave, where it can be expressed as;

$$\tau_{rise} = \frac{\rho}{2k^2\eta} \qquad \text{Equation (4.4.3)}$$

Where:

ρ : is the density of liquid [g.cm^{-3}]

If accommodation takes place, the value of the wave vector must be very high to change the harmonic motion of the local mode of the capillary wave to anharmonic motion. This happens when the capillary waves need more time to fall into the liquid bulk than to rise from the planar surface of the liquid.

The accommodation coefficient of the gas molecule into the bulk liquid is expressed as:

$$\alpha = S \cdot \frac{k_{sol}}{k_{sol} + k_{des}} \qquad \text{Equation (4.4.4)}$$

The sticking coefficient is equal to unity, in the case of mid layer stratosphere. Then the accommodation coefficient can be rewritten as [Davidovits et al. 2006]:

$$\alpha = \frac{k_{sol}}{k_{sol} + k_{des}} \qquad \text{Equation (4.4.5)}$$

The desorption rate of HCl gas from the ice surface can be presented as [Isakson & Sitz, 1999]:

$$k_{des} = \nu_{des} \cdot \exp\left(\frac{-E_{des}}{RT}\right)$$ Equation (4.4.6)

where:

E_{des} : is the activation kinetic energy for the HCl desorption, $E_{des} = 28\,kJ\,.mol^{-1}$

ν_{des} : is the pre exponential factor, $\nu_{des} = 2\times10^{+14}\,s^{-1}$

However, this desorption rate does not take into account the acidity of the sulphuric acid. In contrast, it depends on the temperature of surface. The value of the desorption rate becomes higher with the increase of the temperature of the liquid. Based on the capillary wave theory, this rate can be computed with inserting the angular cosine square factor, because the previous desorption rate was determining the desorbing molecules from the solid surface. Therefore this equation can be improved:

$$k_{des} = \nu_{ads} \cdot \exp\left(\frac{-E_{ads} \cdot \cos^2\theta}{RT}\right)$$ Equation (4.4.7)

The values of the desorption rate in three different temperatures are illustrated in figure (4.18).

The solvation rate of the gas molecules can be calculated based on the local mode of the capillary wave theory. This rate is equal to inverse proportional of fall time in local mode as presented [Behr et al. 2009]:

$$k_{sol} = \frac{1}{\tau_{fall}}$$ Equation (4.4.8)

Combining the equations (4.4.2) and (4.4.8), the solvation rate can be represented as:

$$k_{sol} = \frac{k\gamma}{2\eta}$$ Equation (4.4.9)

In the case of accommodation, the wave vector (k) is equal to ($3.14\times10^{+9} m^{-1}$) and the wave length (λ) is equal to ($2\times10^{-8} cm$). The wave length is very short and the capillary wave is damped by the viscosity of solution (local mode).

According to Williams and Long (1994), the viscosity of sulphuric acid can be calculated at temperatures of 213, 218 and 228 K for concentrations of between 40-75 wt%. As illustrated in figure (4.16) the viscosity of sulphuric acid above 64 wt% increases very rapidly. The high values of the viscosity play an important role in reducing the solvation rate of HCl in the sulphuric acid solution.

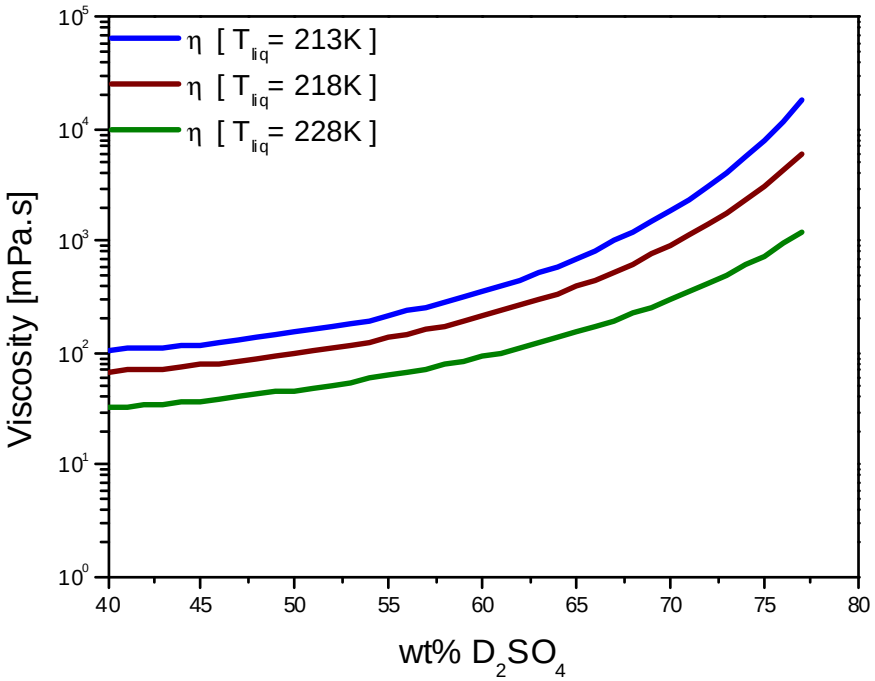

Figure (4.16) Diagram of the viscosity of the sulphuric acid versus the weight percent concentration of sulphuric acid at 213, 218 and 228 K

From equation (4.4.9) it can be concluded that the surface tension of the sulphuric acid may be computed by three different models. These models are from Sabinina (1935), Tabazadeh (2000) and Myhre (1998). The Myhre model accords mostly with the results of the mass accommodation coefficient, which is measured by using the molecular beam technique. In the following, this model will be presented to calculate the surface tension of sulphuric acid. The model simulates the surface tension of the aqueous sulphuric acid, which is based on many other measurements and takes into account the parameterization, which is used to calculate the surface tension of the sulphuric acid solution under the experimental conditions.

The equation of surface tension of aqueous sulphuric acid is given as:

$$\gamma(w,T) = \sum_{i=0}^{7}\sum_{j=0}^{3} \gamma_{i,j} \cdot w^i \left(T - 273.15\right)^j \quad \text{Equation (4.4.10)}$$

where:

$\gamma(w,T)$: is the surface tension as a function of concentration and temperature

w: is the mass fraction of the sulphuric acid

$\gamma_{i,j}$: is the coefficient's temperature parameter, which is listed in the table below (4.1):

Table (4.1):

$\gamma_{i,j}$	j = 0	1	2	3
i = 0	75.640 X 10^{-3}	-13.818 X 10^{-5}	-31.807 X 10^{-8}	
1	23.033 X 10^{-4}	-35.768 X 10^{-4}	26.948 X 10^{-5}	-38.605 X 10^{-7}
2	12.516 X 10^{-2}	55.742 X 10^{-2}	-39.071 X 10^{-4}	55.691 X 10^{-6}
3	-12.516 X 10^{-1}	-30.759 X 10^{-2}	21.360 X 10^{-3}	-30.419 X 10^{-5}
4	-42.193 X 10^{-1}	83.258 X 10^{-2}	-57.881 X 10^{-3}	82.448 X 10^{-5}
5	64.995 X 10^{-1}	-11.910 X 10^{-1}	83.310 X 10^{-3}	-11.865 X 10^{-4}
6	-47.546 X 10^{-1}	86.407 X 10^{-2}	-60.908 X 10^{-3}	86.653 X 10^{-5}
7	13.185 X 10^{-1}	-24.979 X 10^{-2}	17.746 X 10^{-3}	-25.204 X 10^{-5}

Figure (4.17) shows the surface tensions for three different temperatures and different concentrations, which are computed by using the Dolphin program.

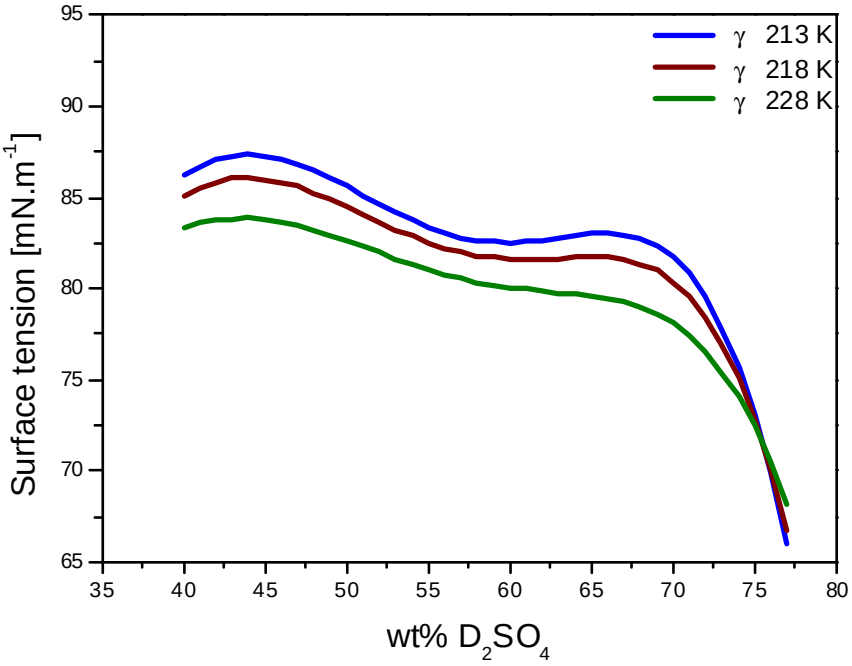

Figure (4.17) Diagram of the surface tension versus sulphuric acid concentration at 213, 218 and 228 K

In the case of low concentrations of sulphuric acid, the values of the desorption rate become smaller than those of the solvation rate at three different temperatures. This framework is shown in figure (4.18). The dashed curves are the calculated solvation rate of HCl in the sulphuric acid solution in regard to the capillary wave theory. The solid lines are the desorption rate of HCl molecules from the D_2SO_4 / D_2O solution, which is calculated using the equation (4.4.7) at the three temperatures of 213, 218 and 228 K. The molecules dissolve faster in the liquid than they desorb from it. That means the velocity of transfer molecules in the liquid is higher than the speed of desorbing molecules from the surface of the liquid. Hence, the accommodation coefficient is determined through the speed of desorption. In other words, the desorption rate is stronger influenced by the temperature than the solvation rate.

The mass accommodation coefficient decreases with the increase of temperature as well as with higher values of concentration of the sulphuric acid. This process is presented in figure (4.19).

At concentrations between 65- 66 wt% of sulphuric acid, the desorption rate is equal to the solvation rate ($k_{sol} = k_{des}$). That is predicted in figure (4.18).

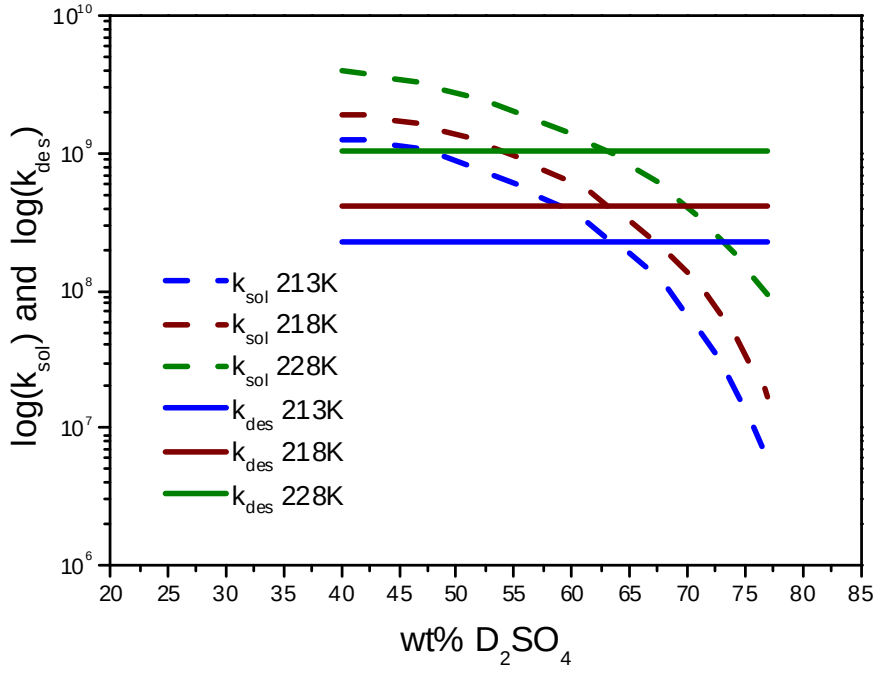

Figure (4.18) The logarithms of desorption and solvation rates versus the weight per cent of the concentration of the sulphuric acid at temperatures of 213, 218 and 228K

The transfer velocity of the molecules into the solution is the same as the desorbing speed of the molecules from the surface. In this case, the accommodation of the gas molecules is affected by this equilibrium situation between the desorbing and dissolving molecules. Therefore, the accommodation coefficient is independent from the temperature of the liquid and it has the same value ($\alpha = 0.45$). This is illustrated in figure (4.19). At the point of intersection of the isotherm the mass accommodation coefficient curves at the concentration of the sulphuric acid of between 65- 66 wt%.

In the case of high concentrations of the solution of over 67 wt%, the figure (4.18) shows that the values of the desorption rate are higher than these of the solvation rate. The speed of the dissolving gas molecules is slower than the speed of the desorbing molecules from the surface of the liquid. The viscosity of the sulphuric acid

becomes higher, when the concentration of the sulphuric acid increases in the solution as well as, when the temperature of the solution decreases. Hence, the transfer of molecules in the liquid at a higher temperature and a lower concentration of the sulphuric acid solution is better than that which is on inverse conditions.

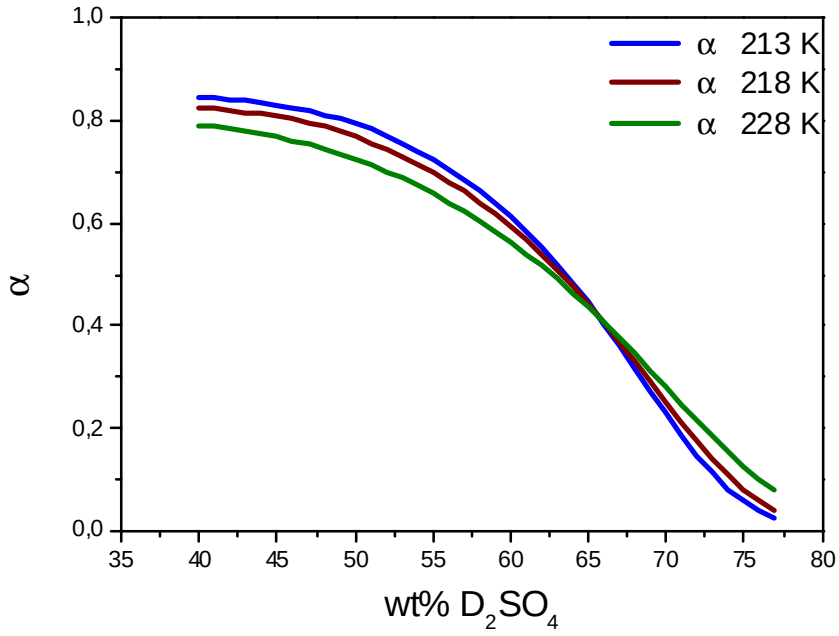

Figure (4.19) The diagram of the accommodation coefficient as a function of the concentration of sulphuric acid at 213, 218 and 228 K

Taking into account the velocity of transfer molecules in the sulphuric acid solution and the dynamic of the capillary waves in local mode, the accommodation coefficient increases as the temperature of the sulphuric acid increases, as shown in figure (4.19). The reason for that condition is that the solvation rate is stronger influenced by the temperature than the desorption rate.

The measured and calculated values of the mass accommodation coefficient of HCl for each temperature of 213, 218 and 228 K will be presented separately. After that, the temperature effect on the mass accommodation coefficient will be outlined.

Figure (4.19) is a plot of the mass accommodation coefficient versus the concentration of the sulphuric acid solution at the temperature of 213 K. The black points and gray stars are the measured (α) of HCl with an incident energy of 6 kJ.mol^{-1} and 140 kJ.mol^{-1}, respectively. The measured mass accommodation coefficient associates with the calculated one, which is based on the local mode of the capillary wave theory, as illustrated above. Overall and as a result, the mass accommodation coefficient of the HCl gas on the surface of the sulphuric acid solution can be described and calculated through the capillary wave theory in the range of concentrations of between (40- 75 wt%).

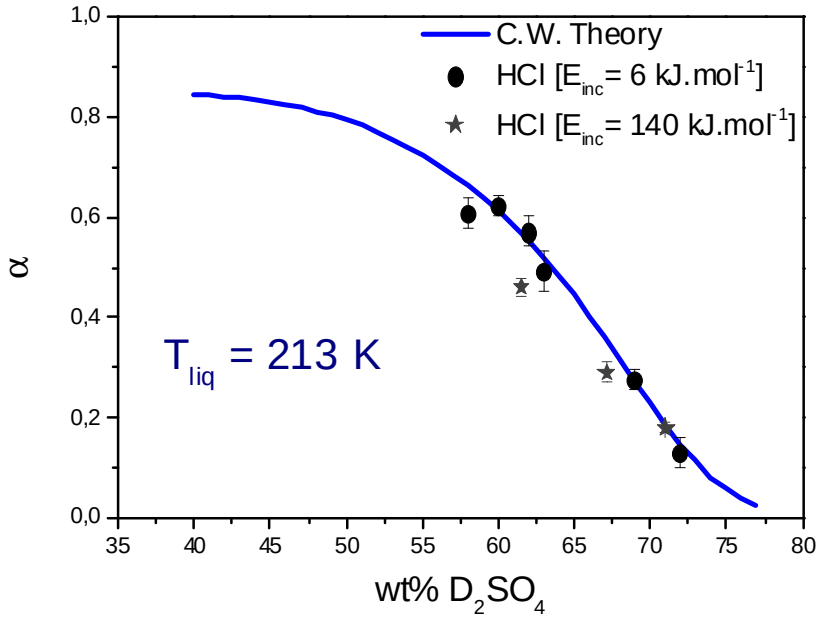

Figure (4.20) The accommodation coefficient of HCl versus the weight percent of deuterated sulphuric acid solution at temperature 213 K

A plot of mass accommodation coefficient of HCl against the concentration of the sulphuric acid is illustrated in the following figure (4.21). The values of (α) are extracted empirically through the comparison of thermal desorption intensities of DCl and these of HCl at the temperature of 218 K of the sulphuric acid. The squares and triangles are the measurements of the accommodation coefficient of HCl with the incident energy 6 kJ.mol^{-1} and 140 kJ.mol^{-1}, respectively. The brown solid curve is the calculated mass accommodation coefficient according to the capillary wave theory at the temperature of 218 K.

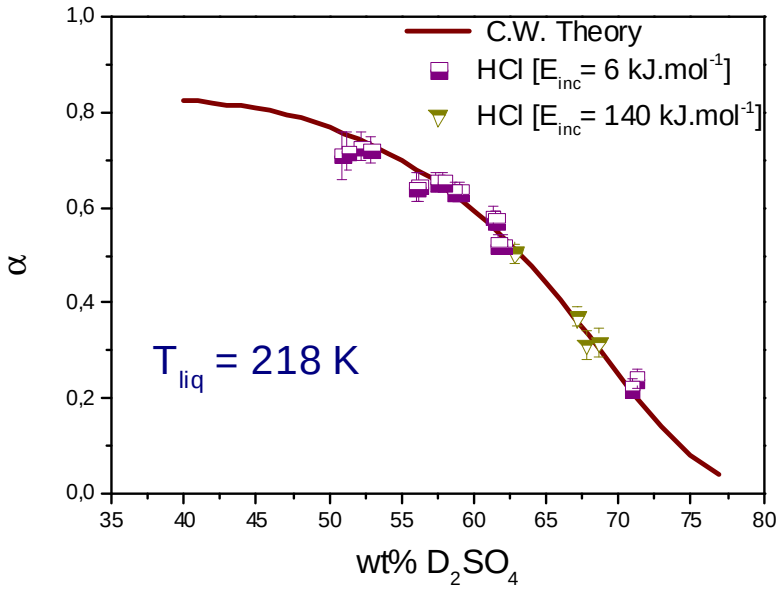

Figure (4.21) The diagram of (α) of HCl versus the concentration of the sulphuric acid at the temperature of 218 K

The results correspond very well with the theoretical values of the mass accommodation coefficient based on the capillary wave theory. The collision energy of HCl molecules has no effect on the values of the mass accommodation coefficient, because the molecules that thermally equilibrate at the surface undergo an ($H \rightarrow D$) exchange. The accommodation coefficient decreases with increasing the concentration of the sulphuric acid solution at a temperature of 218 K the same happens at a temperature of 213 K.

The figure (4.22) shows that the measured value of (α) for the HCl gas molecules with the incident energy of 6 kJ.mol^{-1} accords with the calculated value of the mass accommodation coefficient at the temperature of 228 K. As a result, the capillary wave theory gives a good example of how to describe the behaviour of the HCl gas molecules which are accommodated on and into the surface of the deuterated sulphuric acid solution. As outlined above, the solvation of the HCl gas molecules depends on the dynamic of the surface molecules.

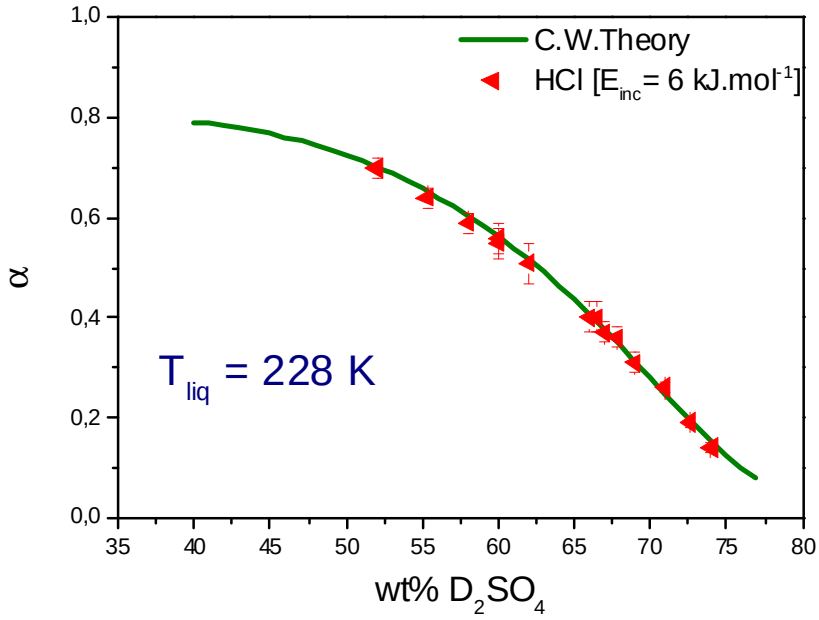

Figure (4.22) The accommodation coefficient is as a function of the concentration of the sulphuric acid at the temperature of 228 K

These surface molecules oscillate faster at the lower concentration of the sulphuric acid than at the higher concentration, because the solution's viscosity has an effect on their motion. This means, when the concentration of the sulphuric acid increases, the oscillation's velocity of the surface molecules is damped sharply through the increasing viscosity. Therefore, the accommodating molecules in the surface decrease with an increase of the concentration of the sulphuric acid at the constant of the solution's temperature.

The calculated isothermal values of the mass accommodation coefficient and the measured ones are displayed as solid lines as well as points, respectively, in figure (4.23), at the different temperatures of 213, 218 and 228 K. The results demonstrate that the values of the ($H \rightarrow D$) exchange fraction increases with the reduction of the temperature of sulphuric acid solution in the range of a concentration of between (40-64 wt %). For example, at the concentration of sulphuric acid of 62 wt%, the measured values of the mass accommodation coefficient are 0.51, 0.54 and 0.57 at the temperatures of 228, 218 and 213 K, respectively. In contrast, the empirical values of the mass accommodation coefficient of HCl are 0.28, 0.24 and 0.18 at the

temperatures of 228, 218 and 213 K, respectively, at the concentration of the sulphuric acid solution of 71 wt%. Therefore, the values of the accommodation coefficient increase with increasing temperature of the sulphuric acid solution in the range of the concentrations of between (67- 78 wt %).

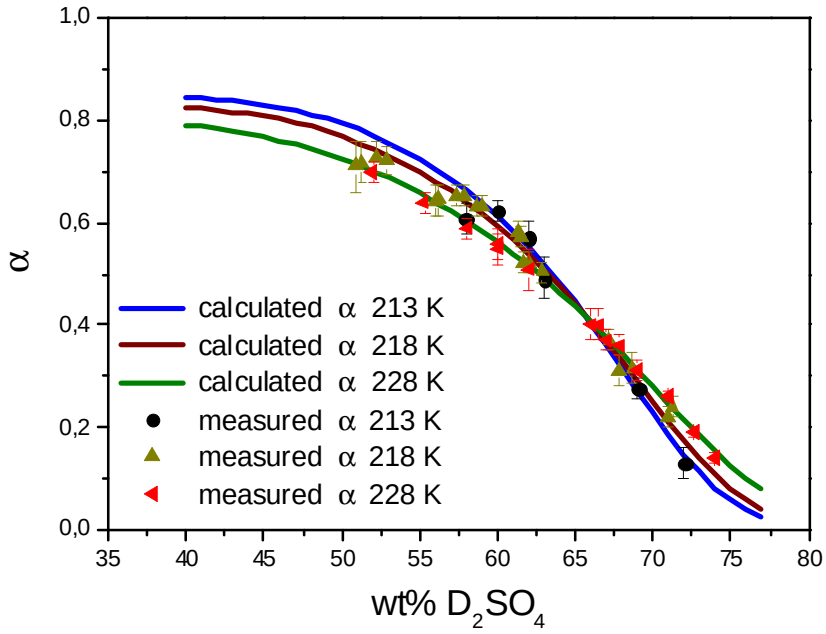

Figure (4.23) The diagram of isotherm calculated and measured (α) of HCl versus the concentration of the sulphuric acid at the temperature of 213, 218 and 228 K

Overall and as illustrated previously, on the one hand, the mass accommodation coefficient is limited through the desorption rate (k_{des}) of HCl from the surface of the sulphuric acid in the case of lower concentrations of the sulphuric acid of between (40- 64 wt %). On the other hand, the solvation rate (k_{sol}) affects the mass accommodation coefficient at higher concentrations of the sulphuric acid of between (67- 75 wt %).

5. The residence time of HCl in a D_2SO_4 / D_2O solution

The residence time of HCl gas in the bulk of the D_2SO_4 solution is measured by the comparison of the pre- chopper TOF spectra and the TOF spectra of the post-chopper. Both of these TOF spectra are observed the DCl desorbing molecules, where the exchange reaction ($H \rightarrow D$) has occurred in the bulk of the D_2SO_4 solution. After that, the experimental results of the residence time of HCl will be compared respectively to the calculated residence time according to the following models: the Tabazadeh model, the Carslaw model and the capillary wave theory model.

The calculated residence time which is based on the two different values of the Henry's law constant is named the solubility residence time, which is computed with the aid of the Tabazadeh model and the Carslaw model. Furthermore, the calculated residence time based on the capillary wave theory is named the time constant of the transport of HCl gas into the sulphuric acid solution.

5.1 Experimental data

The pre- and post- chopper TOF spectra will be presented first in order to extract the residence time of HCl gas molecules in the deuterated sulphuric acid solution. These TOF spectra for DCl (after they have undergone an exchange reaction) are compared in order to determine the residence time, as outlined in (section 2). Moreover, the results of the residence time will be compared with other previous measurements. After that, the measured values of the residence time of HCl in the sulphuric acid solution will be outlined at three different temperatures of 213, 218 and 228 K.

Figure (5.1) reveals the pre- and post- chopper spectra for DCl, which thermally desorb from the deuterated sulphuric acid of 70 wt% at temperature of 218 K. The measured DCl pre- and post- chopper signals are presented as red and black

squares. The calculated curve corresponds to the DCl post- chopper spectrum at the residence time of (0 µs), because the start time of this spectrum begin after the molecules desorb from the surface.

In contrast, the best calculated curve corresponds to the DCl pre- chopper spectrum at the residence time of 130 µs. The start time of this spectrum begins before the molecules strike the liquid surface. The reduction in intensity as well as the shift in arrival time for the pre- chopper spectrum is due to the residence time of the HCl molecules, which impinge the surface before they desorb as DCl. In this case, the HCl gas molecules need 130 µs in order to be transported into the solution, to dissolve in the solution, to undergo exchange reactions and desorb from the surface of the sulphuric acid at the concentration of 70 wt%.

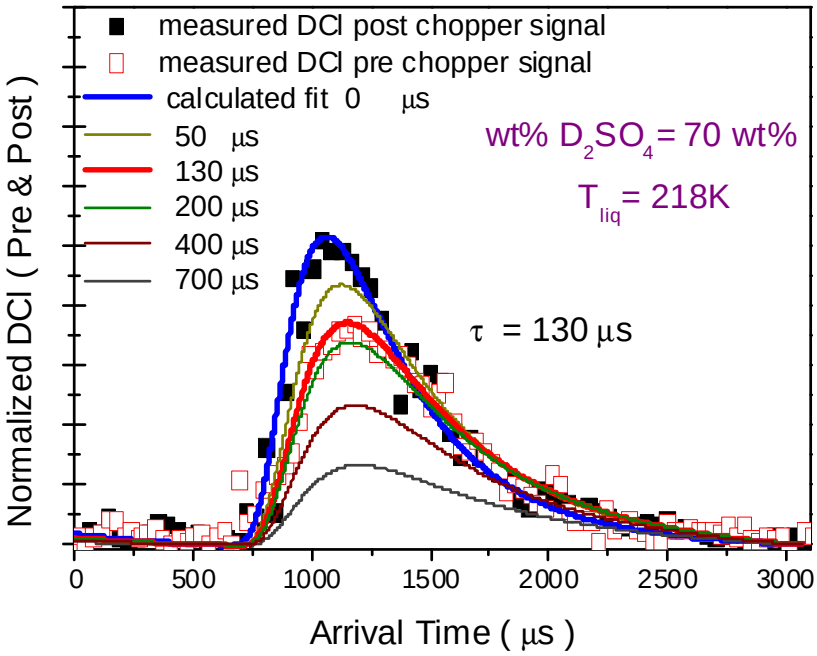

Figure (5.1) Pre- and post- chopper spectrum of DCl desorbing molecules from the D_2SO_4 solution in the concentration of 70 wt% and at the temperature of 218 K, the residence time is 130 µs

The calculated fitting signal that corresponds with the pre chopper TOF spectrum is at the residence time of 500 µs. In this case, the concentration of the sulphuric acid is of 58 wt% and its temperature reaches 218 K, as shown in the following figure (5.2).

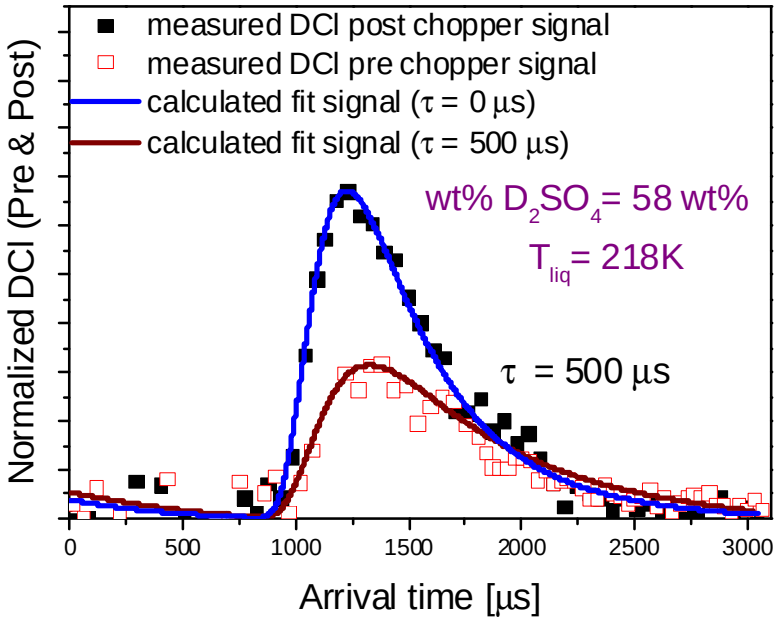

Figure (5.2) Pre- and post- chopper spectrum of DCl desorbing molecules from the D_2SO_4 solution in concentration of 58 wt% and at the temperature of 218 K, the residence time is 500 μs

The longer residence time reflects that the HCl impinging molecules dissolve deeply in the solution of sulphuric acid. As a result, the residence time of HCl in the sulphuric solution depends on the concentration of the sulphuric acid as well as on its temperature. Therefore, in the next step, the effect of the concentration and temperature of the sulphuric acid solution on its residence time will be studied.

Figure (5.3) shows the residence time of HCl in the bulk of the solution as a function of the concentration of the sulphuric acid solution. The measured values of the residence time are presented in this figure. The red stars are the values of residence time that were measured by Behr et al. 2000. The triangles and circles are measurements of the residence time of HCl gas which impinge the surface of the sulphuric acid with incident energies of 6 $kJ.mol^{-1}$ and 140 $kJ.mol^{-1}$, respectively. All measured values are carried out at the temperature 213 K. the measured residence time of this work corresponds to the measured one of Behr et al. 2000.

In addition, the measured values do not depend on the incident energy. The residence time reduces with an increase in the concentration of the sulphuric acid in the range of concentrations of between (50- 65 wt %). However, at the concentrations above of 65 wt%, the residence time becomes longer as the value of the concentration increases.

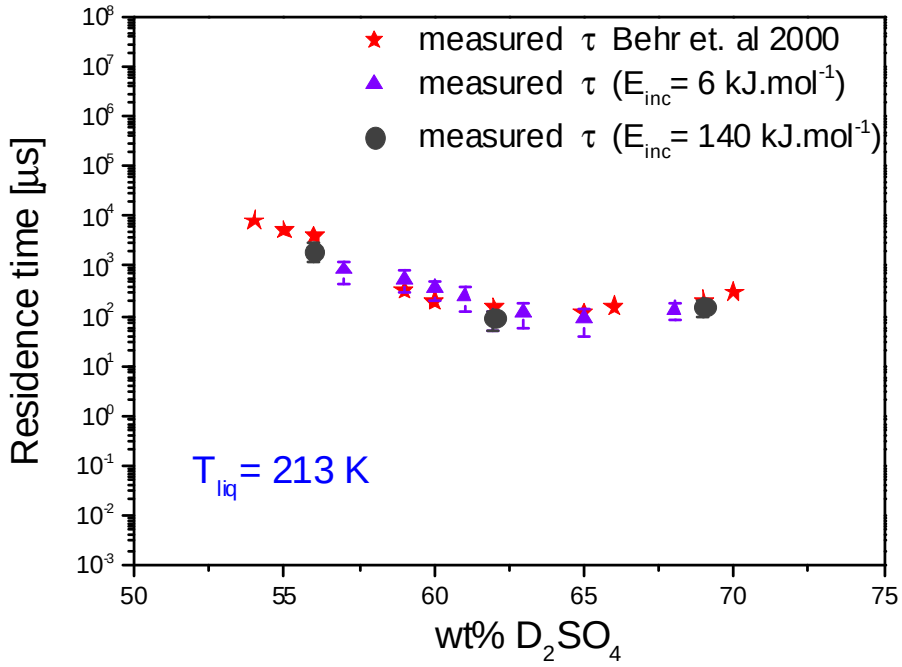

Figure (5.3) The diagram of residence time versus the concentration of D_2SO_4 at the temperature of 213 K

The diagram of the residence time as a function of the concentration of the deuterated sulphuric acid solution in weight percent is displayed in figure (5.4).

The black and red triangles are the measured values of the residence time of HCl gas in a D_2SO_4 / D_2O solution at the temperatures of 213 and 228 K.

The results demonstrate that the residence time of HCl decreases as the concentration of the sulphuric acid solution increases up to 63 wt%. In contrast, the measured residence time of HCl in the solution becomes longer with an increase of concentration of the sulphuric acid solution.

However, the measurements of the residence time of HCl in a D_2SO_4/ D_2O decreases as the temperature of the sulphuric acid solution increases in the whole range of the solution's concentration.

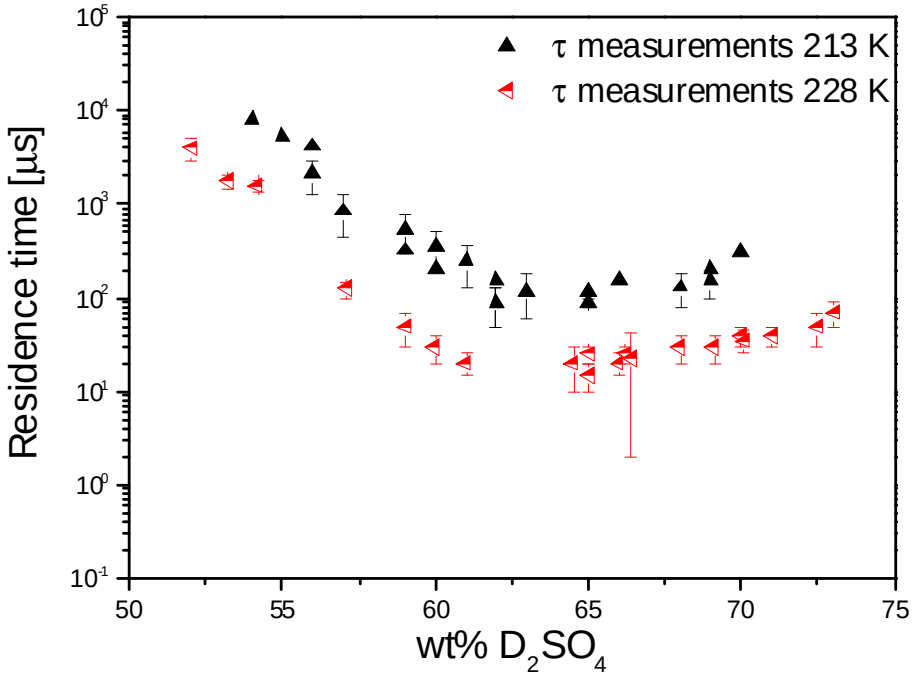

Figure (5.4) The measured values of residence time of HCl gas versus the concentration of the sulphuric acid at the temperatures of 213 and 228 K

5.2 Theoretical analysis using the Tabazadeh model

The residence time of the HCl in the sulphuric acid solution can be calculated depending on the kinetic theory of gases, which has been considered by Dankwerts 1970, is given by:

$$\tau = D\left(\frac{H^* RT}{\alpha.\bar{v}}\right)^2 \qquad \text{Equation (5.2.1)}$$

Where:

D : is the diffusion coefficient of HCl in the sulphuric acid solution ($cm^2.s^{-1}$)

R : is the universal constant (atm.l.mol^{-1}.K^{-1})

T : is the temperature of the sulphuric acid solution (K)

α : is the accommodation coefficient, which is calculated by using the capillary wave theory, as described in the next chapter (dimensionless)

$\overline{v}$: is the average velocity of the gas species, $\overline{v} = \frac{3}{2}RT$ (m.s^{-1})

H^* : is the effective Henry's law constant (mol.l^{-1}.atm^{-1})

The residence time is related to the concentration and the temperature of the sulphuric acid solution. Therefore, the diffusion coefficient for HCl in the sulphuric acid solution must be computed first. This diffusion coefficient can be estimated by using Stockes- Einstein relation:

$$D = c \cdot \frac{T}{\eta} \qquad \text{Equation (5.2.2)}$$

c : is the constant, = 7.8x10^{-8} cm^2.cP.s^{-1}.K^{-1}, which is determined by [Klassen et al. 1998].

T : is the temperature of the sulphuric acid solution in this work; 213, 218 and 228 K

η : is the viscosity of the sulphuric acid in centipoise.

The viscosity of the super cooled sulphuric acid can be determined by the equation [Williams & Long, 1995]:

$$\eta_{(w)} = A_{(w)}.T^{n(w)} \exp\left(B_{(w)} / T - T_{0(w)}\right) \qquad \text{Equation (5.2.3)}$$

$\eta_{(w)}$: is the viscosity of the sulphuric acid solution as a function of the weight percent (wt %)

T : is the temperature of the solution (K)

And the parameters:

$B_{(w)}$ = 425 and n = -1.43

The expression of $A(w)$ and $T_0(w)$ are given in the following equation:

$$A(w) = 279,4 - 8,8w + 0,358\,w^2 \quad \text{Equation (5.2.4)}$$

$$T_0(w) = 203 - 2,63w + 0,0287\,w^2 \quad \text{Equation (5.2.5)}$$

Figure (5.5) reveals the decrease of the diffusion coefficient as the concentration of the sulphuric acid increases. In addition, the diffusion coefficient increases with increasing temperature of the sulphuric acid solution.

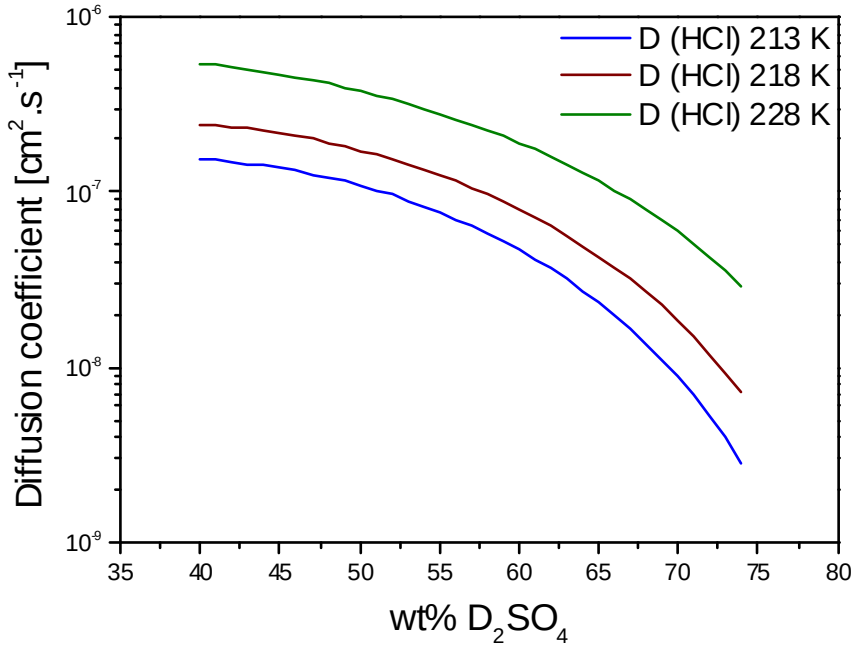

Figure (5.5) The diffusion of HCl gas in the sulphuric acid solution against the concentration of D_2SO_4 / D_2O solution at temperatures of 213, 218 and 228 K

The values of the residence time are stronger affected by the Henry's law constant than by the diffusion coefficient.

As a next step, the Henry's law constant, which is based on the Tabazadeh model for the solubility of trace gas HCl in the sulphuric acid solution in atmospheric ambient will be calculated. The calculated Henry's constant of HCl depends on the temperature and on the concentration of the binary sulphate aerosol:

$$H^*(T, m_s^0) = \frac{m_{Cl}}{p_{Cl}} = \frac{K_s(T)}{2 m_s^0 \left[\gamma_{Cl}^{mix}(T, m_s^0)\right]^2} \cdot \frac{M_{(H_2SO_4)}}{m_{(H_2SO_4)}}$$ Equation (5.2.6)

Where:

$H^*(T, m_s^0)$: is the effective Henry's law constant (mol.l^{-1}.atm^{-1})

$K_s(T)$: is the gas solubility constant

This constant depends on the solution's temperature, thus it can be approximated using Van't Hoff equation:

$$\ln\left[\frac{K_s(T)}{K_s(T^0)}\right] = \frac{\Delta H^0}{R}\left(\frac{1}{T^0} - \frac{1}{T}\right) + \frac{\Delta C_p^0}{R}\left(\frac{T^0}{T} - 1 - \ln\left(\frac{T^0}{T}\right)\right)$$ Equation (5.2.7)

In the course of this work, there will only be computed the solubility constant for HCl in the aqueous H_2SO_4 concentrations of between (40- 75 wt %) and at temperatures of (213, 218 and 228 K). Thus:

T : is the experimental temperature of the sulphuric acid solution

T^0 : is the standard temperature of (= 298.15 K)

$K_s(T^0)$: is the solubility constant of HCl gas at the standard temperature of (= 2.04 x10^{+6} mol^2.kg^{-2}.atm^{-1})

ΔC_p^0 : is the standard heat capacity of HCl of (= -3.95793 x10^{+1} cal.K^{-1}.mol^{-1})

ΔH^0 : is the standard enthalpy of HCl of (= -1.78967 x10^{+1} kcal.mol)

Tabazadeh had taken these parameters at standard temperature from [Brimblecomble & Clegg 1988].

m_s^0 : is the molality of H_2SO_4, which is the major component of the aerosol in the solution; $m_s = m_s^0$:

$$m_s^0 = \frac{1000 \cdot w_s^0}{M\,(100 - w_s^0)}$$ Equation (5.2.8)

This equation is used to convert the weight percent of the aqueous electroly concentration into molality, where:

M = 100 g.mol^{-1} for D_2SO_4

w_s^0 : is the weight percent of the electrolyte in the solution, which is calculated as a function with respect to water vapour pressure (p_w), which is calculated by [Tabazadeh et al. 1997] in units of torr. The equation is:

$$w_s^0 = \sum_{i=0}^{5} (-1)^i S_i(T) \cdot P_w^i \quad \text{Equation (5.2.9)}$$

S_i : the temperature coefficients are given in table (5.1):

$$\ln S_i(T) = a_0 + a_1/T + a_2/T^2 + a_3/T^3 + a_4/T^4$$

Coefficients	a_0	a_1	a_2	a_3	a_4
S_0	4.9306007769	-281.24576227	36171.943540	-739210.80947	-116409364.69
S_1	-10.6902946223	5784.329174	-1246284.8248	31325022.591	-2206827530.8
S_2	-39.722280419	12350.60747	-3429949.4505	62642389.672	-3970969449.3
S_3	-55.968384906	12922.351288	1350408.6346	-178905338.60	8849811933.4
S_4	-82.938840352	22079.294414	294696.83691	-31424855.089	1088487564.6
S_5	-106.47596744	27525.067463	420618.52240	-51877378.665	284983818.2

The mean activity coefficient can be calculated in the following equation. And the result can be added to the Henry's law constant equation:

$$\ln \gamma_{Cl}^{mix} = \frac{1}{2I}\left[m_s^0\left(2\ln \gamma_{Cl}^0(I,T) + 2{,}25 \ln \gamma_s^0(I,T)\right)\right] \quad \text{Equation (5.2.10)}$$

where $I = 3m_s^0$

The mean activity coefficient for the pure of HCl can be computed by the equation:

$$\ln \gamma_{Cl}^0 = \sum_{i=0}^{3} a_{ci}(T).m_{Cl}^i \quad \text{Equation (5.2.11)}$$

The concentration of HCl in the sulphuric acid solution is very small; therefore it will be assumed that the concentration is approximately 0,001 mol.kg^{-1}.

The mean activity coefficient for H_2SO_4 can be computed by the following equation:

$$\ln \gamma_s^0 = \sum_{i=0}^{3} a_{si}(T).m_s^i$$ Equation (5.2.12)

The (a_c) and (a_s) variables are temperature coefficients for the mean activity coefficients of HCl and H_2SO_4, respectively, which can be calculated through the table (5.2) below:

$$a_{ij} = b_0 + b_1 T + b_2 T^2 + b_3 T^3 + b_4 T^4$$

Coefficients	b_0	b_1	b_2	b_3	b_4
a_{s0}	-98.727713620	1.5892180900	-1.0611069051e-2	3.1437317659e-5	-3.5694366687e-8
a_{s1}	26.972534510	-0.41774114259	2.7534704937e-3	-8.0885350553e-6	9.0919984894e-9
a_{s2}	-3.1506575361	5.1477027299e-2	-3.4697470359e-4	1.0511865215e-6	-1.2167638793e-9
a_{s3}	0.089194643751	-1.4398498884e-3	9.5874823381e-6	-2.8832930837e-8	3.319971759e-11
a_{c0}	-63.192805354	9.1254642395	-5.0869838292e-3	1.2864402271e-5	-1.2449266080e-8
a_{c1}	-4.3827430062	7.1340939436e-2	-4.0096139965e-4	1.0068383723e-6	-9.703889501e-10
a_{c2}	1.1661208715	-1.6494974438e-2	9.0259619393e-5	-2.2549127848e-7	2.167004813e-10
a_{c3}	-0.02003266808	2.6583489579e-4	-1.4088333815e-6	3.4600826715e-9	-3.298437535e-12

Hence, it can be extracted that the residence time depends on the calculation of Henry's law constant using Tabazadeh model. The diagram (5.6) illustrates the residence time of HCl gas, which is plotted as a function in respect with the weight percent concentration of the sulphuric acid.

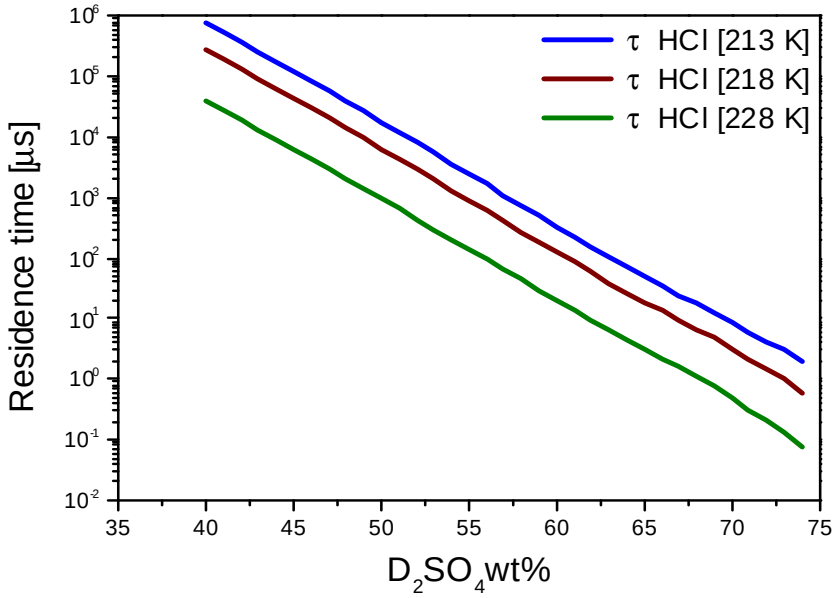

Figure (5.6) Diagram of τ_{HCl} as a function of D_2SO_4 wt%, at the temperature of 213, 218 and 228K

The blue, brown and green solid lines illustrate the calculated residence time based on the Tabazadeh model at temperatures of the sulphuric acid solution of 213, 218 and 228 K, respectively.

The results demonstrate that the calculated residence time according to the Tabazadeh model becomes shorter, when the concentration of the sulphuric acid solution increases and the values of the temperature of this solution become higher. The Henry's law constant of HCl gas in the sulphuric acid solution decreases as the concentration and the temperature of the sulphuric acid solution increase.

Figure (5.7) is a plot of the residence time of HCl in microsecond against the concentration of the deuterated sulphuric acid solution at the temperature of 228 K. The measured values of the residence time with the collusion energy of 6 $kJ.mol^{-1}$ are displayed as the red triangles. The solid line is the calculated residence time according to the Tabazadeh model at temperature of 228 K.

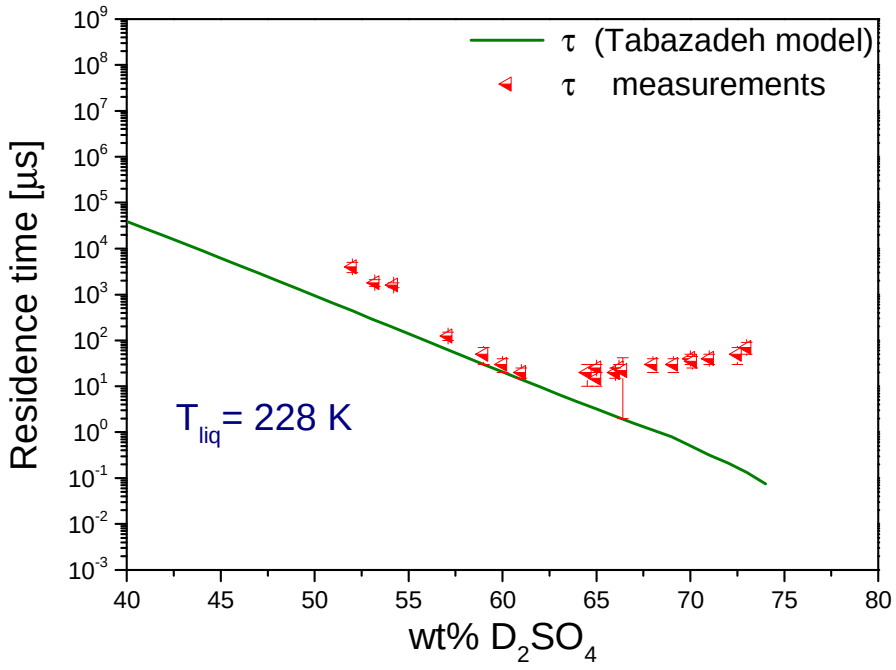

Figure (5.7) The residence time as a function of the weight percent concentration of the sulphuric acid at the temperature of 228 K

The measured value of the residence time associates with the calculated one in the range of concentrations of between (57- 61 wt %). There are two significant

deviations between the calculated and the measured values of this characteristic time at the concentrations of above 61 wt% and at the ones lower than 57 wt%.

The results indicate that the calculated residence time based on Tabazadeh model cannot describe the residence time of HCl gas in the bulk of the sulphuric acid solution. Therefore, another model will be used to describe the residence time.

5.3 Theoretical analysis using the Carslaw model

The residence time of the HCl in the sulphuric acid solution is calculated indirectly from the effective Henry's law constant, which is computed from the Carslaw model. The Carslaw's model is used to determine the solubility of HCl in the aqueous solution of the sulphuric acid. The Henry's law constant is calculated as a function of temperature of the liquid, which is given in the following equation:

$$\ln\left[{}^{x}K_{H}(HCl)\right] = 6.4954 - 9.0027\times10^{+3}\left(\frac{1}{T^{0}} - \frac{1}{T}\right) - 65.346\left(\frac{T^{0}}{T} - 1 + \ln\left(\frac{T}{T^{0}}\right)\right)$$
$$+ 0.078178\left[\left(T^{0}/T - 1\right)\cdot T^{0} + T - T^{0}\right]$$

Equation (5.3.1)

where:

T^{0} = 298,15 K; is a standard temperature

${}^{x}K_{H}(HCl)$: is Henry's law constant on a mole fraction (atm^{-1})

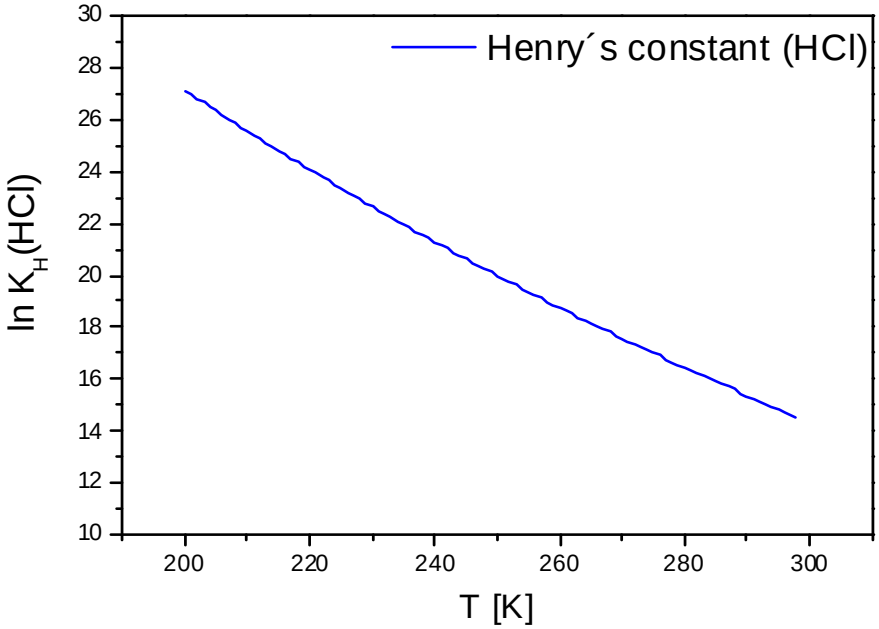

Figure (5.8) Diagram of Henry's law constant of HCl versus temperature

The relationship between the Henry's law constant above and the molal Henry's law constant is:

$$K_H = \frac{{}^{x}K_H}{(m_{H_2O})^2} = \frac{{}^{x}K_H}{(18/1000)^2} \quad ; \; K_H \text{ (kg}^2\text{.mol}^{-2}\text{.atm}^{-1}\text{)} \qquad \text{Equation (5.3.2)}$$

Diagram (5.8) plots the molal Henry's law constant of HCl in the sulphuric acid solution as a function of the temperatures in a range of between (200- 298K).

On the other hand, [Carslaw et al. 1995] presents the effective Henry's law constant H* (mol.l^{-1}.atm^{-1}) of HCl as a function of the concentration of the sulphuric acid solution:

$$H^* = \frac{K_H}{m_H \cdot \gamma_{\mp}^2} \cdot \frac{M_{(H_2SO_4)}}{m_{(H_2SO_4)}} \qquad \text{Equation (5.3.3)}$$

while:

m_H : is the molality of free hydrogen ion in solution; the sulphuric acid must be complete dissociation as:

$$H_2SO_4 \Leftrightarrow SO_4^{2-} + 2H^+ \qquad \text{Reaction (5.3.1)}$$

$\gamma_{\mp}$: is the mean molal activity coefficient only for HCl, which can be found in the internet on the website "EAIM" inorganic composition (HCl, HBr, HF in solution model 2 and 3).

$M_{(H_2SO_4)}$: is the molarity of the aqueous sulphuric acid solution (mol.l^{-1})

$m_{(H_2SO_4)}$: is the molality of the aqueous sulphuric acid solution (mol.kg^{-1})

Then, the molality of the aqueous H_2SO_4 can be calculated from the weight percent concentration of the sulphuric acid with the help of this equation:

$$m_{H_2SO_4} = \frac{1000.(H_2SO_4 wt\%)}{98.(100 - H_2SO_4 wt\%)} \qquad \text{Equation (5.3.4)}$$

In addition to that, the density of the solution at lower temperatures such as 213, 218 and 228 K can be computed by the following equation [Carslaw et al. 1995]:

$$d = 1000 + a_1 m + a_2 m^{\frac{3}{2}} + a_3 m^2$$ Equation (5.3.5)

where:

m: is the stoichiometric molality of the sulphuric acid solution

The a_1, a_2 and a_3 are the temperature coefficients, which can be calculated from the following equations:

$$a_1 = 123.64 - 5.6 \times 10^{-4} T^2$$ Equation (5.3.6)

$$a_2 = -29.54 + 1.814 \times 10^{-4} T^2$$ Equation (5.3.7)

$$a_3 = 2.343 - 1.487 \times 10^{-3} T - 1.324 \times 10^{-4} T^2$$ Equation (5.3.8)

Thus, the molarity of the sulphuric acid can be found through multiplication of both of the results of the modality of the sulphuric acid as well as the density:

$$M_{H_2SO_4} = m_{H_2SO_4} \cdot d \cdot 1000$$ (mol.l^{-1}) Equation (5.3.9)

As it was mentioned before, the residence time depends on the Henry's law constant of HCl, which is calculated with the help of the Carslaw model. Diagram (5.9) shows that the characteristic time of HCl gas solubility in the solution decreases with increasing concentration of the sulphuric acid.

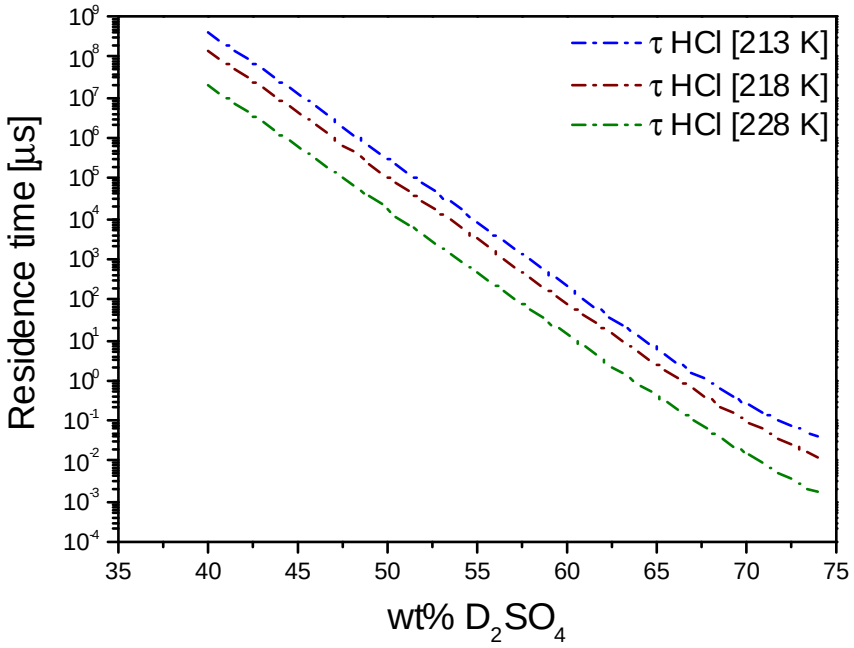

Figure (5.9) Diagram of the isotherm residence time versus the concentration of the sulphuric acid

The blue, brown and green dotted dashed lines are the calculated residence time according to the Carslaw model at temperatures of the sulphuric acid solution of 213, 218 and 228 K, respectively.

The calculated residence time of HCl which is based on the Carslaw model decreases as the temperature of the D_2SO_4 / D_2O solution increases, because the Henry's law constant decreases with increasing temperature of the sulphuric acid solution, as explained in figure (5.8).

The calculated values of the residence time are represented as dotted dashed lines based on the Carslaw model at the temperature of 228 K, as shown in figure (5.10) below. The measured values of the residence time are the same values that are displayed in figure (5.7). In this case, the calculated residence time accords with the measured one in the range of concentrations of between (50- 62 wt %). At concentrations of above 62 wt% lead to an increasing deviation between the measured and calculated residence time. As a result, the residence time which is based on the Carslaw model can only describe the solubility of the HCl gas in the sulphuric acid solution at the lower concentrations up to 62 wt%.

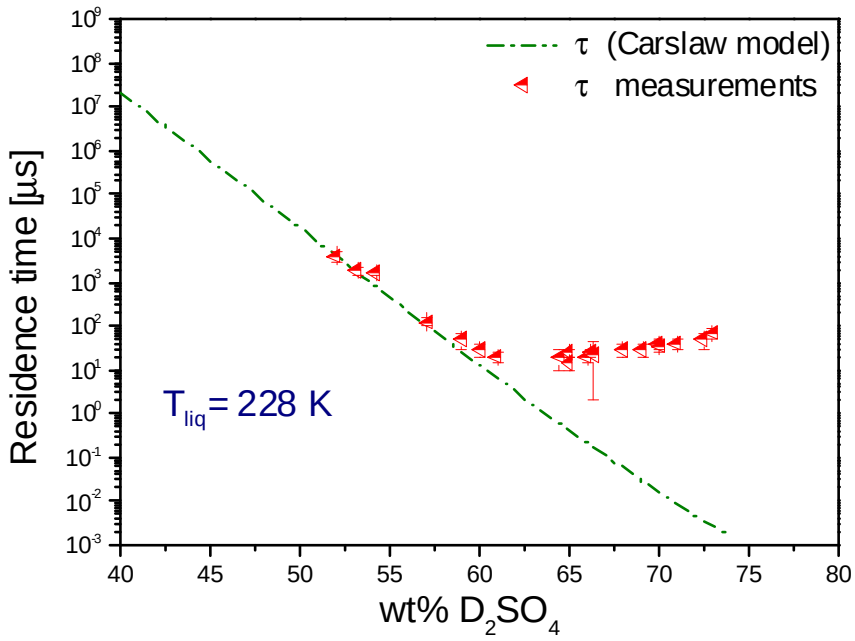

Figure (5.10) The residence time against the concentration of the sulphuric acid, at the temperature of 228 K, the dashed line is the calculated residence time based on the Carslaw model

To sum up, the greatest difference between the two models is that the Henry's law constant of HCl has been calculated by the Tabazadeh model which depends on the mean activity coefficient for all species which exist in the sulphuric acid solution. In contrast, the effective Henry's law constant has been extracted by the Carslaw model which is based on the mean activity coefficient only for the solute HCl in the sulphuric acid solution.

In figure (5.11) will be pointed out that the reduction in the calculated residence time regarding to the Carslaw model is sharper than that which is based on Tabazadeh model. On the one hand, the measurements of the residence time correspond to the calculated ones based on the Carslaw model in the range of the low concentration of the sulphuric acid at a lower temperature. On the other hand, the measurements are partly associated with the calculated residence time according to Tabazadeh model.

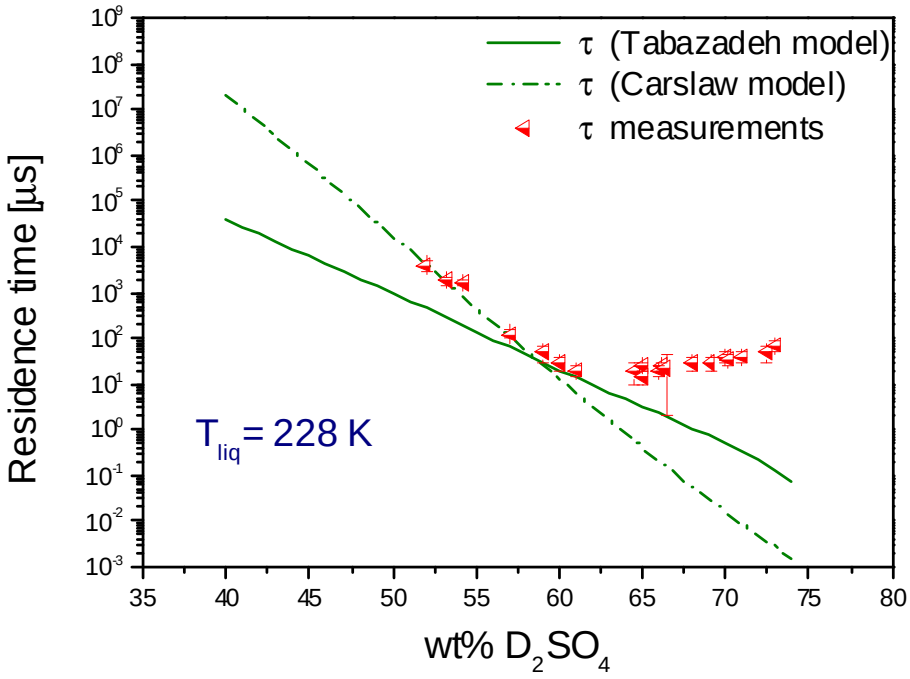

Figure (5.11) The residence time versus the concentration of the sulphuric acid solution at the temperature of 228 K. The solid line represents the Tabazadeh model and the dotted dashed one the Carslaw model

Figure (5.13) illustrates that the difference between the measured values of residence time and the calculated values based on Carslaw model does not only exist at the temperature of 228 K, but also at temperatures of 213 and 218 K. Additionally, the values of the residence time at lower temperatures are higher than those at higher temperatures. The measured values of the residence time associate with the calculated ones in the lower concentrations of the sulphuric acid at the three different temperatures of 213, 218 and 228 K.

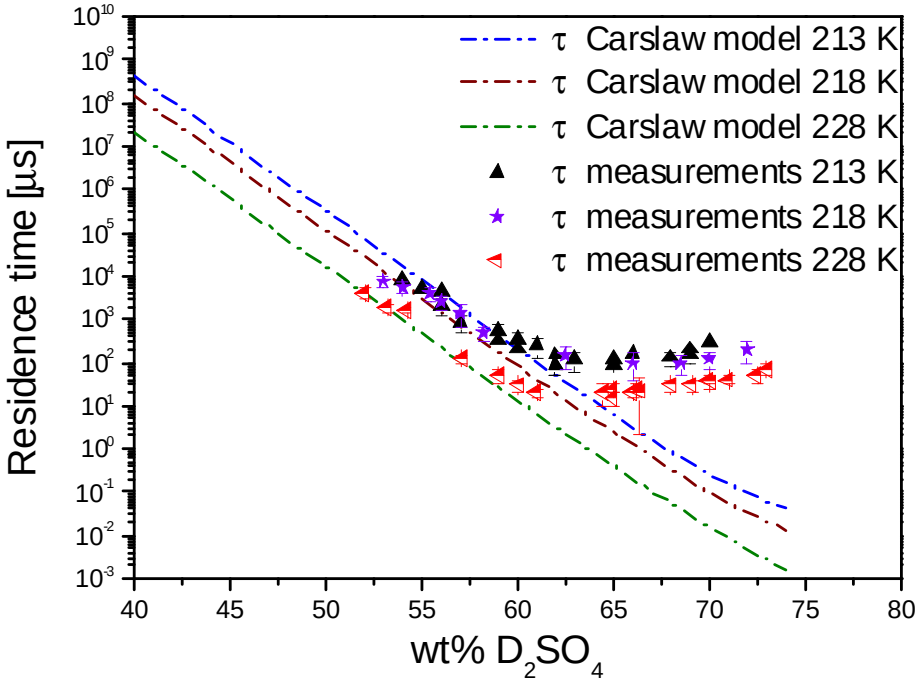

Figure (5.13) The diagram of the measured and calculated residence time versus the weight percent concentration of the sulphuric acid at temperatures of 213, 218 and 228 K

These results support the residence time of HCl gas molecules in the solution that depends only on the solubility time of this gas in the sulphuric acid solution at the lower concentrations of the solution.

One study suggests that the higher solubility of HCl gas in the sulphuric acid of concentrations of above 60 wt% is caused by the reaction of HCl with H_2SO_4 to form chlorosulphonic acid (HSO_3Cl) [Robinson et al. 1998].

Other study observes that the solubility of HCl in the sulphuric acid becomes better at concentration of over 65 wt% of the sulphuric acid and the reaction of forming

chlorosulphonic acid might be more enhanced with increasing concentration of the sulphuric acid. Hence, the observed residence time of HCl of above 65 wt% becomes longer than it was expected by using the molecular beam technique [Behr et al. 2000].

5.4 Theoretical analysis using the capillary wave theory

The capillary wave theory is adapted to describe the unexpected behaviour of the solubility of HCl gas in higher concentrations of the sulphuric acid solution. In higher concentrations it is used to estimate the solubility of HCl gas based on the transport time of HCl into the sulphuric acid solution.

The residence time associates with the solubility coefficient of gas molecules in the liquid (Henry's constant), which is calculated by using the Carslaw model. This model does not take into consideration the kinetics of the solubility at higher concentration of the sulphuric acid. Thus the residence time of the gas molecules in the solution accords with this model at the lower concentration of the binary solution.

In the case of the higher concentration of the sulphuric acid, the residence time becomes longer after 65 wt%. That is caused by the decay time for the dissociation and recombination of the solute in the liquid bulk before it desorbs from the surface. This decay time can be computed by using the local mode capillary wave theory from Phillips (2001 b):

The transport constant of the element into the bulk of the liquid is independent from the surface tension. In contrast, the viscosity of the liquid affects to reduce the transport velocity of the solute in the liquid. That is given as:

$$k_{trans} = \frac{k_B T}{2\eta\sigma^2} \qquad \text{Equation (5.4.1)}$$

Where:

k_{trans} : is the transport constant in the liquid bulk ($m.s^{-1}$)

k_B : is the Boltzmann constant [= 1.38 X 10^{-16} g.cm^2.s^{-2}.K^{-1}]

σ^2 : is the collision surface of the solute molecule on the super position of the local mode. When HCl is in contact with the sulphuric acid it is estimated to be [9.02 X 10^{-15} cm^2]

The transport time, which must be spent by the penetrating molecules in the bulk liquid to dissociate and immediately recombine, is given as:

$$\tau_{trans} = \frac{2\eta\sigma^2 l}{k_B T} \qquad \text{Equation (5.4.2)}$$

where:

l : is the thickness of the bulk liquid, where the dissociation and recombination take place in (10 A°) [Ringeisen et al, 2002].

Figure (5.14) reveals that the viscosity of the sulphuric acid is responsible for the enhancement of HCl solubility in the sulphuric acid at concentrations of above 65 wt%.

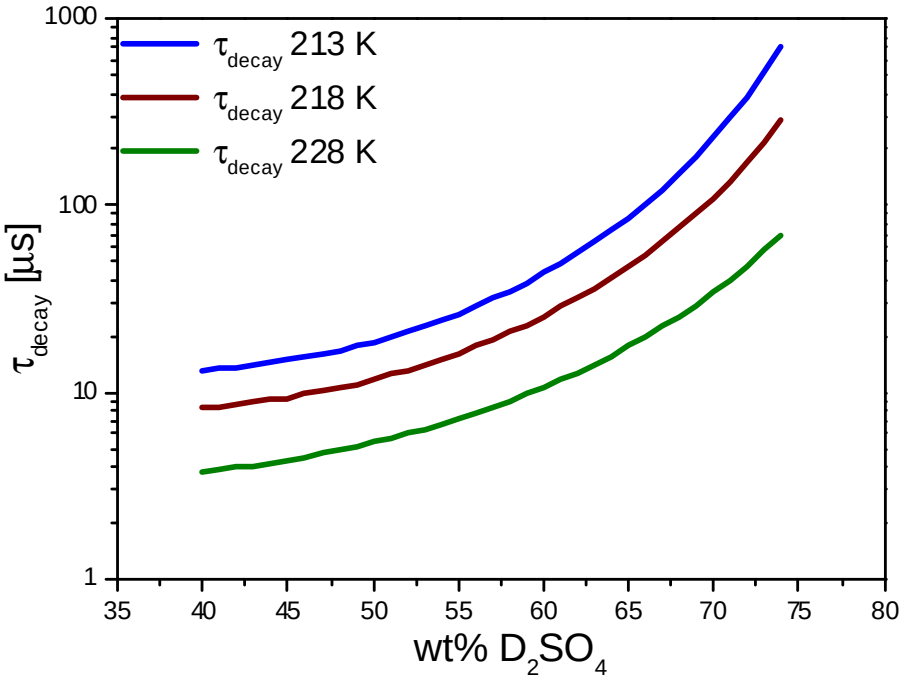

Figure (3.12) The diagram of the decay time of HCl in solution as a function of weight percent of the sulphuric acid

As a result, the true residence time is extracted from the sum of the residence time which is based on the solubility constant of the Carslaw model (solubility residence time) plus the residence time of the kinetic transport of HCl gas into the bulk liquid depending on the local mode capillary wave theory (transport time). The true residence time is given as:

$$\tau = \tau_S + \tau_{trans} \quad \text{Equation (5.4.3)}$$

Combining this equation with equations (5.4.3) and (5.2.1) it may be rewritten:

$$\tau = \left[D\left(\frac{4H^* RT}{\alpha \bar{v}} \right)^2 \right] + \left[\frac{2\eta\sigma^2 l}{k_B T} \right] \quad \text{Equation (5.4.4)}$$

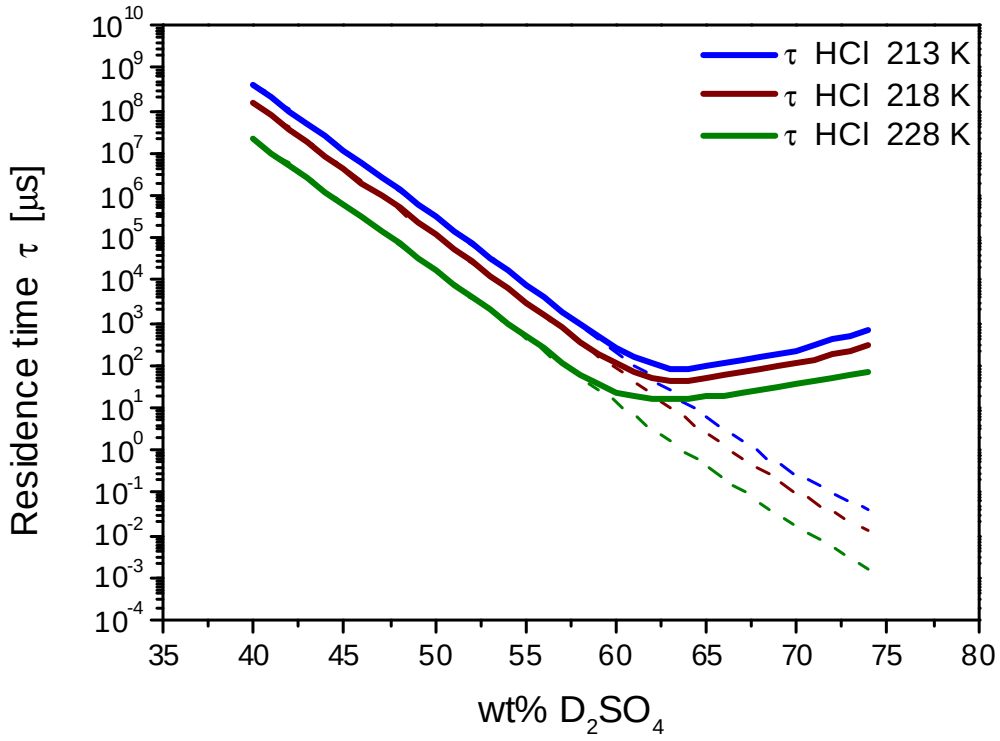

Figure (5.15) The diagram of the true residence time (solid lines) and the solubility residence time (dashed lines) versus the concentration of the sulphuric acid at temperature of 213, 218 and 228 K

In the case of lower concentrations of the sulphuric acid, the values of the solubility residence time are a good deal higher than the decay time. The effect of the kinetic transport is negligible for the true residence time. Therefore, the residence time based on the Carslaw model corresponds with the true residence time, when the concentration of the sulphuric acid is lower than 63 wt%.

The true residence time increases with increasing concentration of the sulphuric acid in the field of concentrations of above 63 wt%. This depends on an effective kinetic transport of the solute into the bulk solvent. The difference between the true residence time and the solubility residence time increases significantly with increasing concentration of the sulphuric acid, because the viscosity of the solution is responsible for the slow desorption of the gas molecules from the surface. The deviation of the true residence time from the solubility residence time becomes obvious in figure (5.15).

The temperature plays an important role determining the residence time of the gas molecules in the solution. The true residence time reduces with an increase in the temperature of the sulphuric acid. This is because the residence time depends on the Henry's law constant of HCl as well as the viscosity of the sulphuric acid solution. Furthermore, when the temperature increases, the Henry's law constant of HCl falls and the viscosity of the sulphuric acid solution decreases rapidly. Figure (5.15) shows this behaviour of the residence time at the three different temperatures of liquid of 213, 218 and 228K.

As explained above, the deviation between the measured and calculated values of residence time is caused by the transport time of HCl gas molecules into the bulk of the sulphuric acid solution at the higher concentrations. Therefore, the measured values of the residence time accord with the calculated residence time based on the local mode of the capillary wave theory. At the lower concentrations of the sulphuric acid, the values of the transport time of HCl gas molecules are negligible in comparison with the solubility residence time. By this means, the measured values of residence time correspond with its calculated values, which are not only based on the Carslaw model, but also on the capillary wave theory, as shown in figure (5.16).

The measured values of residence time associate with its calculated values based only on the capillary wave theory, because the values of the transport time are a good deal higher than the solubility time. In addition, the measured residence time increases with increasing concentration of the sulphuric acid. These results demonstrate that the transport time of HCl gas into bulk solution increases with increasing viscosity of the sulphuric acid.

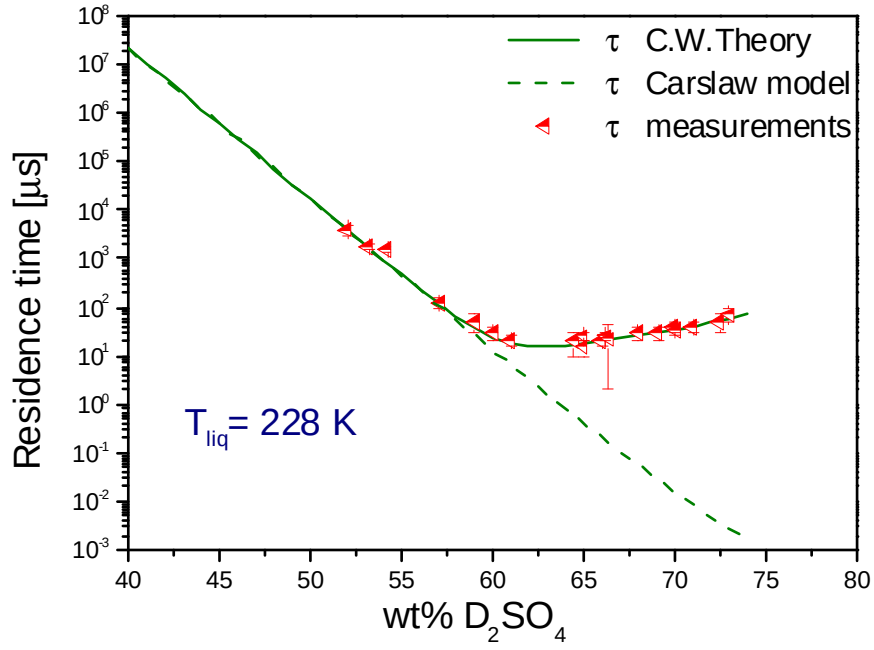

Figure (5.16) The diagram of the residence time against the concentration of the sulphuric acid solution at the temperature of 228 K, the dashed line and the solid curve represent the calculated residence time based on Carslaw model and the capillary wave theory, respectively

The effect of the temperature on the residence time is shown in figure (5.17). The values of the residence time reduce with increasing temperature of the sulphuric acid solution. This increase in the residence time does not only depend on the Henry's law constant of the solubility HCl but also on the kinetic transport of HCl into the solution.

On the one hand, in the case of lower concentrations of the sulphuric acid, the Henry's law constant of HCl decreases with increasing temperature of the sulphuric

acid solution. Thus, the measured values of the residence time become shorter, if the values of the temperature increase.

On the other hand, in the case of higher concentrations of the sulphuric acid solution, the residence time becomes shorter for the transfer of HCl molecules into the bulk of the solution with increasing temperature of the sulphuric acid solution. Hence, the measured values of residence time decrease, when the temperature of the sulphuric acid increase due to decreasing viscosity of the sulphuric acid.

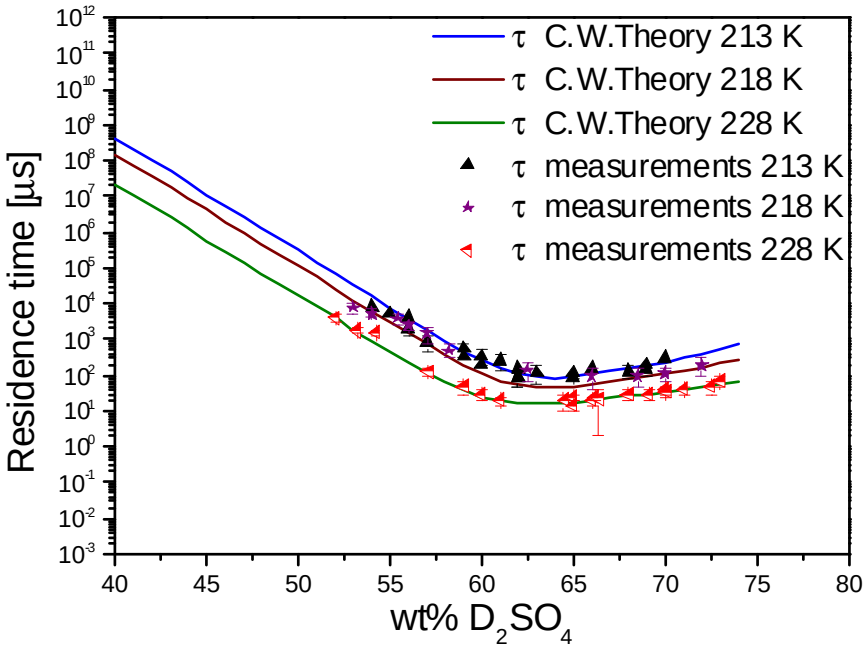

Figure (5.17) The residence time as a function of the concentration at the three different temperatures of 213, 218, 228 K, the solid lines are calculated according to the true residence time

To summarize, the kinetics of the HCl solubility in the sulphuric acid solution can be described in the whole concentrations of the sulphuric acid solution using the both the Carslaw model and the local mode of the capillary wave theory.

6. Summary

In this thesis, there are three main points that can be concluded as follows:

1. Water desorption from the surface:

The vacuum evaporation experiments are used to monitor the loss of deuterium oxide from the surface of the liquid and the solid of deuterated sulphuric acid solution at temperatures of 213, 218 and 228 K with different spectral angles in the range from 0° to 65°.

The velocity distribution with the angular cosine square factor in exponent is expressed for the velocity distribution of D_2O molecules, which desorb from the liquid surface. The angle in this factor can be calculated through the root mean slope of the capillary wave. This root mean slope depends on the temperature of the liquid surface. The capillary wave theory includes that the surface of the capillary wave expands with increasing temperature of the liquid surface. Hence, when the temperature of the liquid surface increases, the diameter of the capillary wave becomes wider, which needs molecules to desorb from the surface of the capillary wave. In contrast, the spectral angle and the concentration of the sulphuric acid solution have no effect on the slope of the capillary wave. This velocity distribution is named as non-Maxwell-Boltzmann velocity distribution. In the case of the solid surface, the velocity distribution of the desorbing D_2O molecules associates with the Maxwell-Boltzmann velocity distribution. Besides, the spectral angle has also no effect on the energy distribution.

However, the intensity of Maxwellian and non Maxwellian velocity distribution depends on the concentration of the sulphuric acid solution and spectral angle. This intensity of velocity distribution decreases with increasing concentration of the sulphuric acid solution. This reduction associates with the number of D_2O molecules on the surface of the solution. Moreover, the reduction in intensity of the velocity distribution is as a function of the angular cosine of the spectral angle (cos Φ).

2. The mass accommodation coefficient:

The molecular beam techniques are used to investigate the proton exchange function of HCl gas in collision with the bare deuterated sulphuric acid solution at temperatures of 213, 218 and 228 K in the range of concentrations of between (52- 74 wt %).

This proton exchange function is measured through the comparison of the DCl post-chopper TOF spectrum with the HCl post- chopper TOF spectrum. The value of the ($H \rightarrow D$) exchange is equal to the mass accommodation coefficient, which can be determined by the solvation rate of the HCl gas molecule into the liquid phase of the sulphuric acid solution as well as the desorption rate of HCl from the liquid surface of solution.

In the case of constant temperature, the mass accommodation coefficient of HCl decreases as the concentration of the sulphuric acid solution increases. This behaviour depends on the increase in the viscosity of the sulphuric acid solution. The solvation rate constant decreases with increasing concentration of the D_2SO_4 / D_2O solution.

In the case of concentrations of between (50- 64 wt %), the measured values of accommodation coefficient increases with decreasing temperature of the sulphuric acid solution. In addition to that, the values of the desorption rate are lower than the values of solvation rate. Further, the kinetics of HCl molecules to dissolve in the sulphuric acid solution is faster than the kinetics of desorption from the liquid surface. As a result, the proton exchange fraction decreases as the temperature of the D_2SO_4 solution increases at the same concentration, because the desorption rate is stronger influenced by temperature than the solvation rate constant.

On the other hand, in the case of concentrations of between (67- 75 wt %), it is found that the proton exchange fraction becomes higher with increasing temperature of the sulphuric acid solution at constant concentration of the D_2SO_4 / D_2O solution. In addition, the viscosity of the sulphuric acid solution decreases as the temperature of

the sulphuric acid solution increases. The solvation rate constant is stronger influenced by temperature than the desorption rate. Therefore, the mass accommodation coefficient of HCl decreases with falling temperature of the sulphuric acid solution.

3. The residence time of HCl:

Time- of- flight molecular beam scattering techniques are used to explore the residence time of HCl- molecules, which collide with the binary sulphuric acid water solution. The experiments are carried out in a concentration range from 52 to 75 wt% at temperatures of 213, 218 and 228 K. The residence time of HCl is recorded through the comparison of the DCl pre- chopper TOF spectrum with the DCl post-chopper TOF spectrum after the time off set is corrected.

In the case of concentration of (52- 63 wt %), the residence time of the HCl molecules in the solution decreases as the concentration of the sulphuric acid solution increases. The reduction in the residence time accords with the calculated residence time based on the Carslaw model. The residence time depends on the Henry's law constant of HCl gas molecules in the solution (the solubility of gas molecules).

In the case of concentration of (63- 75 wt %), the residence time of HCl increases with increasing concentration of the sulphuric acid solution. The residence time corresponds with the time constant of the transfer HCl molecules in the solution of the sulphuric acid. The effect of the HCl solubility is negligible in the residence time. In contrast, this characteristic residence time corresponds with the transport of HCl molecules in the solution. The velocity of transport HCl molecules becomes slower with increasing viscosity of the sulphuric acid solution.

However, the residence time of HCl gas molecules reduces, when the temperature of solution increases, because the Henry's law constant of the HCl solubility and the transport of HCl in the sulphuric acid decreases with increasing temperature of a D_2SO_4 /D_2O solution.

7. References

Aarts D. G. A. L., M. Schmidt, H. N. W. Lekkerkerker, *Direct visual observation of thermal capillary wave*, Science, 304, 847- 850, **2004.**

Abbatt J. P. D., M. J. Molina, *The heterogeneous reaction of HOCl +HCl* $\longrightarrow$ Cl_2 + H_2O *on ice and nitric acid trihydrate: reaction probability and stratospheric implications*, Geo. Res. Lett., 19, 461- 464, **1992**.

Anderson P. U., M. B. Nagard, J. B. C. Pettersson, *Molecular beam studies of HCl interactions with pure and HCl covered ice surface*, J. Phys. Chem., 104, 1596- 1601, **2000**.

Ardura D., D. J. Donaldson, *Where does acid hydrolysis take place?*, Phys. Chem. Chem. Phys., 11, 857- 863, **2009**.

Bar-Nun A., T. Owen, *Astrophysics Space,* Sci.-Libr., 227, 353, **1998**.

Baron P. A., K. Willeke, *Aerosol measurement principles, techniques, and applications,* John Wiley and Sons, p. 91, **2001**.

Behr P., J. R. Morris, M. D. Antman, B. R. Ringeisen, J. R. Splan, G. M. Nathanson, *Reaction and desorption of HCl and HBr following collisions with supercooled sulphuric acid*, Geo. Res. Lett., 28, 1961- 1964, **2001**.

Behr P., U. Scharfenort, K. Ataya, R. Zellner, *Dynamic and mass accommodation of HCl molecules on surface acid- water surfaces*, Phys. Chem. Chem. Phys., 11, 1- 8, **2009**.

Behr P., U. Scharfenort, R. Zellner, *Collision of nobel gases with supercooled sulphuric acid- water solution*, Phys. Chem. Chem. Phys., 11, 7292- 7302, **2009 a**.

Bianco R., J. T. Hynes, *Heterogeneous reactions important in atmospheric ozone depletion: a theoretical perspective,* Acc. Chem. Res., 39, 159-165, **2006**.

Brastad S. M., G. M. Nathanson, *Molecular beam studies of HCl dissolution and dissociation in cold salty water*, Phys. Chem. Chem. Phys., DOI: 10.1039/ C0cp02540b, **2011**.

Brimblecombe P., S. L. Clegg, *The solubility and behaviour of acid gases in the marine aerosols*, J. Atoms. Chem., 7, 1- 18, **1998**.

Brown R. L., *Tubular Flow reactors with first order kinetics*, J. Res. Natl. Bur. Stand, 83, 1- 8, **1978**.

Burden D.K., A. M. Johnson, G. M. Nathanson, *HCl uptake through films of pentanoic acid and pentanoic acid/ hexanol mixtures at the surface of sulphuric acid*, J. Phys. Chem., 113, 14131- 14140, **2009**.

Calz F., F. Fenter, K. D. Tabor, M. J. Rossi, I. Paper, *Design and construction of a Knudsen- cell reactor for the study of heterogeneous reactions over the temperature range 130- 750 K, Performances and limitations*, Rev. Sci. Instrum., 68, 3172- 3179, **1997**.

Carslaw K. S., S. L. Clegg, P. Brimblecombe, *A thermodynamic model of the System HCl- HNO_3- H_2SO_4- H_2O, Including solubilities of HBr, from fewer 200 to 328 K*, J. Phys. Chem., 99, 11557- 11574, **1995**.

Cheng S., J. B. Lechman, S. J. Plimpton, G. S. Grest, *Evaporation of Lennard- Jones fluids*, arXiv: 1101.5349v2 [cond- mat.soft], **2011**.

Dankwerts P. V., *Gas- Liquid Reactions*, Mc Graw- Hill, New York, 30- 69, **1970**.

Davidovits P., J. H. Hu, D. R. Worsnop, M. S. Zahniser, C. E. Kolb, *Entry of gas molecules into liquids*, Faraday Discuss., 100, 65- 82, **1995**.

Davidovits P., C. E. Kolb, L. R. Williams, J. T. Jayne, D. R. Worsnop, *Mass accommodation and chemical reactions at Gas- Liquid interfaces*, Chem. Rev., 106, 1323- 1354, **2006**.

De More W. B., *Tests of stratospheric models: The reactions of atomic chlorine with O_3 and CH_4 at low temperature*, J. Geo phys. Res, 96, 4995- 5000, **1991**.

Deshler T., D. J. Hoffmann, B. J. Johnson, W. R. Rozier, *Balloonborne measurements of Pinatubo aerosol size distribution and volatility at Laramie, Wyoming during the summer of 1991,* Geophys. Res. Lett., 19, 199-202, **1992***.*

Donaldson D. J., A. R. Ravishankara, D. R. Hanson, *Detailed study of HOCl + HCl* $\longrightarrow$ *Cl_2 + H_2O in sulphuric acid*, J. Phys. Chem., 101, 4717- 4725, **1997**.

EIAM, internet web site inorganic composition (HCl, HBr, HF) in solution model 2 and 3.

Eizenberg D., W. Kauzmann, *The structure and prosperities of water*, Oxford University press, New York, **1969**.

Faubel M., S. Schlemmer, J. P. Toennies, *A molecular beam study of the evaporation of water from a liquid jet, Z. Phys. D- Atoms, Molecules and Cluster*, 10, 269- 277, 1988.

Fowler R., G. A. Guggenheim, *Statistical thermodynamics*, Cambridge press, Cambridge, 124, **1965**.

Giauque W. F., E. W. Hornung, J. E. Kunzler and T. R. Rubin, The thermodynamic properties of aqueous sulphuric acid solution and hydrates from 15 to 300 K, Vol. 82, 62- 70, **1960**.

Hanson D. R., R. A. Ravishankara, *Heterogeneous chemistry of Bromine species in sulphuric acid under stratospheric conditions*, Geo phys. Res. Lett., 22, 385- 388, **1995**.

Hanson D. R., E. R. Lovejoy, *Heterogeneous reactions in liquid sulfuric acid: HOCl + HCl as a model system*, J. Phys. Chem., 100, 6397-6405, **1996**.

Hobbs P. V., *Ice physics*, Clarendon press, Oxford, **1974**.

Hurlbut F. C., D. E. Beck, U. C. Eng. Proj. Report No. HE-150-166, University of California, **1959**.

Isakson M.J., G. O. Sitz, *Adsorption of HCl on ice*, J. Phys. Chem., 103, 2044- 2049, **1999**.

King M. E., G. M. Nathanson, M. A. Hanning-Lee, T. K. Minton, *Probing the microscopic corrugation of liquid surface with gas-liquid collision*, J. American Phys. Soc., 70, 1026- 1029, **1993.**

Klassen J. K., Z. Hu, L. R. Williams, *Diffusion coefficient for HCl and HBr in 30 wt% to 72 wt% sulphuric acid at temperatures between 220 and 300 K*, J. Geo phys. Res., 103, 16197- 16202, **1998**.

Knox C. J. H., L. F. Phillips, *Maxwell versus Non- Maxwell velocity distributions for molecules emitted from a liquid surface*, J. Phys. Chem., 102, 10515- 10520, **1998**.

Kolb C. E., R. A. Cox, J. P. D. Abbatt, M. Ammann, E. J. Davis, D. J. Donaldson, B. C. Garrett, C. George, P.T. Griffiths, D. R. Hanson, M. Kulmala, G. McFiggans, U. Pöschl, I. Riipinen, M. J. Rossi, Y. Rudich, P. E.Wagner, P. M. Winkler, D. R. Worsnop, and C. D. O' Dowd, *An overview of current issues in the uptake of atmospheric trace gases by aerosols and clouds,* atmos. Chem. Phys.,10,10561-10605, **2010**.

Mora S., J. Daillant, K. Mecke, D. Luzet, A. Braslau, M. Alba, B. Struth, *X- ray synchrotron study of liquid- vapour interface at short length scales: effect of long-range forces and bending energies*, Phys. Rev. Lett., 90, 216101/1- 216101/4, **2003**.

Morris J.R., P. Behr, M. D. Antman, B. R. Ringeisen, J. Splan, G. M. Nathanson, *molecular beam scattering from supercooled sulphuric acid: collisions of HCl, HBr and HNO_3 with 70 wt% D_2SO_4*, J. Phys. Chem., 104, 6738- 6751, **2000**.

Myhre C. E. L., C. J. Nielsen, O. W. Saastad, *Density and surface tension of aqueous H_2SO_4 at low temperature*, J. Chem. Eng. Data, 43, 617- 622, **1998**.

Nagayama G., T. Tsuruta, *A general expression for the condensation coefficient based on transition state theory and molecular dynamics simulation*, J. Chem. Phys., 118, 1392- 1399, **2003**.

Nathanson G. M., P. Davidovits, D. R. Worsnop, C. E. Kolb, *Dynamics and kinetics at the Gas- Liquid interface*, J. Phys. Chem., 100, 13007- 13020, **1996**.

Nathanson G. M., *Molecular Beam Studies of Gas- Liquid Interface*, Annu. Rev. Phys. Chem., 55, 231- 255, **2004**.

Packwood D. M., L. F. Phillips*, A stochastic local mode treatment of high- energy gas- liquid collisions*, J. Phys. Chem., 113, 7647- 7653, **2009**.

Phillips L. F., *Velocity and angular distributions and evaporation at the surface of a drop*, Chem. Phys. Lett., 266, 161- 168, **1997**.

Phillips L. F., *Capillary wave, slope correlations, and evaporation at the surface of a drop*, Chem. Phys. Lett., 320, 398- 404, **2000**.

Phillips L. F., *Local Modes and surface- bulk exchange rate at a liquid interface*, J. Phys. Chem., 105, 1041- 1046, **2001a**.

Phillips L. F., *Gaussian modes of liquid interface*, J. Phys. Chem., 105, 11283- 11289, **2001b**.

Phillips L. F., *A molecular- scale model for the coupling of heat and matter fluxes at a gas- liquid interface*, J. Phys. Chem., 107, 9059- 9062, **2003**.

Phillips L. F., *A geometrical explanation for the enhanced small- scale roughness of a liquid surface*, J. Phys. Chem., 108, 1986- 1991, **2004a**.

Phillips L. F., *Surfing the Nanowaves: progress in understanding the Gas- Liquid interface*, Acc. Chem. Res., 37, 982- 988, **2004b**.

Phillips L. F., *Capillary- wave model for evaporation of a liquid*, Chemical Phys. Lett., 407, 249- 253, **2005**.

Pollack G. L., *Why gases dissolve in liquids*, Science, Vol. 251, 1323- 1330, **1991**.

Rabinson GH, D. R. Worsnop, T. J. Jayre, C. E. Kolb, E. Swartz, P. Davidovits, *Heterogeneous uptake of HCl by sulphuric acid solution*, J. Geo phys. Res, 103, 25371- 25381, **1998**.

Rahimi P., C. A. Ward, *Kinetic of evaporation: statistical rate theory approach*, Int. J. of Thermo., Vol. 8, 1- 14, **2005**.

Reid J. P., R. M. Sayer, *Heterogeneous atmospheric aerosol chemistry: laboratory studies of chemistry on water droplets*, Chem. Soc. Rev., 32, 70- 79, **2003**.

Ringeisen B. R., PhD Thesis, *collisions and reactions of HCl and HBr with liquid glycerol*, University of Wisconson, **2000**.

Ringeisen B. R., A. H. Muenter, G. M. Nathanson, *collisions of DCl with liquid Glycerol: evidence for rapid, near- interface D* $\longrightarrow$ *H exchange and desorption*, J. Phys. Chem., 106, 4999- 5010, **2002**.

Ronk W. R., D. V. Kowalski, M. Manning, G. M. Nathanson, *Inert gas scattering from molten metals: probing the stiffness and roughness oft he surfaces of atomic liquids,* J. Chem. Phys., 104, 4842-4848, **1996**.

Sabinina L., L. Terpugow, *Surface tension of the sulphuric acid- water system*, Z. Phys. Chem., A173, 237- 241, **1935**.

Sadtchenko V., K. Knutsen, C. F. Giese, W. R. Gentry, *Interactions of CCl_4 with thin D_2O amorphous ice films, Part I: a nanoscale probe of ice morphology*, J. Phys. Chem., 104, 2511-2521, **2000a**.

Sadtchenko V., C. F. Giese, W. R. Gentry, *Interaction of hydrogen chloride with thin ice films: the effect of ice morphology and evidence for unique surface species on crystalline vapor-deposited ice*, J. Phys. Chem., 104, 9421-9429, **2000b**.

Saecker M. E., G. M. Nathanson, *Collisions of protic and aprotic gases with hydrogen bonding and hydrocarbon liquids*, J. Chem. Phys., 99, 7056- 7075, **1993**.

Samuel G. V., S. Park, G. M. Nathanson, *Evaporation of water and uptake of HCl and HBr through Hexanol films at the surface of supercooled sulphuric acid*, J. Phys. Chem., 110, 7593- 7601, **2006**.

Scharfenort U., PhD Thesis*, Atom- /Molekülstrahlen und ihre Interaktion mit Schwefelsäuregrenzflächen unter stratosphärischen Temperaturbedingungen*, university Essen Duisburg, **2007**.

Scharge R. W., *A theoretical study of inter phase mass transfer*, Columbia University press, New York, Ch. 3, **1953**.

Schwell M., H. Baumgärtel, I. Weidinger, B. Krämer, H. Vortisch, L. Wöste, T. Leisner, E. Rühl, *Uptake dynamics and diffusion of HCl in sulphuric acid solution measured in single levitated micro droplets*, J. Phys. Chem., 104, 6726- 6732, **2000**.

Scoles G., D. Bassi, U. Buck, D. Laine, *Atomic and molecular beam methods*, Oxford University press, New York, Vol. 1, 189, 366, **1988**.

Smith J. D., C. D. Cappa, W. S. Drisdell, R. C. Cohen, R. J. Saykally, Raman thermometry measurements of free evaporation from liquid water droplets, J. AM. CHEM. SOC., 128, 12892- 12898, **2006**.

Tabazadeh A., R. P. Turco, M. Z. Jacobson, *A model for studying the composition and chemical effects of stratospheric aerosol*, J. Geo phys. Res.,99, 12897- 12914, **1994**.

Tabazadeh A., O. B. Toon, S. L. Clegg, P. Hamill, *A new parameterization of H_2SO_4/ H_2O aerosol composition: Atmospheric implications*, Geo. Res. Lett., 24, 1931- 1934, **1997**.

Tabazadeh A., S. T. Martin, J. Lin, *The effect of particle size and nitric acid uptake on the homogeneous freezing of aqueous sulphuric acid particles*, 27, 1111- 1114, **2000**.

Tolbert M. A., M. J. Rossi, R. Malhotra, D. M. Golden, *Reaction of chlorine nitrate with hydrogen chloride and water at Antarctic stratospheric temperatures*, Science, 238, 1258- 1260, **1987**.

Ward C. A., G. Fang, *Expression for predicting liquid evaporation flux: Statistical rate theory approach*, Amer. Phys. Society, Vol. 59, 429- 440, **1999**.

Ward C. A., F. Duan, *Turbulent transition of thermo capillary flow induced by water evaporation*, Phys. Rev. E., Vol. 69, 056308- 1, **2004**.

Waschewsky G. C. G., J. P. D. Abbatt, *HOBr in sulphuric acid solution: solubility and reaction with HCl as a function of temperature and concentration*, J. Phys. Chem., 103, 5312- 5320, **1999**.

Williams L. R., F. S. Long, *Viscosity of supercooled sulphuric acid solution*, J. Phys. Chem., 99, 3748- 3751, **1995**.

Worsnop D.R., M. S. Zahniser, C. E. Kolb, J. A. Gardner, L. R. Waston, J. M. Van Doren, J. T. Jayne, P. Davidovits, *Temperature dependence of mass accommodation of sulphuric dioxide and hydrogen peroxide on aqueous surfaces*, J. Phys. Chem., 93, 1159- 1172, **1989**.

Zhang R., M. T. Leu, L. F. Keyser, *Heterogeneous reactions of $ClONO_2$, HCl and HOCl on liquid sulfuric acid surfaces*, J. Phys. Chem., 98, 13563-13574, **1994**.